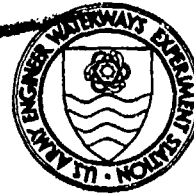LEVEL

MISCELLANEOUS PAPER HL-80-3

VAHM - A VERTICALLY AVERAGED HYDRODYNAMIC MODEL USING BOUNDARY-FITTED COORDINATES

by

Billy H. Johnson

Hydraulics Laboratory
U. S. Army Engineer Waterways Experiment Station
P. O. Box 631, Vicksburg, Miss. 39180

DTIC
ELECTE
JAN 2 8 1981
C

September 1980

Final Report

AD A094247

DDC FILE COPY

81 1 27 108

REPORT DOCUMENTATION PAGE		READ INSTRUCTIONS BEFORE COMPLETING FORM
1. REPORT NUMBER Miscellaneous Paper HL-80-3	2. GOVT ACCESSION NO. AD-A094 347	3. RECIPIENT'S CATALOG NUMBER
4. TITLE (and Subtitle) VAHM - A VERTICALLY AVERAGED HYDRODYNAMIC MODEL USING BOUNDARY-FITTED COORDINATES		5. TYPE OF REPORT & PERIOD COVERED Final report
		6. PERFORMING ORG. REPORT NUMBER
7. AUTHOR(s) Billy H. Johnson		8. CONTRACT OR GRANT NUMBER(s)
9. PERFORMING ORGANIZATION NAME AND ADDRESS U. S. Army Engineer Waterways Experiment Station Hydraulics Laboratory P. O. Box 631, Vicksburg, Miss. 39180		10. PROGRAM ELEMENT, PROJECT, TASK AREA & WORK UNIT NUMBERS Project 4A061101A91D
11. CONTROLLING OFFICE NAME AND ADDRESS Assistant Secretary of the Army (R&D) Department of the Army Washington, D. C. 20310		12. REPORT DATE September 1980
		13. NUMBER OF PAGES 108
14. MONITORING AGENCY NAME & ADDRESS(if different from Controlling Office) WES/MH/HL-80-3		15. SECURITY CLASS. (of this report) Unclassified
		15a. DECLASSIFICATION/DOWNGRADING SCHEDULE

16. DISTRIBUTION STATEMENT (of this Report)

Approved for public release; distribution unlimited.

17. DISTRIBUTION STATEMENT (of the abstract entered in Block 20, if different from Report)

18. SUPPLEMENTARY NOTES

19. KEY WORDS (Continue on reverse side if necessary and identify by block number)

Computerized models   Numerical analysis
Coordinates   Salinity
Hydrodynamics   VAHM (Vertically Averaged Hydrodynamic Model)
Mathematical models

20. ABSTRACT (Continue on reverse side if necessary and identify by block number)

    A numerical model called VAHM for computing the vertically averaged hydrodynamics of a water body, including salinity effects, has been developed. The model employs the concept of boundary-fitted coordinates to allow for an accurate representation of the boundary of the region being modeled while retaining the simplicity of the finite difference method of solution. Although a general curvilinear coordinate system covers the

(Continued)

20. ABSTRACT (Continued).

physical domain, all computations to solve the governing fluid dynamic
equations, as well as the computation of the boundary-fitted coordinate
system, are performed in a transformed rectangular plane with square grid
spacing.

A combination implicit-explicit finite difference scheme has been
employed to numerically solve the governing equations. With such a scheme,
the water surface elevation is computed implicitly using the Accelerated
Gauss-Seidel solution technique, whereas the velocity and salinity fields
are solved in an explicit manner. The major advantage of such a scheme
is that the speed of a surface gravity wave is removed from the stability
criteria while many desirable features of an explicit scheme are retained.

Although additional work on VAHM remains to be completed before the
model can be considered fully operational, results from the three applica-
tions of river and ocean boundaries demonstrate that the basic model be-
haves properly.

PREFACE

The study reported herein was conducted during the period October 1978 to September 1980 by the Hydraulics Laboratory of the U. S. Army Engineer Waterways Experiment Station (WES) under the general supervision of Messrs. H. B. Simmons, Chief of the Hydraulics Laboratory, and M. B. Boyd, Chief of the Hydraulic Analysis Division (HAD). The study was funded by Department of the Army Project 4A061101A91D, "In-House Laboratory Independent Research," sponsored by the Assistant Secretary of the Army.

Dr. B. H. Johnson, HAD, conducted the study and prepared this report. Special thanks are extended to Dr. Joe F. Thompson of the Aerophysics and Aerospace Department of the College of Engineering at Mississippi State University for his invaluable consultation throughout the study. In addition, the typing of the report by Mrs. Elaine Seeley and Mrs. Connie Johnson is gratefully acknowledged.

Commanders and Directors of WES during the conduct of this study and the preparation and publication of this report were COL John L. Cannon, CE, and COL Nelson P. Conover, CE. Technical Director was Mr. Fred R. Brown.

Accession For

NTIS   GRA&I

DTIC TAB

Unannounced

Justification

By

Distribution/

Availability Codes

Avail and/or

Dist   Special

A

1

CONTENTS

CONVERSION FACTORS, U. S. CUSTOMARY TO METRIC (SI)
UNITS OF MEASUREMENT

U. S. customary units of measurement used in this report can be con-
verted to metric (SI) units as follows:

Multiply	By	To Obtain
feet	0.3048	metres
miles (U. S. statute)	1.609344	kilometres

VAHM - A VERTICALLY AVERAGED HYDRODYNAMIC MODEL
USING BOUNDARY-FITTED COORDINATES

PART I: INTRODUCTION

1. The mathematical modeling of the hydrodynamics of a body of water plus the transport and dispersion of a conservative constituent within that body involves the solution of a set of partial differential equations expressing the conservation of mass, momentum, and energy of the flow field along with a transport equation for the constituent. These equations involve derivatives with respect to time as well as three spatial dimensions. However, a simplification that is often made in treating relatively shallow bodies of water that are well mixed over the depth is to vertically average the three-dimensional (3D) equations to yield a two-dimensional (2D) set for nearly horizontal flows.

Numerical Techniques

2. Since the governing equations are nonlinear, analytic solutions in general cannot be found and one is forced to resort to numerical techniques to obtain solutions. The two most common such techniques are the finite difference method (FDM) and the finite element method (FEM). There are, of course, both advantages and disadvantages to each of these approaches.

3. Perhaps the most often quoted advantage of the finite element method is that with this approach physical boundaries coincide with computational net points. Therefore, the modeling of flow within an irregular domain can be more accurately handled than with the normal finite difference method where the approach is to construct a rectangular grid over the domain, which forces the boundaries to be represented in a "stair stepped" fashion. However, a disadvantage of finite element methods is that they involve dense matrices rather than the sparse matrices involved in finite difference methods. This results in more

computational time being required in a finite element model having the same number of mesh points as a finite difference model. An additional disadvantage is that the finite element method is more cumbersome to code into a computer model than the finite difference method. This can be a problem not only during the development of the model but can also increase the level of effort required during later model modifications.

Boundary-Fitted Coordinates Concept

4. Accepting that the finite difference method possesses an advantage in simplicity and perhaps computational costs, a logical question is whether or not one can develop ways to circumvent the major disadvantage of having to represent irregular boundaries in a "stair stepped" fashion. One such technique which has been developed by Thompson, et al.[1,2,3] involves the use of boundary-fitted coordinates. Thompson's method generates curvilinear coordinates as the solution of two elliptic partial differential equations with Dirichlet boundary conditions, one coordinate being specified to be constant on the boundaries, and a distribution of the other specified along the boundaries. However, the numerical computations to solve the governing flow equations, as well as computations for the solution of the coordinate system, are not made in the physical curvilinear coordinate system but rather are made on a rectangular grid with square mesh spacing.

Purpose and Scope

5. Since the early to mid 1960's, many finite difference, plus a few finite element, computational models for vertically averaged flows have been developed.[4,5,6,7] The purpose of this report is to describe the development of a new vertically averaged hydrodynamic model which is fully coupled with the water salinity through its influence on the water density. The finite difference method of solution is employed but, unlike the previously developed models, solutions are obtained on a

boundary-fitted coordinate system to provide an accurate representation of boundary geometry.

6. The first part of the report summarizes Thompson's method for computing boundary-fitted coordinates. A portion of this discussion has been taken from a previous Independent Laboratory Inhouse Research (ILIR) report by Johnson and Thompson.[8] The second part of the report presents the basic equations to be solved and a discussion of their transformation in a fully conservative form from the physical plane to a transformed rectangular plane, wherein computations are made. The third part then deals with the numerical aspects of the solution scheme and presents the difference equations to be solved, along with associated boundary conditions. The final part of the report describes the computer model as it is developed to date and presents results from three applications that demonstrate, in a qualitative sense, that the model is behaving properly.

7.   Thompson's work on the generation of boundary-fitted coordi-
nates can be found in References 1, 2, and 3. The discussion below is a
summary of the more important theoretical aspects of the subject.

The Basic Idea

8.   Suppose one is interested in solving a differential system
involving two concentric circles, such as shown in Figure 1, where
r = constant = η_1 on the inner circle and r = constant = n_2 on the
outer circle and θ varies monotonically over the same range over both
the inner and outer boundaries, i.e., 0° to 360°.

9.   A cylindrical coordinate system is the obvious choice since a
coordinate line, i.e., a line of constant radius, coincides with each
boundary. If one now pulls the interior region between the two circles
apart at θ = 0° (or θ = 360°) and folds outward, it is easy to visu-
alize the region D_1 becoming the rectangular region D_2 .

10.   The general boundary-fitted system is completely analogous
to the system discussed above. In Figure 2 the curvilinear coordinate,
η , is defined to be constant on the inner boundary in the same way that
the curvilinear coordinate, r , is defined to be constant on the inner
circle in the cylindrical coordinate system. Similarly, η is defined
to be constant at a different value on the outer boundary. The other
curvilinear coordinate, ξ , is defined to vary monotonically over the
same range on both the inner and outer boundaries, as the curvilinear
coordinate, θ , varies from 0 to 2π around both the inner and outer
circles in cylindrical coordinates. It would be just as meaningless to
have a different range for ξ on the inner and outer boundaries as it
would be to have θ increase by something other than 2π around one of
the circles in cylindrical coordinates. It is this fact that ξ has the
same range on both boundaries that causes the transformed field to be
rectangular. Note that the actual values of the coordinates, η and

ξ , are irrelevant, in the same way that r and θ may be expressed in different units in cylindrical coordinates.

11. Now that the values of the coordinates, η and ξ , have been completely specified on all the boundaries of a closed field, it remains to define the values in the interior of the field in terms of these boundary values. Such a task immediately calls to mind elliptic partial differential equations, since the solution of such an equation is completely defined in the interior of a region by its values on the boundary of the region. Thus if the coordinates, ξ and η , are taken as the solutions of any two elliptic partial differential equations, say $L(\xi) = 0$, $D(\eta) = 0$, where L and D represent elliptic operators, then ξ and η will be determined at each point in the interior of the field by the specified values on the boundary. One condition must be put on the elliptic system chosen since the same pair of values (ξ, η) must not occur at more than one point in the field or the coordinate system will be ambiguous. This condition can be met by choosing elliptic partial differential equations exhibiting extremum principles that preclude the occurrence of extrema in the interior of the field.

Mathematical Development

12. From the discussion above, a logical choice of the elliptic generating system is Poisson's equation. Thus, based upon Figure 2, the basic problem is to solve

$$\xi_{xx} + \xi_{yy} = P$$

$$\tag{1}$$

$$\eta_{xx} + \eta_{yy} = Q$$

with boundary conditions,

8

$$\xi = \xi_1(x,y) \text{ on } \Gamma_1$$

$$\eta = \text{constant} = \eta_1 \text{ on } \Gamma_1$$

(2)

$$\xi = \xi_2(x,y) \text{ on } \Gamma_2$$

$$\eta = \text{constant} = \eta_2 \text{ on } \Gamma_2$$

The arbitrary curve joining Γ_1 and Γ_2 in the physical plane specifies a branch cut for the multiple-valued function, $\xi(x,y)$. Thus the values of the coordinate functions $x(\xi,\eta)$ and $y(\xi,\eta)$ are equal along Γ_3 and Γ_4 , and these functions and their derivatives are continuous from Γ_3 to Γ_4 . Therefore boundary conditions are neither required nor allowed on Γ_3 and Γ_4 .

13. The functions P and Q may be chosen to cause the coordinate lines to concentrate as desired. As discussed in Reference 1, negative values of Q result in a superharmonic solution and cause η lines to move toward the η-line having the lowest vaue of η , while positive values have the opposite effect. Considering the ξ solution to be superharmonic results in the interior of the ξ = constant lines being rotated in a clockwise direction in the physical plane, whereas if the ξ equation is subharmonic, i.e., P is positive, the lines are rotated in the counterclockwise direction.

14. The form of these functions incorporated by Thompson,[2] based upon much computer experimentation, is that of decaying exponentials. For example, let Q be taken as

$$Q = -a \exp\left(- d\left|\eta - \eta_i\right|\right)$$

where a and d are constants, and η_i is some specified η-line. This function reaches its maximum magnitude on the η_i line and decays away from that line on either side at a rate controlled by d .

9

15. This function would cause η-lines to concentrate on one side of the η_i-line and to move away from the other side. If, however, a sign-changing function is incorporated so that

$$Q = - a \; sgn \; (\eta - \eta_i) \; exp \; (- \; d|\eta - \eta_i|)$$

where $sgn(x)$ is simply the sign of x, the η-lines will concentrate on both sides of the η_i-line. In a similar fashion, it is possible to cause concentration of η_i-lines near a point (ξ_i, η_i) with the function

$$Q = - a \; sgn \; (\eta - \eta_i) \; exp \left[\; - d \sqrt{\left(\xi - \xi_i \right)^2 + \left(\eta - \eta_i \right)^2} \; \right]$$

Finally, concentration near more than one line and/or point is achieved by writing Q as a sum of functions of the above form. In this case the attraction amplitude a and the decay factor d may be different for each line or point of attraction. The decay factor should be large enough to cause the effects of each attraction line or point to be confined essentially to its immediate vicinity. Thompson has found that attraction amplitudes of 100 are moderate, 10 is weak and 1000 is fairly strong. A decay factor of 1.0 causes the effects to be confined to a few lines near the attraction source, while 0.1 gives a fairly widespread effect. Control of ξ-lines is accomplished by an analogous form of the function P. Such control is useful to improve grid spacing and configuration when complicated geometries are involved.

16. Since all numerical computations are to be performed in the rectangular transformed plane, it is necessary to interchange the dependent and independent variables in Equation 1. Using the relations

$$\xi_x = y_\eta / J$$

$$\xi_y = -x_\eta / J$$

$$\eta_x = -y_\xi / J$$

$$\eta_y = x_\xi / J$$

10

$$\xi_{xx} = (\xi_x y_{\xi\eta} + \eta_x y_{\eta\eta})/J - (\xi_x^2 J_\xi + \xi_x \eta_x J_\eta)/J$$

$$\xi_{yy} = - (\eta_y x_{\eta\eta} + \xi_y x_{\xi\eta})/J - (\xi_y \eta_y J_\eta + \xi_y^2 J_\xi)/J$$

$$\eta_{xx} = - (\xi_x y_{\xi\xi} + \eta_x y_{\xi\eta})/J - (\xi_x \eta_x J_\xi + \eta_x^2 J_\eta)/J$$

$$\eta_{yy} = (\eta_y x_{\xi\eta} + \xi_y x_{\xi\xi})/J - (\xi_y \eta_y J_\xi + \eta_y^2 J_\eta)/J$$

equation 1 becomes

$$\alpha x_{\xi\xi} - 2\beta x_{\xi\eta} - \gamma x_{\eta\eta} + J^2(P x_\xi + Q x_\eta) = 0$$

$$\alpha y_{\xi\xi} - 2\beta y_{\xi\eta} + \gamma y_{\eta\eta} + J^2(P y_\xi + Q y_\eta) = 0$$

(3a)

where

$$\alpha = x_\eta^2 + y_\eta^2$$

$$\beta = x_\xi x_\eta + y_\xi y_\eta$$

$$\gamma = x_\xi^2 + y_\xi^2$$

(3b)

$$J = \text{Jacobian of the transformation} = x_\xi y_\eta - x_\eta y_\xi$$

with the transformed boundary conditions

11

$$x = f_1(\xi,\eta_1) \text{ on } \Gamma_1^*$$

$$y = g_1(\xi,\eta_1) \text{ on } \Gamma_1^*$$

$$x = f_2(\xi,\eta_2) \text{ on } \Gamma_2^* \tag{4}$$

$$y = g_2(\xi,\eta_2) \text{ on } \Gamma_2^*$$

Again considering Figure 2, the functions $f_1(\xi,\eta_1)$, $g_1(\xi,\eta_1)$, $f_2(\xi,\eta_2)$, and $g_2(\xi,\eta_2)$ are specified by the known shape of the contours Γ_1 and Γ_2 and the specified distribution of ξ thereon. Although the new system of equations is more complex than the original system, the boundary conditions are specified on straight boundaries and the coordinate spacing in the transformed plane is uniform. Computationally, these advantages far outweigh any disadvantages resulting from the extra complexity of the equations to be solved.

17. The boundary-fitted coordinate system so generated has a constant η-line coincident with each boundary in the physical plane. The ξ-lines may be spaced in any manner desired around the boundaries by specification of x,y at the equispaced ξ-points on the Γ_1^* and Γ_2^* lines of the transformed plane.

18. The rectangular transformed grid is set up to be the size desired for a particular problem. Since the values of ξ and η are meaningless in the transformed plane, the η lines are assumed to run from 1 to the number of η lines desired in the physical plane. Likewise, the ξ lines are numbered 1 to the number specified on the boundaries of the physical plane. The grid spacing in both the ξ and η directions of the transformed plane is taken as unity. Second order central difference expressions are used in Thompson's coordinate generation code, TOMCAT,[2] to approximate all derivatives in Equations 3a and 3b. The resulting set of nonlinear difference equations, two for each point, are solved in TOMCAT by accelerated Gauss-Seidel (SOR) iteration using overrelaxation. Some discussion of this technique is presented in Reference 2.

12

19. The same procedure may be extended to regions that are more than doubly connected, i.e. have more than two closed boundaries, or equivalently, more than one body within a single outer body. A river reach containing more than one island would be an example.

Types of Boundary-Fitted Coordinate Systems

20. Previous discussion of the generation of boundary-fitted coordinates has centered around the idea of using branch cuts to reduce multiply connected regions to simply connected ones in the transformed plane. Thompson's TOMCAT code employs such branch cuts. The other type of coordinate system transformation available leaves the multiplicity of the region unchanged. In this case, bodies in the interior of the physical field are transformed to rectangular slabs or even slits in the transformed plane. In the case of slits, the physical coordinates and solution variables generally have different values at points on the two sides of the slit, even though such points are coincident in the transformed plane. This does not introduce any approximations, but simply adds a little more bookkeeping to the code. Fields with more than one body in the interior simply result in a like number of slabs and/or slits in the transformed plane.

21. Different types of transformation may be more appropriate for different physical configurations. Generally, the slit/slab form is more appropriate for channel-like physical configurations having bodies in the interior, while the branch cut form works particularly well for "unbounded" regions involving external flow about bodies and for regions having an outer boundary that forms a continuous circuit without pronounced corners around the field. The slab is generally superior to the slit unless the boundary has a sharp point. The case of a single channel without any interior bodies would be the same in either form.

Data Required for Generation of Boundary-Fitted Coordinates

22. The basic input or data required to generate a boundary-fitted

13

coordinate system are the physical coordinates of points on the boundaries. This will be discussed in more detail in PART V in connection with the applications presented.

Computer Time Required for Generation of Boundary-Fitted Coordinates

23. The computing cost for generating a boundary-fitted coordinate system is trivial. Approximately 3 sec of CPU time on a CRAY I computer were required to generate the coordinate system shown in Figure 3. It might be noted that no coordinate control was employed. The use of such control would result in a slight increase in computational time.

PART III: BASIC HYDRODYNAMIC EQUATIONS

24. The Navier Stokes equations express the conservation of mass and momentum of a flow field and are the basic governing equations for the solution of any fluid dynamics problem. Written in tensor notation these equations are

$$\text{\underline{Continuity}:} \quad \frac{\partial \rho}{\partial t} + \frac{\partial \rho u_i}{\partial x_i} = 0 \tag{5}$$

$$\text{\underline{Momentum}:} \quad \frac{\partial \rho u_i}{\partial t} + \frac{\partial (\rho u_i u_j)}{\partial x_j} = \frac{-\partial P}{\partial x_i} + \rho g_i - 2\varepsilon_{ijk}\Omega \, \rho u_k + \frac{\partial T_{ij}}{\partial x_j} \tag{6}$$

where

ρ = water density

t = time

u_i = tensor notation for velocity

x_i = tensor notation of spatial coordinate

g_i = acceleration of gravity

ε_{ijk} = cyclic tensor

Ω_j = Coriolis parameter

T_{ij} = laminar stress tensor

μ = molecular eddy viscosity

δ_{ij} = Kronecker delta

and where

$$T_{ij} = \mu \left(\frac{\partial u_i}{\partial x_j} + \frac{\partial u_j}{\partial x_i} \right) - \frac{2}{3} \mu \frac{\partial u_i}{\partial x_j} \delta_{ij} \tag{7}$$

represents the viscous molecular stress arising as a result of the continuum approach. All symbols used are defined in Appendix A. It will

be recalled from tensor theory that repeated indicies imply a summation and also that ε_{ijk} in the Coriolis term is the cyclic tensor defined as

$$\varepsilon_{ijk} = \begin{matrix} 1 \text{ - for an even permutation of ijk} \\ -1 \text{ - for an odd permutation of ijk} \\ 0 \text{ - otherwise} \end{matrix}$$

In addition, the Kronecker Delta, δij, is defined as

$$\delta_{ij} = \begin{matrix} 1 \text{ - if } i = j \\ 0 \text{ - otherwise} \end{matrix}$$

25. In addition to the above equations, a conservation of mass equation must also be written for any constituent being transported. Such an equation for the salinity becomes

$$\underline{\text{Salinity}}: \quad \frac{\partial s}{\partial t} + \frac{\partial (su_i)}{\partial x_i} = \frac{\partial \left(D_{ij} \frac{\partial s}{\partial x_j} \right)}{\partial x_i} \tag{8}$$

This equation states that the salinity can change as a result of advection by the flow field and molecular diffusion.

26. Since the salinity is coupled to the flow equations through its influence on the density, one additional equation remains to be written in order to close the system. An equation of state expressing the density as a function of the temperature and salinity must be employed.

$$\underline{\text{Equation of State}}: \quad \rho = \rho(T,s) \tag{9}$$

With the closure of the system, there exists six equations to be solved for the six unknowns; density -ρ , three velocity components -u,v,w , pressure -p , and salinity -s.

16

27. The above equations written with molecular values of viscosity and diffusivity are only applicable in a practical sense to laminar flow fields where the flow does not exhibit random irregular fluctuations in time. However, most fluids in motion exhibit such fluctuations and are referred to as turbulent flows.

28. Following Reynolds, the approach normally taken to make the equations applicable to turbulent flows is to assume that the dependent variables are composed of an average time-varying component plus a small randomly varying component about the average value. This is illustrated below.
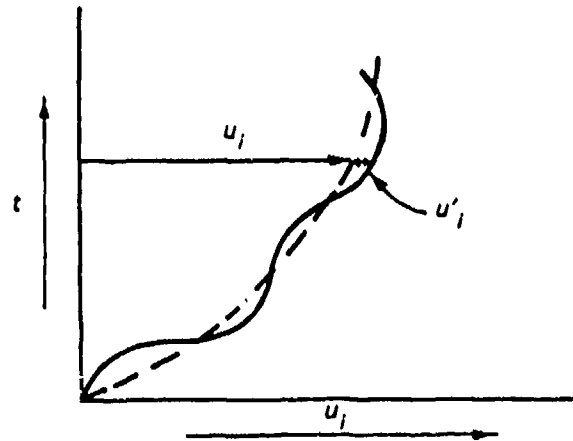
Thus, one writes

$$u_i(x,y,z,t) = \bar{u}_i(x,y,z,t) + u_i'(x,y,z,t)$$

where

$$\bar{u}_i = \frac{1}{\Delta t} \int_{t-\Delta t/2}^{t+\Delta t/2} u_i(x,y,z,t) \, dt$$

17

and

$$\frac{1}{\Delta t} \int_{t-\Delta t/2}^{t+\Delta t/2} u_i'(x,y,z,t) \, dt = 0$$

u_i' = deviation between instantaneous velocity and time-averaged velocity

$\bar{u}_i$ = time-averaged velocity

Δt = time step

With all the dependent variables written in the form above, substitution into Equations 5, 6, and 8 and then integration over the time increment Δt produces the same form of the previous equations, but now written with the time-averaged components as the dependent variables, plus the additional terms

$$\frac{1}{\Delta t} \int_{t-\Delta t/2}^{t+\Delta t/2} u_i' u_j' \, dt$$

and

$$\frac{1}{\Delta t} \int_{t-\Delta t/2}^{t+\Delta t/2} s' u_i' \, dt$$

where s' = deviation between instantaneous and time-averaged salinity.

29. The first term is referred to as the turbulent Reynolds stress, since the high frequency turbulent fluctuations manifest themselves as viscous stresses acting on the average component of flow. Using Boussinesq's concept of eddy viscosity, the first term is written as

18

$$\frac{1}{\Delta t} \int_{t-\Delta t/2}^{t+\Delta t/2} u_i' u_j' \, dt = \varepsilon_{ij}\left(\frac{\partial \bar{u}_i}{\partial x_j} + \frac{\partial \bar{u}_j}{\partial x_i}\right) \text{(no summation over i)}$$

In analogy with the laminar flow case, ε_{ij} is referred to as the turbulent or eddy viscosity tensor.

30. In a similar fashion, the second term above, which arises from the time averaging of the salinity equation, is commonly written as

$$\frac{1}{\Delta t} \int_{t-\Delta t/2}^{t+\Delta t/2} s' u_i' \, dt = A_{ij} \frac{\partial \bar{s}}{\partial x_j}$$

where A_{ij} is called the "eddy diffusivity tensor" and $\bar{s}$ is the time-averaged salinity.

31. The equations commonly applied to turbulent flow problems can now be written as

$$\text{\underline{Continuity}:} \quad \frac{\partial \bar{\rho}}{\partial t} + \frac{\partial \overline{\rho u_i}}{\partial x_i} = 0 \tag{10}$$

$$\text{\underline{Momentum}:} \quad \frac{\partial \overline{\rho u_i}}{\partial t} + \frac{\partial(\overline{\rho u_i u_j})}{\partial x_j} = -\frac{\partial \bar{\bar{p}}}{\partial x_i} + \bar{\rho} g_i$$

$$- 2\varepsilon_{ijk}\Omega_j \overline{\rho u}_k + \frac{\partial}{\partial x_j}\left[\varepsilon_{ij}\left(\frac{\partial \bar{u}_i}{\partial x_j} + \frac{\partial \bar{u}_j}{\partial x_i}\right)\right] \tag{11}$$

19

$$\underline{\text{Salinity}}: \quad \frac{\partial \bar{s}}{\partial t} + \frac{\partial \overline{su_i}}{\partial x_i} = \frac{\partial}{\partial x_i}\left(A_{ij}\, \frac{\partial \bar{s}}{\partial x_j}\right) \tag{12}$$

$$\underline{\text{Equation of State}}: \quad \bar{\rho} = \bar{\rho}(\bar{T}, \bar{s}) \tag{13}$$

where

$\bar{\rho}$ = time-averaged water density

$\bar{P}$ = time-averaged pressure

and where the assumption has been made that the eddy coefficients are much larger than the molecular values; i.e.,

$$\varepsilon_{ij} \gg \mu$$

$$A_{ij} \gg D_{ij}$$

Depth Averaging for Nearly Horizontal Flow

32. A solution of the above set of equations constitutes a fully time varying, three-dimensional model of the flow and salinity fields. However, when modeling nearly horizontal flow in relatively shallow and well-mixed water bodies the usual approach is to employ a spatial averaging to yield a two-dimensional model.

33. The basic assumption in the spatial averaging of the three-dimensional equations is that the dependent variables can be represented by an average value over one or more of the spaial coordinates plus some small random deviation; e.g., the velocity would be written as

$$\bar{u}_i = \tilde{\bar{u}}_i + \bar{u}_i' \tag{14}$$

where

20

$$\widetilde{\bar{u}}_i = \frac{1}{\Delta x_i} \int\limits_{x_i - \Delta x_i/2}^{x_i + \Delta x_i/2} \bar{u}_i \; dx_i$$

$$\frac{1}{\Delta x_i} \int\limits_{x_i - \Delta x_i/2}^{x_i + \Delta x_i/2} \bar{u}_i' \; dx_i = 0$$

and

$\widetilde{\bar{u}}_i$ = time- and space-averaged velocity

Δx_i = spatial step

$\bar{u}'$ = deviation between time-averaged velocity and time- and space-averaged velocity

In an x, y, z coordinate system (with x referring to the longitudinal; y, the lateral; and z, the vertical), if $i = 2$, the integration is over the width and a width-averaged model results. However, if $i = 3$, the integration is taken over the depth and a depth-averaged model will result. Many depth-averaged models have been developed since Leendertse's[5] work, whereas laterally averaged models have only been developed over the past five years or so. If the integration is performed over the complete cross section, a one-dimensional model with variations allowed only in the longitudinal direction results.

34. As was done in the time-averaging of the instantaneous equations, expressions such as Equation 14 are substituted into the turbulent time-averaged equations to yield a set of equations with the time-averaged and spatially averaged components of the flow and salinity as dependent variables plus the additional terms

$$\frac{1}{\Delta x_i} \int\limits_{x_i - \Delta x_i/2}^{x_i + \Delta x_i/2} \bar{u}_i' \bar{u}_j' \; dx_i$$

21

and

$$\frac{1}{\Delta x_i} \int_{x_i - \Delta x_i/2}^{x_i + \Delta x_i/2} \overline{s'}\,\overline{u_i'} \; dx_i$$

As in the time-averaging case, these terms are normally approximated by

$$\frac{1}{\Delta x_i} \int_{x_i - \Delta x_i/2}^{x_i + \Delta x_i/2} \overline{u_i'}\,\overline{u_j'} \; dx_i = \varepsilon'_{ij} \left(\frac{\partial \widetilde{\overline{u}}_i}{\partial x_j} + \frac{\partial \widetilde{\overline{u}}_j}{\partial x_i} \right)$$

and

$$\frac{1}{\Delta x_i} \int_{x_i - \Delta x_i/2}^{x_i + \Delta x_i/2} \overline{s'}\,\overline{u_i'} \; dx_i = A'_{ij} \frac{\partial \widetilde{\overline{s}}}{\partial x_i}$$

where ε'_{ij} and A'_{ij} are referred to as "eddy dispersion coefficients" by Holley[9] to distinguish them from the turbulent eddy diffusion coefficients arising from the time averaging, and $\widetilde{\overline{s}}$ is the time-averaged and and spatially averaged salinity.

35. The resulting spatially averaged equations take different forms, depending upon whether the averaging is performed over the depth or the width. For the depth averaged case, the equations below are obtained. It should be noted that the Boussinesq approximation has been made which removes the effect of density variations in all terms except those multiplied by the acceleration of gravity.

$$\underline{\text{Continuity:}} \quad \frac{\partial \phi}{\partial t} + \frac{\partial (uh)}{\partial x} + \frac{\partial (vh)}{\partial y} = 0$$

22

x-momentum: $\quad \dfrac{\partial(hu)}{\partial t} + \dfrac{\partial(hu^2)}{\partial x} + \dfrac{\partial(huv)}{\partial y} = -\dfrac{h}{\rho}\dfrac{\partial P}{\partial x}$

$$+ \dfrac{\partial\left(hD_{xx}\dfrac{\partial u}{\partial x}\right)}{\partial x} + \dfrac{\partial\left(hD_{xy}\dfrac{\partial u}{\partial y}\right)}{\partial y}$$

$$+ \tau_{s_x} - \tau_{B_x} + fhv \qquad (16)$$

y-momentum: $\quad \dfrac{\partial(hv)}{\partial t} + \dfrac{\partial(huv)}{\partial x} + \dfrac{\partial(hv^2)}{\partial y} = -\dfrac{h}{\rho}\dfrac{\partial P}{\partial y}$

$$+ \dfrac{\partial\left(hD_{yx}\dfrac{\partial v}{\partial x}\right)}{\partial x} + \dfrac{\partial\left(hD_{yy}\dfrac{\partial v}{\partial y}\right)}{\partial y}$$

$$+ \tau_{s_v} - \tau_{B_y} - fhu \qquad (17)$$

Salinity: $\quad \dfrac{\partial(hs)}{\partial t} + \dfrac{\partial hus}{\partial x} + \dfrac{\partial(hvs)}{\partial y} = \dfrac{\partial\left(hE_x\dfrac{\partial s}{\partial x}\right)}{\partial x} + \dfrac{\partial\left(hE_y\dfrac{\partial s}{\partial y}\right)}{\partial y} \qquad (18)$

The equation of state relating the water density to the salinity and water temperature (assumed constant) has been taken from Leendertse[10] and is given as

$$\rho(s,T) = 1000\left(\frac{PO}{AL} + ALO * PO\right) \qquad (19)$$

where

$\quad AL = 1779.5 + 11.25T - 0.0745T^2 - (3.80 + 0.01T)s$

$\quad ALO = 0.6980$

$\quad PO = 5890.0 + 38T - 0.375T^2 + 3s$

36. In the above equations the surface wind shear is

$$\tau_{s_x} = \frac{W_c}{\rho_o} \rho_a v_w^2 \cos \alpha \tag{20}$$

$$\tau_{s_y} = \frac{W_c}{\rho_o} \rho_a v_w^2 \sin \alpha \tag{21}$$

and the bottom shear is

$$\tau_{B_x} = gu \sqrt{u^2 + v^2}\Big/ C^2 \tag{22}$$

$$\tau_{B_y} = gv \sqrt{u^2 + v^2}\Big/ C^2 \tag{23}$$

The coriolis parameter, f , is computed from

$$f = 2\omega_e \sin \lambda \tag{24}$$

where ω_e = earth's angular velocity and λ is the angle of latitude of the center of the area being modeled.

37. In order to finalize the above system of equations it remains to couple the salinity computations with those of the flow field. This is accomplished in the following manner. Assuming that the pressure is hydrostatic,

$$\frac{\partial P}{\partial z} = -\rho g$$

one can determine the pressure at any depth z from

$$\int_z^\phi \frac{\partial F}{\partial z} \, dz = - \int_z^\phi \rho g dz$$

24

where the coordinate system is
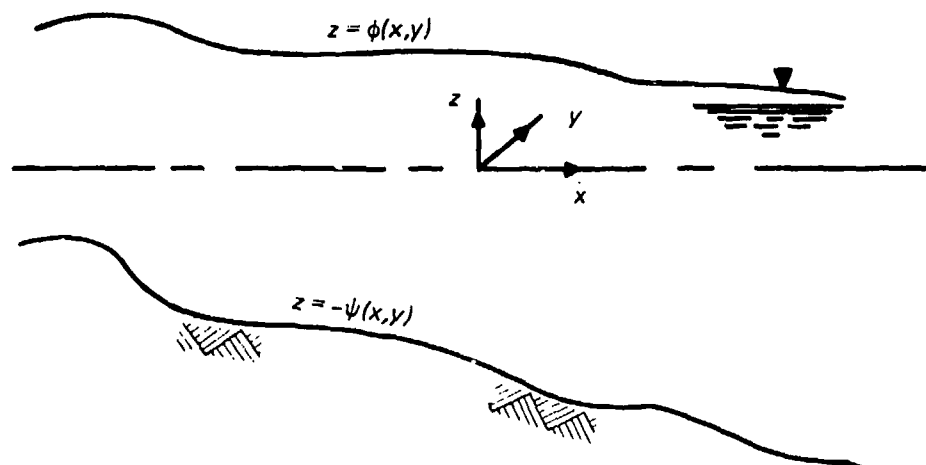
Integrating the above eq one obtains

$$P = P_a + \int_z^\phi \rho g dz$$

where P_a is the atmospheric pressure. Differentiating with respect to the x-coordinate yields

$$\frac{\partial P}{\partial x} = \frac{\partial P_a}{\partial x} + \frac{\partial}{\partial x} \int_z^\phi \rho g dz$$

As was done in the continuity and momentum equations above, one now assumes that the pressure and density are composed of a depth averaged plus a fluctuating component. The resulting equation is then integrated over the depth to yield

$$h \frac{\partial P}{\partial x} = h \frac{\partial P_a}{\partial x} + hg\rho \frac{\partial \phi}{\partial x} + \frac{1}{2} h^2 g \frac{\partial \rho}{\partial x} \tag{25}$$

25

Similarly,

$$h \frac{\partial P}{\partial y} = h \frac{\partial P_a}{\partial y} + hg\rho\frac{\partial \phi}{\partial y} + \frac{1}{2} h^2 g \frac{\partial \rho}{\partial y} \qquad (26)$$

Substituting Equations 20-26 into equations 15-18 yields the final form of the equations in cartesian coordinates.

Continuity: $\dfrac{\partial \phi}{\partial t} + \dfrac{\partial (uh)}{\partial x} + \dfrac{\partial (vh)}{\partial y} = 0$ $\qquad (27)$

x-momentum: $\dfrac{\partial (hu)}{\partial t} + \dfrac{\partial (hu^2)}{\partial x} + \dfrac{\partial (huv)}{\partial y} = - \dfrac{h}{\rho_o} \left(\dfrac{\partial P_a}{\partial x} + g\rho\dfrac{\partial \phi}{\partial x} + \dfrac{hg}{2} \dfrac{\partial \rho}{\partial x} \right)$

$$+ \frac{\partial \left(hD_{xx} \frac{\partial u}{\partial x} \right)}{\partial x} + \frac{\partial \left(hD_{xy} \frac{\partial u}{\partial y} \right)}{\partial y} + \frac{W_c}{\rho_o} \, \rho_a v_w^2 \cos \alpha$$

$$- gu \sqrt{u^2 + v^2} \Big/ C^2 + fhv \qquad (28)$$

y-momentum: $\dfrac{\partial (hv)}{\partial t} + \dfrac{\partial (huv)}{\partial x} + \dfrac{\partial (hv^2)}{\partial y} = - \dfrac{h}{\rho_o} \left(\dfrac{\partial P_a}{\partial x} + g\rho\dfrac{\partial \phi}{\partial y} + \dfrac{hg}{2} \dfrac{\partial \rho}{\partial y} \right)$

$$+ \frac{\partial \left(hD_{yx} \frac{\partial v}{\partial x} \right)}{\partial x} + \frac{\partial \left(hD_{yy} \frac{\partial v}{\partial y} \right)}{\partial y} + \frac{W_c}{\rho_o} \rho_a v_w^2 \sin \alpha$$

$$- gv \sqrt{u^2 + v^2} \Big/ C^2 - fhu \qquad (29)$$

Salinity: $\dfrac{\partial (hs)}{\partial t} + \dfrac{\partial (hus)}{\partial x} + \dfrac{\partial (hvs)}{\partial y} = \dfrac{\partial \left(hE_x \frac{\partial s}{\partial x} \right)}{\partial x} + \dfrac{\partial \left(hE_y \frac{\partial s}{\partial y} \right)}{\partial y}$ $\qquad (30)$

Equation of state: $\rho = \rho(s,T)$ $\qquad (31)$

26

38. As previously discussed, the above set of equations must now be transformed into a (ξ,η) boundary-fitted coordinate system such that (ξ,η) are the independent variables. The resulting set of equations will then be solved in a transformed rectangular plane as discussed in PART II. In order to accomplish the transformation, the following expressions derived by Thompson[12] are utilized.

$$f_x = \frac{1}{J}\left[(fy_\eta)_\xi - (fy_\xi)_\eta\right] \tag{32}$$

$$f_y = \frac{1}{J}\left[-(fx_\eta)_\xi + (fx_\xi)_\eta\right] \tag{33}$$

It should be noted that these expressions are written in a fully conservative form which should result in a more accurate solution in highly irregular coordinate systems.

39. Using the above expressions and assuming that the coordinate system is time invariant, one can transform Equations 27-31 into the set below.

Transformed Equations

Continuity:
$$\frac{\partial \phi}{\partial t} + \frac{1}{J}\left[\left(uhy_\eta - vhx_\eta\right)_\xi + \left(vhx_\xi - uhy_\xi\right)_\eta\right] = 0 \tag{34}$$

x-Momentum:
$$\frac{\partial(hu)}{\partial t} + \frac{1}{J}\left[\left(hu^2y_\eta - huvx_\eta\right)_\xi + \left(huvx_\xi - hu^2y_\xi\right)_\eta\right]$$

$$= -\frac{h}{J\rho_o}\left[\left(P_a y_\eta\right)_\xi - \left(P_a y_\xi\right)_\eta\right] - \frac{hg\rho}{J\rho_o}\left[\left(\phi y_\eta\right)_\xi - \left(\phi y_\xi\right)_\eta\right]$$

$$- \frac{h^2 g}{2J\rho_o}\left[\left(\rho y_\eta\right)_\xi - \left(\rho y_\xi\right)_\eta\right] + \frac{1}{J}\left\{\left(\frac{D_{xx}h}{J}\left[\left(uy_\eta\right)_\xi\right.\right.\right.$$

$$\left.\left.\left.- \left(uy_\xi\right)_\eta\right]y_\eta\right)_\xi - \left(\frac{D_{xx}h}{J}\left[\left(uy_\eta\right)_\xi - \left(uy_\xi\right)_\eta\right]y_\xi\right)_\eta\right\}$$

$$+ \frac{1}{J}\left\{-\left(\frac{hD_{xy}}{J}\left[-\left(ux_\eta\right)_\xi + \left(ux_\xi\right)_\eta\right]x_\eta\right)_\xi + \left(\frac{hD_{xy}}{J}\left[-\left(ux_\eta\right)_\xi\right.\right.\right.$$

$$\left.\left.\left.+ \left(ux_\xi\right)_\eta\right]x_\xi\right)_\eta\right\} + \frac{W_c}{\rho_o}\rho_a v_w^2 \cos\alpha - gu\sqrt{u^2+v^2}\bigg/ C^2 + fhv \tag{35}$$

y-Momentum:
$$\frac{\partial(hv)}{\partial t} + \frac{1}{J}\left[\left(hv^2x_\xi - huvy_\xi\right)_\eta + \left(huvy_\eta - hv^2x_\eta\right)_\xi\right]$$

$$= -\frac{h}{J\rho_o}\left[\left(P_a x_\xi\right)_\eta - \left(P_a x_\eta\right)_\xi\right] - \frac{hg\rho}{J\rho_o}\left[-\left(\phi x_\eta\right)_\xi\right.$$

$$\left.+ \left(\phi x_\xi\right)_\eta\right] - \frac{h^2 g}{2J\rho_o}\left[-\left(\rho x_\eta\right)_\xi + \left(\rho x_\xi\right)_\eta\right]$$

$$+ \frac{1}{J}\left\{\left(\frac{D_{yx}h}{J}\left[\left(vy_\eta\right)_\xi - \left(vy_\xi\right)_\eta\right]y_\eta\right)_\xi\right.$$

28

$$-\left(\frac{D_{yx}h}{J}\left[\left(vy_\eta\right)_\xi - \left(vy_\xi\right)_\eta\right]y_\xi\right)_\eta\right\} + \frac{1}{J}\left\{-\left(\frac{D_{yy}h}{J}\left[-\left(vx_\eta\right)_\xi\right.\right.\right.$$

$$\left.\left.\left.+\left(vx_\xi\right)_\eta\right]x_\eta\right)_\xi + \left(\frac{D_{yy}h}{J}\left[-\left(vx_\eta\right)_\xi + \left(vx_\xi\right)_\eta\right]x_\xi\right)_\eta\right\}$$

$$+\frac{W_c}{\rho_o}\,\rho_a v_w^2\,\sin\alpha\ - gv\sqrt{u^2+v^2}\Big/C^2 - fhu \qquad (36)$$

<u>Salinity</u>: $\dfrac{\partial(hs)}{\partial t} + \dfrac{1}{J}\left[\left(husy_\eta - hvsx_\eta\right)_\xi + \left(hvsx_\xi - husy_\xi\right)_\eta\right]$

$$= \frac{1}{J}\left\{\left(\frac{hE_x}{J}\left[\left(sy_\eta\right)_\xi - \left(sy_\xi\right)_\eta\right]y_\eta\right)_\xi\right.$$

$$\left.- \left(\frac{hE_x}{J}\left[\left(sy_\eta\right)_\xi - \left(sy_\xi\right)_\eta\right]y_\xi\right)_\eta\right\} + \frac{1}{J}\left\{-\left(\frac{hE_y}{J}\right.\right.$$

$$\left.\left[-\left(sx_\eta\right)_\xi + \left(sx_\xi\right)_\eta\right]x_\eta\right)_\xi + \left(\frac{hE_y}{J}\left[-\left(sx_\eta\right)_\xi + \left(sx_\xi\right)_\eta\right]x_\xi\right)_\eta\right\} \qquad (37)$$

<u>Eq. of State</u>: $\rho = \rho\left[s(\xi,\eta),T\right]$ \qquad\qquad\qquad\qquad (38)

40. The above set of equations constitute the set for which a numerical solution is sought on a rectangular grid with square grid spacing (e.g., $\Delta\xi = \Delta\eta = 1.0$) . It remains, of course, to specify proper boundary conditions along the sides of the rectangular grid. It is obvious that the transformed equations are more complicated than the original cartesian forms; however, the advantage of being able to make computations on a rectangular grid far outweighs any disadvantage resulting from the more complicated set of equations.

29

PART IV: NUMERICAL ASPECTS

41. In order to obtain a solution of the governing set of Equations 34-38, the method of finite differences is employed. There are many different types of finite difference schemes that have been employed in numerical solutions of partial differential equations. These schemes range from fully explicit to fully implicit, with a combination of an explicit-implicit scheme being employed in some cases, e.g., Edinger and Buchak.[11] A similar scheme is employed here. Basically, the computational cycle will consist of the following steps:

    a. Solve for the water surface from the continuity equation in a fully implicit fashion.

    b. Using the most recent values of the water surface elevations, solve for the u and v velocity components from the x and y momentum equations in an explicit fashion.

    c. Solve for the salinity from the salt transport equation in an explicit fashion.

    d. Compute the density from the equation of state, using the most recently computed salinity field.

    e. Step forward in time and repeat the sequence.

Such a scheme as outlined above will have the stability criterion associated with the speed of a free surface gravity wave removed; although, diffusive criteria as well as the Torrence condition associated with the speed of a water particle remain. However, these criteria are not normally overly restrictive.

Computational Grid

42. The grid upon which Equations 34-38 are solved is rectangular with a grid spacing of $\Delta\xi = \Delta\eta = 1$. The u and v velocity components are computed at the corners of each cell with the water surface

elevation, salinity, and density computed at the center of a cell. Such a grid is illustrated below.
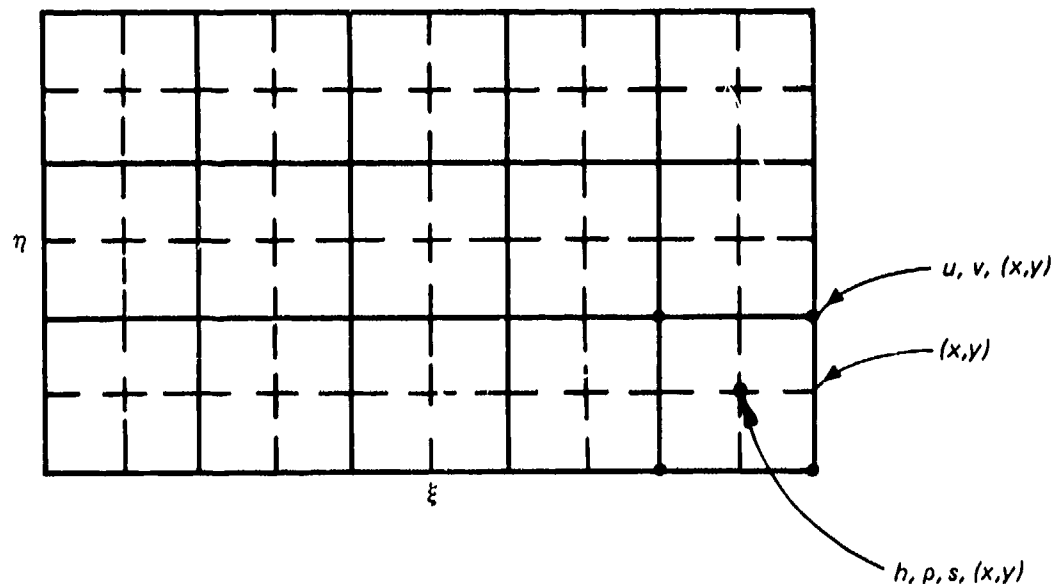
The (x,y) coordinates are specified at the corners, the center, and also at the midpoint of each side of a cell.

43. One might think of the above grid as a global grid. A local grid consisting of 25 points surrounding the (ξ,η) point at which computations are being made is utilized in writing the difference form of the governing equations. This grid is as shown below when velocity computations are being made.
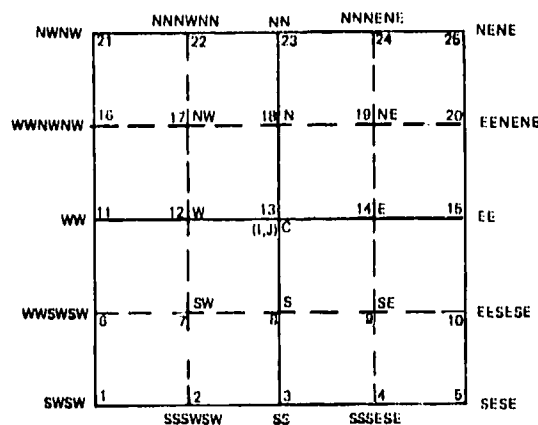
With the above grid, when u and v are being computed at the point labeled c , velocities are defined at points NWNW, NN, WW, NENE, EE, SESE, SS, and SWSW, whereas the water surface and salinity are defined at NW, NE, SE, and SW. When a value of one of the dependent variables is needed at some point where the variable is not defined, an averaging is performed, e.g., $u(W) = \left[u(c) + u(WW)\right]\big/2$.

44. Points in the local grid are assigned to their location in the global grid through functions of the form

$$IFCOR(L) = I + INFCOR(L)$$

$$JFCOR(L) = J + JNFCOR(L)$$

where the 25 values of INFCOR(L) are

$$
\begin{array}{rrrrr}
-1 & 0 & 0 & 0 & 1 \\
0 & -1 & 0 & 0 & 0 \\
-1 & 0 & 0 & 0 & 1 \\
0 & -1 & 0 & 0 & 0 \\
-1 & 0 & 0 & 0 & 1
\end{array}
$$

and the values of JNFCOR(L) are

$$
\begin{array}{rrrrr}
-1 & 0 & -1 & 0 & -1 \\
0 & -1 & 0 & -1 & 0 \\
0 & 0 & 0 & 0 & 0 \\
0 & 0 & 0 & 0 & 0 \\
+1 & 0 & +1 & 0 & +1
\end{array}
$$

Thus, as an example, if one considers the computation for u at (5,5) then the value of u(WW) in the local grid should correspond to the value at (4,5) in the global grid. Using the expressions above, with WW = 11 from the local grid, one obtains

$$u(WW) = u\left(IFCOR(WW) \ , \ JFCOR(WW)\right)$$

$$u(WW) = u\left(IFCOR(11) \ , \ JFCOR(11)\right)$$

where

$$IFCOR(11) = 5 + INFCOR(11) = 5 - 1 = 4$$

$$JFCOR(11) = 5 + JNFCOR(11) = 5 + 0 = 5$$

therefore

$$u(WW) = u(4,5)$$

Similar functions relate the (x,y) coordinates, salinity, and water surface elevations in the local grid to their proper values in the global grid. It should be noted that the grid system described above was suggested by Thompson.[12]

Difference Equations

45. The basic difference equations are developed using forward differences for all time derivatives. Centered differences are used in all spatial derivatives except in the convective terms where one has the option in VAHM of requesting the use of either centered or a form of Roache's second upwind differencing. Examples are presented below.

Forward:
$$\left(\frac{\partial \phi}{\partial t}\right)_c \approx \frac{\phi_c^{n+1} - \phi_c^{n}}{\Delta t}$$

$$\left(\frac{\partial \phi}{\partial \xi}\right)_c^{n} \approx \frac{\phi_E^{n} - \phi_W^{n}}{\Delta \xi} = \phi_E^{n} - \phi_W^{n}$$

Centered:

$$\left(\frac{\partial \phi}{\partial \eta}\right)_c^{n} \approx \frac{\phi_N^{n} - \phi_S^{n}}{\Delta \eta} = \phi_N^{n} - \phi_S^{n}$$

$$\left(\frac{\partial uu}{\partial \xi}\right)_c^n \simeq \frac{u_E - |u_E|}{2} u_E - \frac{u_W + |u_W|}{2} u_W + \frac{u_E + |u_E|}{2} u_c - \frac{u_W - |u_W|}{2} u_c$$

Upwind:

$$\left(\frac{\partial vv}{\partial \eta}\right)_c^n \simeq \frac{v_N - |v_N|}{2} v_N - \frac{v_S + |v_S|}{2} v_S + \frac{v_N + |v_N|}{2} v_c - \frac{v_S - |v_S|}{2} v_c$$

46. As previously noted, the water surface elevations are to be computed using an implicit scheme. Thus, in writing the difference form of the continuity equation all spatial derivatives are taken at the new time level $(n+1)$. Equation 34 becomes

$$\frac{\phi_c^{n+1} - \phi_c^n}{\Delta t} + \frac{1}{J_c} \left[\left(uhy_\eta\right)_E^{n+1} - \left(uhy_\eta\right)_W^{n+1} - \left(vhx_\eta\right)_W^{n+1} + \left(vhx_\eta\right)_E^{n+1} \right.$$
$$\left. + \left(vhx_\xi\right)_N^{n+1} - \left(vhx_\xi\right)_S^{n+1} - \left(uhy_\xi\right)_N^{n+1} + \left(uhy_\xi\right)_S^{n+1} \right] = 0 \qquad (39)$$

47. In the x and y momentum equations, all terms are taken at the old time step except the water surface slope term which is computed at the new time step. Therefore, the difference form of the x and y momentum equations becomes

$$\frac{(hu)_c^{n+1} - (hu)_c^n}{\Delta t} = -\left(\frac{hg\rho}{J\rho_o}\right)_c^n \left[\left(\phi y_\eta\right)_E^{n+1} - \left(\phi y_\eta\right)_W^{n+1} - \left(\phi y_\xi\right)_N^{n+1} + \left(\phi y_\xi\right)_S^{n+1}\right]$$
$$+ F_c^n \qquad (40)$$

$$\frac{(hv)_c^{n+1} - (hv)_c^n}{\Delta t} = -\left(\frac{hg\rho}{J\rho_o}\right)_c^n \left[-\left(\phi x_\eta\right)_E^{n+1} + \left(\phi x_\eta\right)_W^{n+1} + \left(\phi x_\xi\right)_N^{n+1} - \left(\phi x_\xi\right)_S^{n+1}\right]$$
$$+ G_c^n \qquad (41)$$

34

where F and G contain all other terms in Equations 35 and 36, respectively. The difference forms of F and G are

$$
F_c = -\frac{1}{J_c}\left[\left(hu^2y_\eta - huvx_\eta\right)_E - \left(hu^2y_\eta - huvx_\eta\right)_W + \left(huvx_\xi - hu^2y_\xi\right)_N\right.
$$

$$
\left. - \left(huvx_\xi - hu^2y_\xi\right)_S\right] - \left(\frac{h}{J\rho_o}\right)_c\left[\left(P_ay_\eta\right)_E - \left(P_ay_\eta\right)_W - \left(P_ay_\xi\right)_N\right.
$$

$$
\left. + \left(P_ay_\xi\right)_S\right] - \left(\frac{h^2g}{2J\rho_o}\right)_c\left[\left(\rho y_\eta\right)_E - \left(\rho y_\eta\right)_W - \left(\rho y_\xi\right)_N + \left(\rho y_\xi\right)_S\right]
$$

$$
+ \frac{1}{J_c}\left\{\left(\frac{D_{xx}hy_\eta}{J}\right)_E\left[\left(uy_\eta\right)_{EE} - \left(uy_\eta\right)_c - \left(uy_\xi\right)_{NE} + \left(uy_\xi\right)_{SE}\right]\right.
$$

$$
- \left(\frac{D_{xx}hy_\eta}{J}\right)_W\left[\left(uy_\eta\right)_c - \left(uy_\eta\right)_{WW} - \left(uy_\xi\right)_{NW} + \left(uy_\xi\right)_{SW}\right]
$$

$$
- \left(\frac{D_{xx}hy_\xi}{J}\right)_N\left[\left(uy_\eta\right)_{NE} - \left(uy_\eta\right)_{NW} - \left(uy_\xi\right)_{NN} + \left(uy_\xi\right)_c\right]
$$

$$
\left. + \left(\frac{D_{xx}hy_\xi}{J}\right)_S\left[\left(uy_\eta\right)_{SE} - \left(uy_\eta\right)_{SW} - \left(uy_\xi\right)_c + \left(uy_\xi\right)_{SS}\right]\right\} + \frac{1}{J_c}
$$

$$
\left\{-\left(\frac{hD_{xy}x_\eta}{J}\right)_E\left[-\left(ux_\eta\right)_{EE} + \left(ux_\eta\right)_c + \left(ux_\xi\right)_{NE} - \left(ux_\xi\right)_{SE}\right] + \left(\frac{hD_{xy}x_\eta}{J}\right)_W\right.
$$

$$
\left[-\left(ux_\eta\right)_c + \left(ux_\eta\right)_{WW} + \left(ux_\xi\right)_{NW} - \left(ux_\xi\right)_{SW}\right] + \left(\frac{hD_{xy}x_\xi}{J}\right)_N\left[-\left(ux_\eta\right)_{NE}\right.
$$

$$
\left. + \left(ux_\eta\right)_{NW} + \left(ux_\xi\right)_{NN} - \left(ux_\xi\right)_c\right] - \left(\frac{hD_{xy}x_\xi}{J}\right)_S\left[-\left(ux_\eta\right)_{SE} + \left(ux_\eta\right)_{SW}\right.
$$

$$
\left.\left. + \left(ux_\xi\right)_c - \left(ux_\xi\right)_{SS}\right]\right\} + \left[\frac{w_c}{\rho_o}\rho_a v_w^2\cos\alpha\right.
$$

$$
\left. - gu\sqrt{u^2+v^2}\bigg/C^2 + fhv\right]_c \quad (42)
$$

and

$$G_c = -\frac{1}{J_c}\left[\left(hv^2x_\xi - huvy_\xi\right)_N - \left(hv^2x_\xi - huvy_\xi\right)_S + \left(huvy_\eta - hv^2x_\eta\right)_E\right.$$

$$\left. - \left(huvy_\eta - hv^2x_\eta\right)_W\right] - \left(\frac{h}{J\rho_o}\right)_c\left[\left(P_ax_\xi\right)_N - \left(P_ax_\xi\right)_S - \left(P_ax_\eta\right)_E\right.$$

$$\left. + \left(P_ax_\eta\right)_W\right] - \left(\frac{h^2g}{2J\rho_o}\right)_c\left[-\left(\rho x_\eta\right)_E + \left(\rho x_\eta\right)_W + \left(\rho x_\xi\right)_N - \left(\rho x_\xi\right)_S\right]$$

$$+ \frac{1}{J_c}\left\{\left(\frac{D_{yx}hy_\eta}{J}\right)_E\left[\left(vy_\eta\right)_{EE} - \left(vy_\eta\right)_c - \left(vy_\xi\right)_{NE} + \left(vy_\xi\right)_{SE}\right]\right.$$

$$- \left(\frac{D_{yx}hy_\eta}{J}\right)_W\left[\left(vy_\eta\right)_c - \left(vy_\eta\right)_{WW} - \left(vy_\xi\right)_{NW} + \left(vy_\xi\right)_{SW}\right]$$

$$- \left(\frac{D_{yx}hy_\xi}{J}\right)_N\left[\left(vy_\eta\right)_{NE} - \left(vy_\eta\right)_{NW} - \left(vy_\xi\right)_{NN} + \left(vy_\xi\right)_c\right]$$

$$\left. + \left(\frac{D_{yx}hy_\xi}{J}\right)_S\left[\left(vy_\eta\right)_{SE} - \left(vy_\eta\right)_{SW} - \left(vy_\xi\right)_c + \left(vy_\xi\right)_{SS}\right]\right\} + \frac{1}{J_c}$$

$$\left\{- \left(\frac{D_{yy}hx_\eta}{J}\right)_E\left[-\left(vx_\eta\right)_{EE} + \left(vx_\eta\right)_c + \left(vx_\xi\right)_{NE} - \left(vx_\xi\right)_{SE}\right]\right.$$

$$+ \left(\frac{D_{yy}hx_\eta}{J}\right)_W\left[-\left(vx_\eta\right)_c + \left(vx_\eta\right)_{WW} + \left(vx_\xi\right)_{NW} - \left(vx_\xi\right)_{SW}\right] + \left(\frac{D_{yy}hx_\xi}{J}\right)_N$$

$$\left[-\left(vx_\eta\right)_{NE} + \left(vx_\eta\right)_{NW} + \left(vx_\xi\right)_{NN} - \left(vx_\xi\right)_c\right] - \left(\frac{D_{yy}hx_\xi}{J}\right)_S\left[-\left(vx_\eta\right)_{SE}\right.$$

$$\left. + \left(vx_\eta\right)_{SW} + \left(vx_\xi\right)_c - \left(vx_\xi\right)_{SS}\right\} + \left[\frac{W_c}{\rho_o}\rho_a v_w^2 \sin\alpha\right.$$

$$\left. - gv\sqrt{u^2 + v^2}\Big/ C^2 - fhu\right]_c \quad (43)$$

48. Consider the cell below
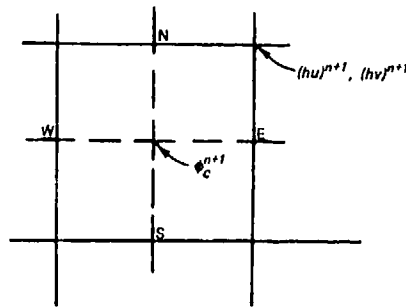
From an inspection of Equation 39, it can be seen that one needs (uh)
and (vh) on the cell faces at time level (n+1) in order to solve for
the water surface elevation at the center of the cell. From Equations 40
and 41, one can determine $(hu)^{n+1}$ and $(hv)^{n+1}$ at the cell corners.
From these values one can determine values on the faces by averaging,
e.g.,

$$(hu)_E^{n+1} = \left[(hu)_{NE}^{n+1} + (hu)_{SE}^{n+1} \right] \Big/ 2$$

Now if one substitues into Equation 39 for the values of $(uh)^{n+1}$ and
$(vh)^{n+1}$ on the faces (from Equations 40 and 41 with appropriate averag-
ing) an equation containing only ϕ at the (n+1) time level results.
This equation is then solved for ϕ_c by using the Accelerated Gauss-
Seidel solution technique.

49. After the water surface elevation at the center of each cell
is determined at the (n+1) time level, values of u^{n+1} and v^{n+1} at
the cell corners are explicitly determined from Equations 40 and 41
using the new ϕ's at the (n+1) time level. It might be noted that
the expressions for F and G in Equations 42 and 43 are only computed
once during each time step. These values are then used in first the
iteration on the water surface and then in the velocity computations.

50. In the computation of ϕ , u , and v , the density is
taken at the old time level. Its value at the new time level is computed
from the equation of state relating the density to the salinity at the
new time level. New salinities are computed from an explicit representa-
tion of the salt transport Equation 37. The difference form becomes

37

$$\frac{(hs)_c^{n+1} - (hs)_c^n}{\Delta t} = -\frac{1}{J_c}\left[\left(husy_\eta - hvsx_\eta\right)_E - \left(husy_\eta - hvsx_\eta\right)_W + \left(hvsx_\xi\right.\right.$$

$$\left.\left. - husy_\xi\right)_N - \left(hvsx_\xi - husy_\xi\right)_S\right] + \frac{1}{J_c}\left\{\left(\frac{hE_x y_\eta}{J}\right)_E\left[\left(sy_\eta\right)_{EE} - \left(sy_\eta\right)_c\right.\right.$$

$$\left. - \left(sy_\xi\right)_{NE} + \left(sy_\xi\right)_{NW}\right] - \left(\frac{hE_x y_\eta}{J}\right)_W\left[\left(sy_\eta\right)_c - \left(sy_\eta\right)_{WW} - \left(sy_\xi\right)_{NW}\right.$$

$$\left. + \left(sy_\xi\right)_{SW}\right] - \left(\frac{hE_x y_\xi}{J}\right)_N\left[\left(sy_\eta\right)_{NE} - \left(sy_\eta\right)_{NW} - \left(sy_\xi\right)_N + \left(sy_\xi\right)_S\right]$$

$$\left. + \left(\frac{hE_x y_\xi}{J}\right)_S\left[\left(sy_\eta\right)_{SE} - \left(sy_\eta\right)_{SW} - \left(sy_\xi\right)_c + \left(sy_\xi\right)_{SS}\right]\right\} + \frac{1}{J_c}$$

$$\left\{-\left(\frac{hE_y x_\eta}{J}\right)_E\left[-\left(sx_\eta\right)_{EE} + \left(sx_\eta\right)_c + \left(sx_\xi\right)_{NE} - \left(sx_\xi\right)_{NW}\right] + \left(\frac{hE_y x_\eta}{J}\right)_W\right.$$

$$\left[-\left(sx_\eta\right)_c + \left(sx_\eta\right)_{WW} + \left(sx_\xi\right)_{NW} - \left(sx_\xi\right)_{SW}\right] + \left(\frac{hE_y x_\xi}{J}\right)_N$$

$$\left[-\left(sx_\eta\right)_{NE} + \left(sx_\eta\right)_{NW} + \left(sx_\xi\right)_{NN} - \left(sx_\xi\right)_c\right] - \left(\frac{hE_y x_\xi}{J}\right)_S\left[-\left(sx_\eta\right)_{SE}\right.$$

$$\left.\left. + \left(sx_\eta\right)_{SW} + \left(sx_\xi\right)_c - \left(sx_\xi\right)_{SS}\right]\right\} \quad (44)$$

51. In summary, the computation cycle is as outlined below.

Step 1: Compute the terms labeled F and G in the x and y momentum equations at the cell corners from Equations 42 and 43.

Step 2: Using the Accelerated Gauss-Seidel solution technique, implicitly solve for the water surface elevation at the center of each cell.

Step 3: Using the new water surface elevations and values of F and G from Step 1, explicitly solve for the velocity components, u and v, from Equations 40 and 41.

Step 4: Explicitly compute the salinity field from Equation 44.

Step 5: Using the new salinities from Step 4, compute the water density from the equation of state.

Step 6: Update all arrays, increment the time, and return to Step 1.

52. This solution scheme removes the gravity wave stability criterion from consideration, although it should be noted that other stability criteria still control the size of the computational time step allowed. These criteria have not been derived for the transformed equations; however, for the cartesian form of the equations they are

$$\Delta t \leq \min\left(\frac{\Delta x}{u}, \frac{\Delta y}{v}\right)$$

$$\Delta t \leq \min\left(\frac{\Delta x^2}{2D_{xx}}, \frac{\Delta y^2}{2D_{yy}}\right) \tag{45}$$

In other words, the time step must be small enough so that a fluid particle does not move more than one grid spacing during the time step. This basic criterion is not nearly as severe as the gravity wave criterion

$$\Delta t \leq \min\left(\frac{\Delta x}{\sqrt{gh}}, \frac{\Delta y}{\sqrt{gh}}\right) \tag{46}$$

for most practical problems.

Boundary Conditions

53. Three types of boundaries are allowed in VAHM; walls, oceans, and rivers. Wall boundaries are characterized by the specification of a no-slip condition, i.e., the velocity components u and v are set to

be zero at walls. Although, physically, the flow must be zero at a
solid boundary, slip conditions on the velocity at a wall often give
more realistic results if the grid spacing is too large near the wall.
Slip conditons would be implemented by setting the normal component of
the velocity equal to zero with the tangential component computed from
the expression for zero vorticity. At the present time, only the no-
slip condition is allowed in VAHM.

54. Ocean boundaries are characterized by the specification of a
time varying water suface elevation at the boundary. Velocities on the
ocean boundary are then computed from a simplified form of the momentum
equation where the diffusive terms have been neglected. One-sided
differences are used to replace derivatives that need points outside the
field. As an example, consider the computation for v on an ocean
boundary that lies on the bottom of the transformed plan.

$\phi(t)$ PRESCRIBED

VELOCITIES COMPUTED HERE
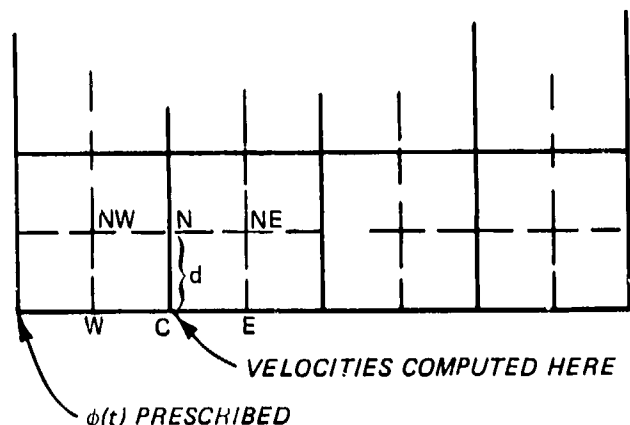
$$v_c^{n+1} = \frac{1}{h_c^{n+1}} \left\{ h_c^n v_c^n - \left(\frac{hg\rho\Delta t}{J\rho_o} \right)_c \left[- \left(\phi x_\eta\right)_E^{n+1} + \left(\phi x_\eta\right)_W^{n+1} + 2\left(\phi x_\xi\right)_N^{n+1} \right. \right.$$

$$\left. - 2\left(\phi x_\xi\right)_c^{n+1} \right] - \frac{\Delta t}{J_c} \left[\left(hvuy_\eta - hvvx_\eta \right)_E^n - \left(hvuy_\eta - hvvx_\eta \right)_W^n \right.$$

$$\left. \left. + 2\left(hvvx_\xi - huvy_\xi \right)_N^n - 2\left(hvvx_\xi - huvy_\xi \right)_c^n \right] \right\} \quad (47)$$

An inspection of Equation 47 reveals that in order to be able to compute
v_c^{n+1} , values of ϕ^{n+1} at the center of the first cell must be known.
These are determined by setting them equal to the boundary values of ϕ ,

but lagged by the time required for a free surface gravity wave to traverse the distance from the boundary to the interior point, e.g.,

$$\phi_{NE}(t) = \phi_E\left(t - \frac{d}{\sqrt{gh_E}}\right)$$

(48)

55. When the flow is directed into the computational field, the boundary condition on the salinity is prescribed as that of the ocean. However, when the flow is moving out of the computational field, the salinity at an ocean boundary is set to be equal to its value at the next point inside.

56. River boundaries are characterized by the specification of the velocity. The salinity is set to be zero and the water surface elevation at the center of a river boundary cell is computed as in any interior cell.

PART V: MODEL APPLICATIONS

57.   In order to demonstrate the versatility of VAHM in its ability
to model flows in rather general multiply-connected regions containing
both river and ocean boundaries, three applications have been made using
the physical geometry in Figure 3.

Generation of Boundary-Fitted Coordinates

58.   The first step in the application of VAHM is the generation
of the boundary-fitted coordinates. This is accomplished through a
coordinate generation code developed by Thompson. Output from the co-
ordinate code is saved on a file for subsequent use by VAHM. The basic
input to the coordinate code is the specification of the (x,y) co-
ordinates of the boundary points noted on Figure 3. Although various
degrees of coordinate control can be exercised, the boundary-fitted
coordinates shown in Figure 3 were computed using no control. Figure 4
illustrates the actual computational grid network that is used in VAHM,
where velocities are computed at the cell corners and salinities and
water elevations at the cell center. However, it should be remembered
that VAHM requires that the (x,y) coordinates be specified at not only
the corners and center of a computational cell but also on the cell
faces. The reason for this is because of the fully geometrically con-
servative transformation of the mass, momentum and salinity equations to
be solved. With such a transformation, one should never use averaged
values of the geometrical derivatives since this can result in the loss
of conservation of the properties being computed. This is the reason
for computing the coordinate system illustrated in Figure 3.

59.   The coordinate system plotted in Figure 3 was the third at-
tempt at generating a useful grid system. Through the movement of bound-
ary points and/or coordinate control one attempts to compute boundary-
fitted coordinates such that the grid spacing does not vary rapidly and
such that (ξ,η) lines never approach being parallel to each other. The
coordinate system in Figure 3 satisfies both of these criteria and thus
is considered to be adequate.

42

Flow Through Problem

60. Before applying the model for the case of time varying boundary conditions, various "debugging" applications were made. Perhaps the most important of these was a "flow through" problem. In a flow through test all velocities are set to be equal, but non zero, (even on the walls), the water surface elevation is constant, but non zero, over the field, and the salinity is set to be a non zero constant over the field. If the coding is correct and all external forces have been set to zero, the initial state should never change. Such tests have helped to correct many errors that might otherwise have gone undetected.

Case 1 - Sloping River

61. The first application was one in which a river boundary with a constant velocity of 0.4 m/s was prescribed at the top with the water surface elevation at the bottom being held constant at 1.0 m. The bottom was assumed to have a slope of 0.005 m/grd cell and the initial depth was set to be 11.0 m. The initial velocity field was set to zero as was the salinity concentration. The Chezy coefficient was set to 35 $m^{1/2}$/s and a time step of 600 sec was prescribed. These plus other input data are presented in Table 1.

62. Three separate runs were made in which the influence of using a form of Roache's second upwind differencing for the convective terms in the momentum equations (CONVEC = UPWIND) as opposed to centered differencing (CONVEC = CENTER) and the influence of increasing the diagonal components of the eddy viscosity from 0.01 m^2/s to 10 m^2s were investigated.

63. Figures 5-8 illustrate the type of phenomena that can occur when using centered differences to represent the convective terms. After 12 hours, a "zig zag" pattern has become well defined. Figures 9-12 demonstrate the effect of using a form of Roache's second upwind differencing. Although a slight pattern can be seen after 12 hours, it isn't nearly as pronounced as when using centered differences. Figures 13-16

Table 1 - Input Data to VAHM

Variable	Case 1	Case 2	Case 3
Δt (sec)	600	600	600
D_{xx} (m^2/s)	0.01 10	10	10
D_{yy} (m^2/s)	0.01 10	10	10
D_{xy} (m^2/s)	0.0	0.0	0.0
D_{yx} (m^2/s)	0.0	0.0	0.0
E_x (m^2/s)	0.01	0.01	0.01
E_y (m^2/s)	0.01	0.01	0.01
C ($m^{1/2}/s$)	35	35	35
Initial depth, m	11.0	11.0	11.0
Bottom slope/cell	0.005	0.0	0.0
CONVEC	CENTER UPWIND	UPWIND	UPWIND
Initial Velocity, m/s	0.0	0.0	0.0
Conv Tolerance	0.005	0.005	0.005

show that by increasing the eddy viscosity, along with upwind differenc-
ing, essentially all of the "roughness" in the computed velocity field
has been removed. Figure 17 presents a time history of the water surface
profile along the $\xi = 6$ line.

Case 2: Closed at Top, Ocean on Bottom

64. The second application was for the case of a closed boundary
at the top and an ocean boundary on the bottom. Once again the initial
velocity and salin ty fields were set to zero and the initial depth was
11.0 m. Unlike the previous application, the bottom was assumed flat.

65. The water surface elevation curve, relative to a depth of
10 m, presented in Figure 18 was prescribed at the ocean boundary along
with a salt concentration of 30 ppt. As in the previous application,
CONVEC = UPWIND, $D_{xx} = D_{yy} = 10$ m^2/s , $\Delta t = 600$ sec and the value of
the Chezy coefficient was 35 m$^{1/2}$/s (see Table 1).

66. The vector plots of the flow field presented in Figures 19-30
illustrate quite clearly the effect of the time varying ocean boundary
which first drives water into the field with water flowing out on the ebb
portion of the tidal cycle. The channelizing effect of the island is
also quite clearly shown. Figure 31 presents a time history of the water
surface profile along the $\xi = 6$ line, whereas Figures 32, 33 and 34
are plots of the water surface at particular points.

67. From an inspection of Figures 26-30 it can be seen that an
oscillation in the flow field has developed in the upper portion of the
modeled area when the flow is pushed toward the boundary. This is
probably due to the influence of the upstream boundary, although the
tolerance on the iterated water surface may also be a factor. The con-
vergence tolerance was set to be 0.005 m in all the runs.

68. Figure 35 demonstrates the movement of the salinity field
over a tidal cycle. As the flooding cycle of the tide curve is experi-
enced, saline water at a concentration of 30 ppt moves into the region.
As the flow reverses at the ocean boundary (see Figure 23), the salinity
at the boundary is set to its value immediately inside to reflect an

45

outflow boundary. This is the reason for the decrease in salt concentra-
tion at the boundary after 5 hours. Figure 36 gives a time history of
the salinity at a point about 12 miles from the ocean boundary.

Case 3: River on Top, Ocean on Bottom

69. The third application was identical to the second except that
a river boundary with a constant velocity of 0.4 m/s in the η-component
was assumed at the top as opposed to the closed boundary in Case 2.

70. Figures 37-49 present "snap shots" of the computed flow field
for 16 hours. With the flow field initialized to zero at a constant
depth of 11.0 m, it can be seen that the influence of the incoming tide
and the river meet after about 4 hours. As in the previous application,
an oscillatory pattern occurs in the upper portion between hours 8 and
12. However, as revealed in Figures 48 and 49, this irregularity is re-
moved as the influence of the ebb portion of the tidal cycle is felt in
the upper reach.

71. Figure 50 is a plot of the time history of the water surface
profile along the $\xi = 6$ line and Figures 51-53 give the time history
of elevations at particular points. Figure 54 presents the time history
of the salinity at a point about 12 miles from the ocean boundary. Com-
paring Figure 54 with Figure 36, it can be seen that the salinities are
essentially the same after 16 hours. Therefore, the influence of the
river has not been felt in the lower reach after this length of time.

Computing Costs and Times

72. Previously it was noted that the major advantage of the FEM
over the FDM was its ability to more accurately handle irregular bound-
aries, whereas its major disadvantages were increased complexity in
coding and perhaps increased computational costs. A finite difference
model such as VAHM which makes computations on a boundary-fitted co-
ordinate system removes the boundary representation advantage of the FEM
in many problems. Although no direct comparison can be made between

46

VAHM and the FEM in the areas of complexity of coding and computational costs, some rather general comparisons can be made.

73. Since VAHM's computational scheme retains much of the character of explicit finite difference schemes, it would appear that VAHM's coding should be much less complicated than any finite element model. With simpler coding, future modifications should be much easier to make, e.g. flooding of boundaries, higher order representation of the advective terms, etc.

74. An approximate comparison of computing costs can be made with a vertically averaged finite element model called RMA-2[13]. This is a flow model that does not include the modeling of salinity and its effect upon the flow field. The model was developed by Resource Management Associates and is currently being used by the Estuaries Division of the Hydraulics Laboratory at WES.

75. The time step employed in the previously presented runs of VAHM was 600 sec, which compares with a time step of perhaps 30 sec that could be employed in a fully explicit finite difference model. With a computational grid that contains 363 velocity points (1365 coordinate points) 12 hours of computations required 43 sec of CPU time at a cost of $21 on a CRAY I computer for the first application presented. The second and third applications required approximately twice as much CPU time at about twice the cost. However, later experimentation with VAHM revealed that stable computations could be achieved using a time step of 1500 sec. Therefore, if such a time step had been used in the cases presented the costs would have been reduced by a factor of about 2.5. The increased time of the last two applications was because of the more rapidly varying water surface. Only one or two iterations each time step were required to achieve a convergence tolerance of 0.005 m in the first case, whereas an average of seven or eight iterations were required in the last two applications.

76. As a comparison, RMA-2 applications to grids containing approximately the same number of net points for a 12 hour tidal cycle, using an 1800 sec time step, cost about $40 on the same CRAY I computer.[14] However, it should be remembered that RMA-2 makes computations for only

the flow field, whereas VAHM also computes the salinity field and its
coupling with the flow field through a relationship with the water
density. Based upon these approximate costs, it would appear that the
FEM, as reflected by RMA-2 costs, is about 3 times more expensive than
VAHM for tidal problems and perhaps 6 times more expensive for river
problems. As a final note, it is believed that after VAHM has been
"cleaned up" to better utilize the vector processing features of the
CRAY I its computational costs will decrease significantly.

PART VI: SUMMARY AND RECOMMENDATIONS

77. A numerical model for computing vertically averaged velocities and salinity plus water surface elevations has been developed. By employing the concept of boundary-fitted coordinates, irregular boundaries can be accurately modeled in either simply or multiply-connected regions. Even though the numerical grid is a nonorthogonal curvilinear grid in the physical region being modeled, all numerical computations are carried out in a transformed rectangular grid with square grid spacing.

78. A feature of the model is the particular solution technique employed to numerically solve the governing equations. A combination implicit-explicit finite difference scheme, patterned after work by Edinger and Buchak[11] in their development of a laterally averaged reservoir hydrodynamic model, has been developed to remove the speed of a gravity wave from stability restrictions on the computational time step while still retaining some of the advantages of explicit schemes. With such a scheme, the water surface elevation is computed implicitly using the Accelerated Gauss-Seidel solution technique while the velocities and salinity are computed in an explicit fashion.

79. The model has been developed for general applications. Any number of river and/or ocean boundaries can be arbitrarily located on the transformed rectangular plane, as can the placement of islands in the interior of the computational field. Even though a great deal of generality does exist, there are restrictions. For example, only no-slip boundary conditions are currently treated at solid boundaries and no flooding of those boundaries is allowed.

80. Although VAHM has been developed to the point where results from the test applications presented are encouraging, additional work is needed before VAHM can be considered fully operational. Recommendations for additional development are listed below.

- In order to expand VAHM's capabilities into the water quality area, it is necessary to devise a scheme for solving the transport equation that accurately transports a "spike" concentration distribution. The present scheme employed in VAHM for computing salinity is sufficient when distributions are fairly

49

smooth. However, it will not do a good job on a spike distribution. Therefore, a major task to be accomplished is the modification of VAHM to allow such computations to be accurately made.

- As previously discussed, at the present time only no-slip conditions are allowed at solid boundaries. Unless a small grid spacing is used near the boundaries, slip conditions may be more appropriate. The slip boundary conditions will be determined by requiring the normal component of the velocity and the vorticity to be zero at a wall. Many of the checks in the basic model have been coded to allow for slip conditions; however, the slip subroutine remains to be developed.

- The capability of handling flooding boundaries is needed in VAHM. Some ideas for incorporating such a capability into VAHM have been considered in the basic coding.

- VAHM uses the Accelerated Gauss-Seidel solution technique to implicitly compute the water surface elevation. At the present time, a constant acceleration parameter is employed. The use of variable acceleration parameters for the purpose of speeding up the computations should be investigated.

- At the present time, a 2D vector plotting program developed by S. A. Adamec of the Hydraulics Laboratory at WES has been coupled with the grid generation code and VAHM to provide plots of the velocity field. Additional plotting capability needs to be coupled with VAHM.

- As noted, the basic coding has been written to allow for an extremely general representation of a physical problem, e.g. specification of islands, river inlets, etc. However, many of these options have not been "debugged." In addition, although VAHM is being run on a CRAY-I computer no attempt at "cleaning up" the code to take advantage of the CRAY's vector processing has been made.

50

REFERENCES

1. Thompson, Joe F., et al., "Automatic Numerical Generation of Body-Fitted Curvilinear Coordinate System for Field Containing Any Number of Arbitrary Two-Dimensional Bodies," Journal of Computational Physics, Vol 15, No. 3, July 1974.

2. Thompson, Joe F., et al., "TOMCAT - A Code for Numerical Generation of Boundary-Fitted Curvilinear Systems on Fields Containing Any Number of Arbitrary Two-Dimensional Bodies," Journal of Computational Physics, Vol 24, No. 3, July 1977.

3. Thompson, Joe F., et al., Boundary-Fitted Curvilinear Coordinate Systems for Solution of Partial Differential Equations on Fields Containing Any Number of Arbitrary Two-Dimensional Bodies, NASA CR-2729, National Aeronautics and Space Administration, Washington, D. C., July 1977.

4. Reid, R. O. and Bodine, B. R., "Numerical Model for Storm Surges in Galveston Bay," Journal Waterways of Harbors Division, Proceedings, ASCE, Vol 94, No. WW1, 1968.

5. Leendertse, J. J., "Aspects of a Computational Model for Long-Period Water-Wave Propagation," RM-5294-PR, the Rand Corporation, Santa Monica, Calif., 1967.

6. Masch, F. D., et al., "A Numerical Model for the Simulation of Tidal Hydrodynamics in Shallow Irregular Estuaries," TR-HYD-12-6901, Hydraulic Engineering Laboratory, University of Texas, Austin, Texas, 1969.

7. Norton, W. R., et al., "A Finite Element Model for Lower Granite Reservoir," prepared for Walla Walla District, U. S. Army Corps of Engineers, 1973.

8. Johnson, B. H. and Thompson, J. F., "A Discussion of Boundary-Fitted Coordinate Systems and their Applicability to the Numerical Modeling of Hydraulic Problems," MP H-78-9, U. S. Army Engineer Waterways Experiment Station, Vicksburg, Miss., Sep 1978.

9. Holley, E. R., "Unified View of Diffusion and Dispersion," Journal of the Hydraulics Division, Proceedings, ASCE, Vol 95, No. HY2.

10. Leendertse, J. J. et al. "A Three-Dimensional Model for Estuaries and Coastal Seas: Vol I, Principles of Computation," R-1417-OWRR, Rand Corporation, Santa Monica, Calif., 1973.

11. Edinger, J. K. and Buchak, E. M., "A Hydrodynamic Two-Dimensional Reservoir Model: Development and Test Application to Sutton Reservoir, Elk River, West Virginia," prepared for U. S. Army Engineer Division, Ohio River, 1979.

12. Personal Communication with J. F. Thompson, Professor, Dept of Aerospace and Aerophysics Engineering, Mississippi State University, June 1979.

13. Norton, W. R. and King, I. P., "Operating Instructions for Computer Program RMA-2 - A Two-Dimensional Finite Element Program for Problems in Horizontal Free Surface Hydormechanics," prepared for Association of Bay Area Governments Environmental Management Plan Bay Modeling Project, Resource Management Associates, Lafayette, Calif., Feb 1977.

14. Personal Communication with M. J. Trawle, Research Hydraulic Engineer, U. S. Army Engineer Waterways Experiment Station, Sep 1980.
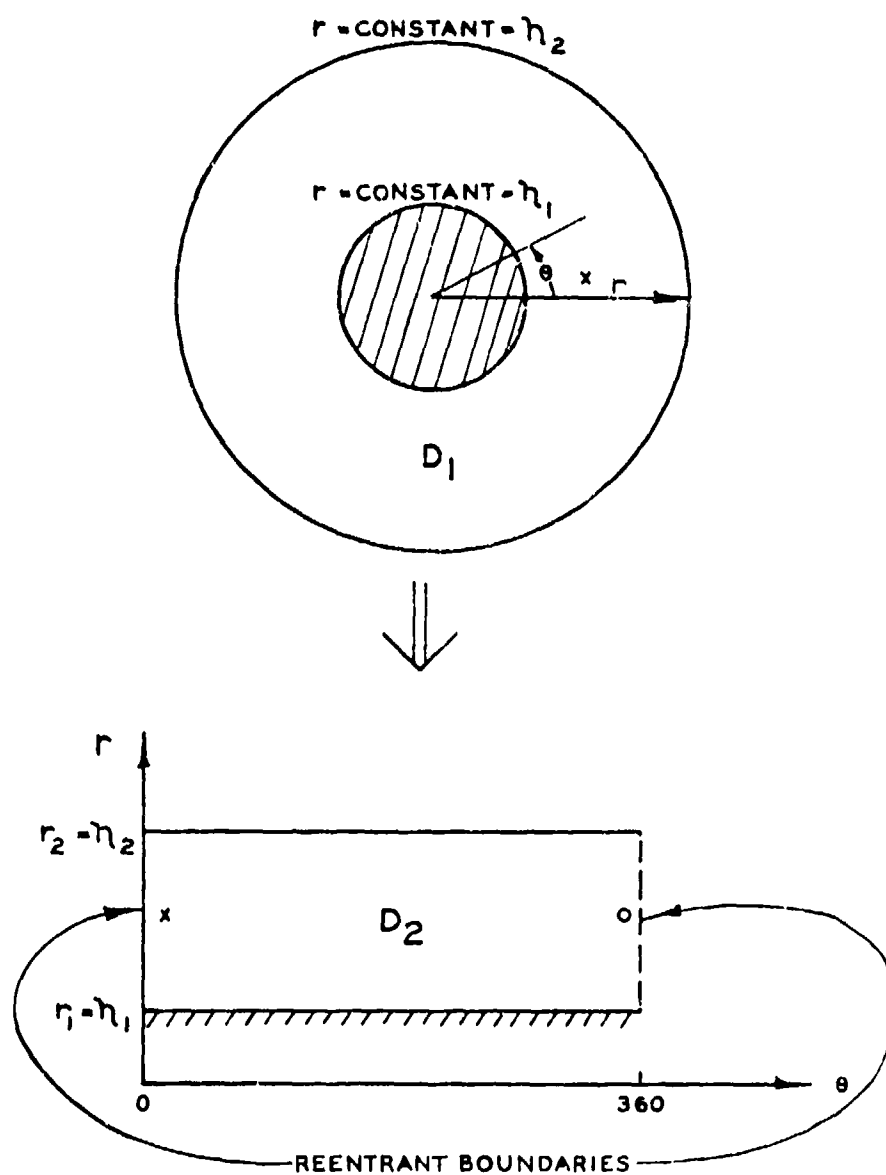
Figure 1. Transformation of domain between concentric cylinders
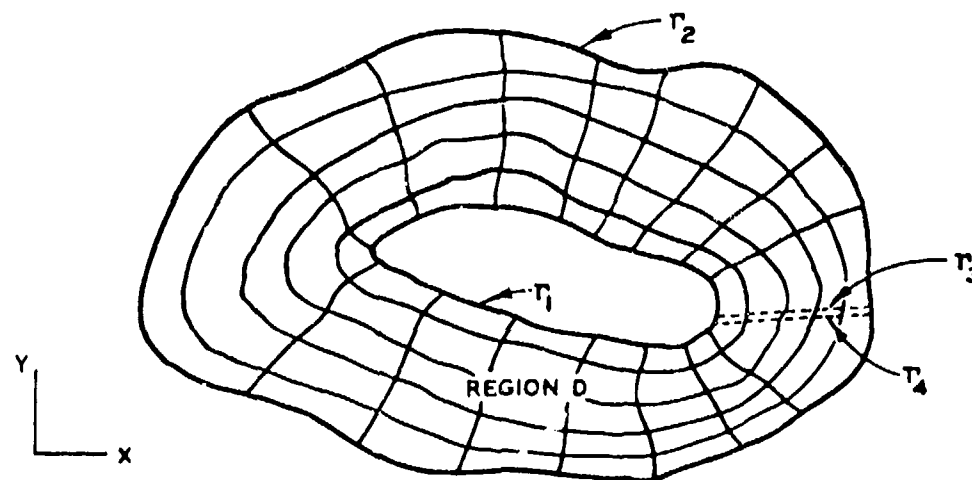
PHYSICAL PLANE
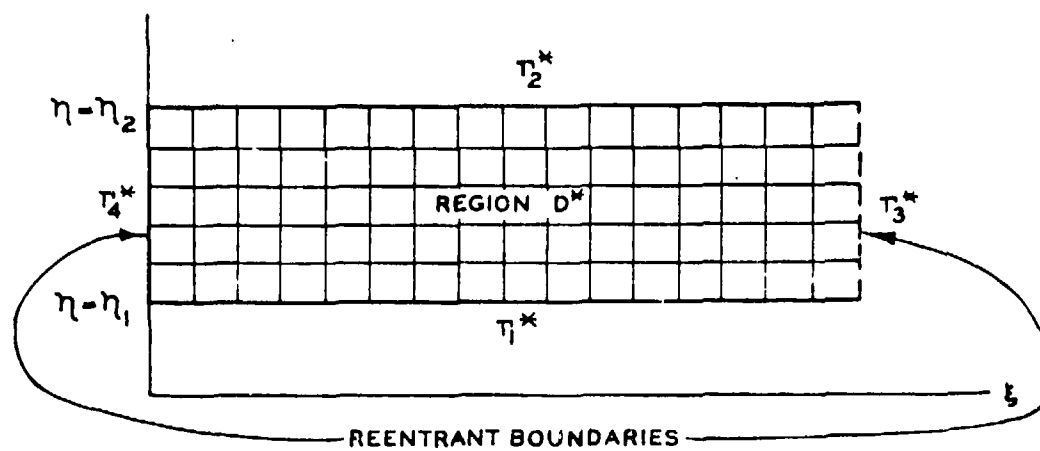
TRANSFORMED PLANE

Figure 2.   Transformation of an irregular domain
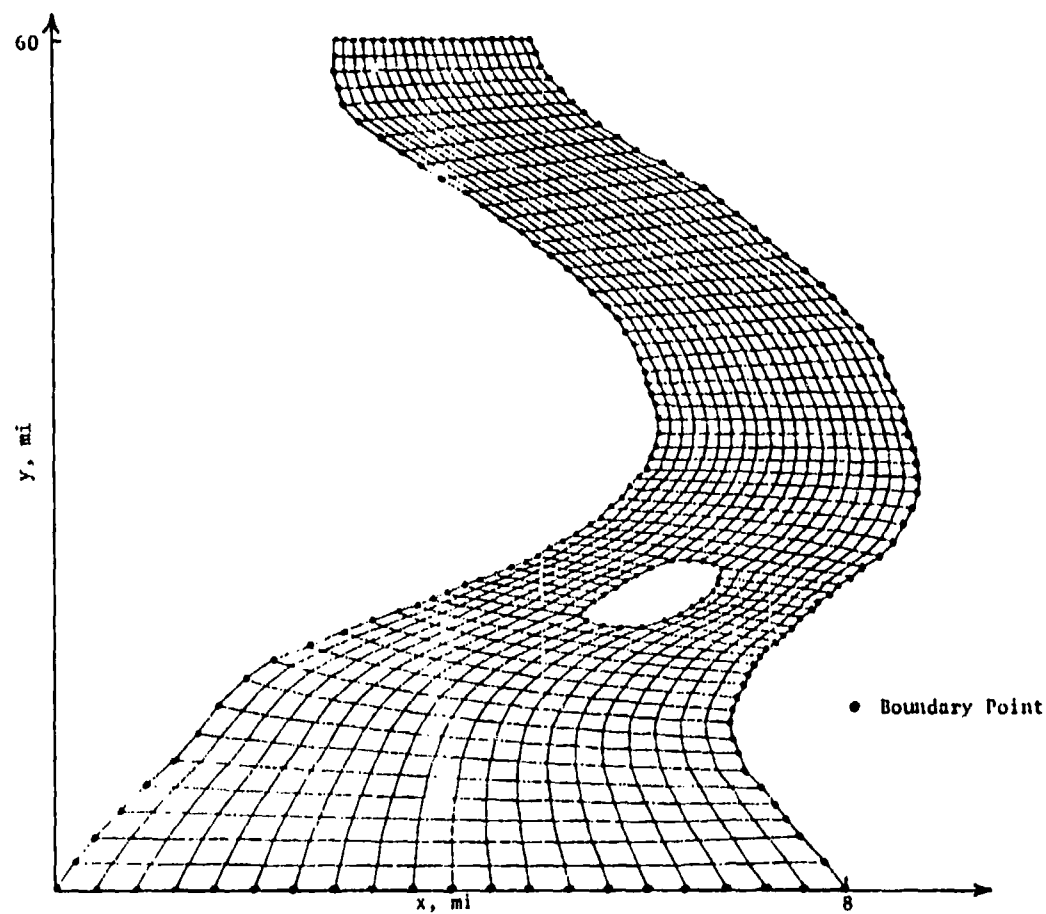
Figure 3. Boundary fitted coordinate system for a multiple connected region
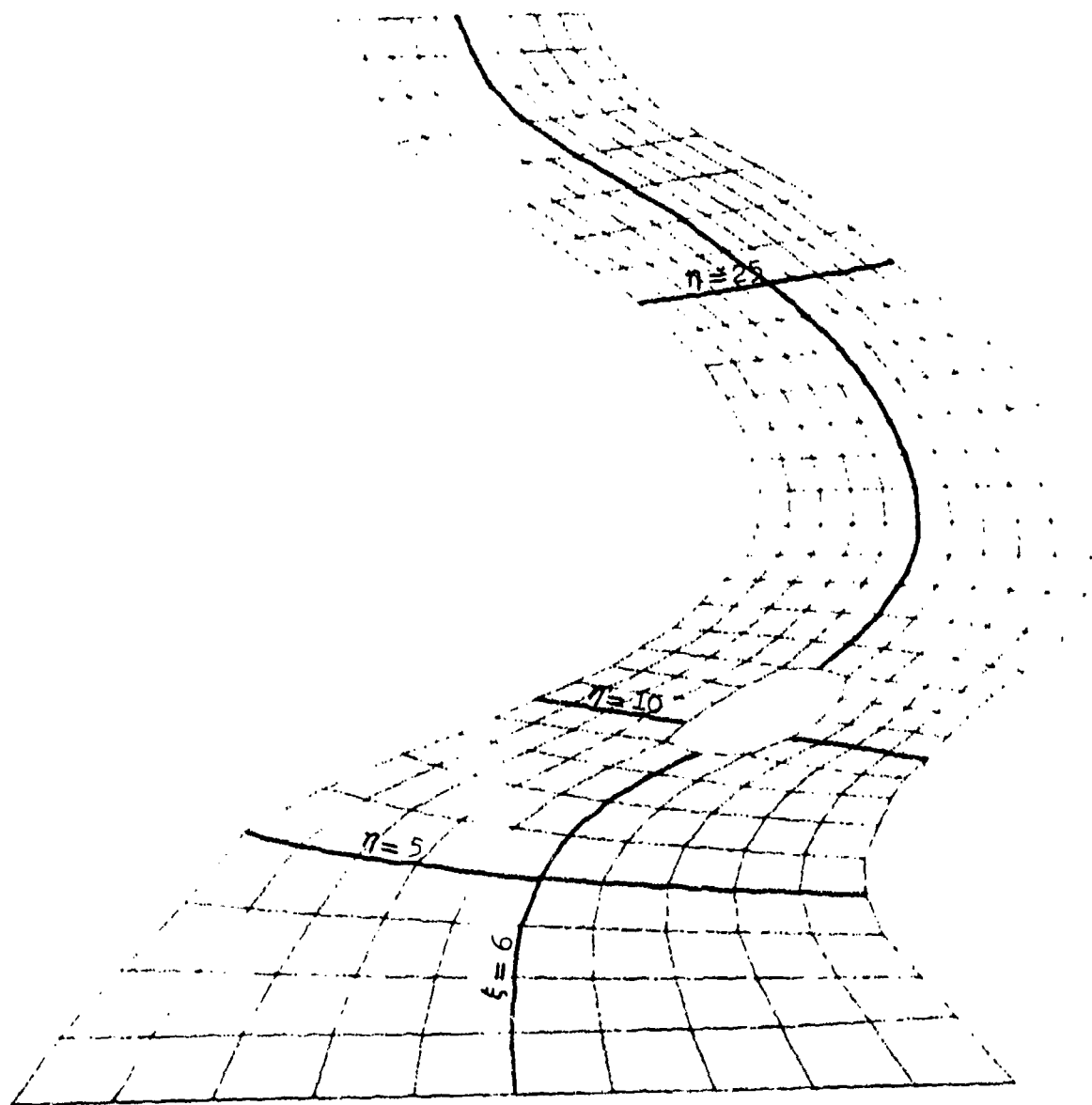
Figure 4.   Computational grid for computing velocities

VELOCITY
VECTOR
SCALE
1.0   (MPS)

1.0

← ———— EXCEEDS PLOT LIMIT

XS =   3.22 KM/IN
YS =   9.66 KM/IN
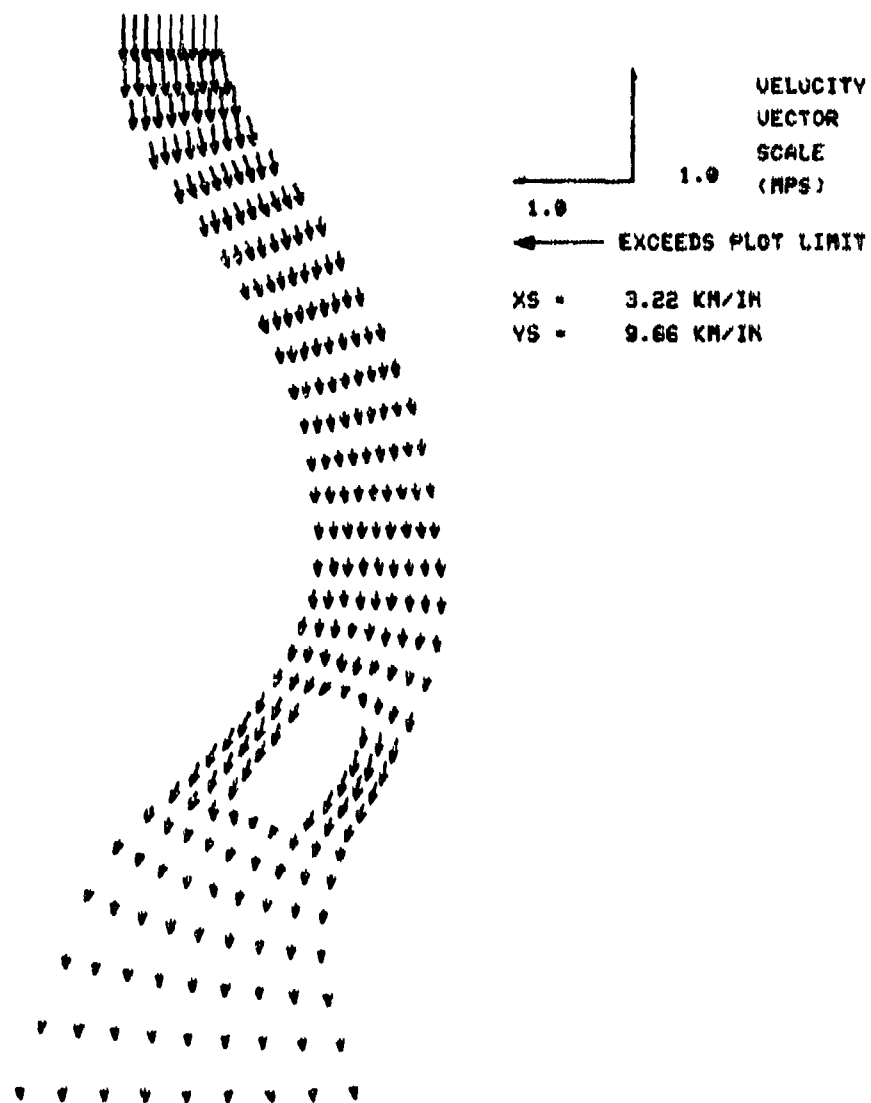
Figure 5. Velocity field after 3 hours, CONVEC = CENTER
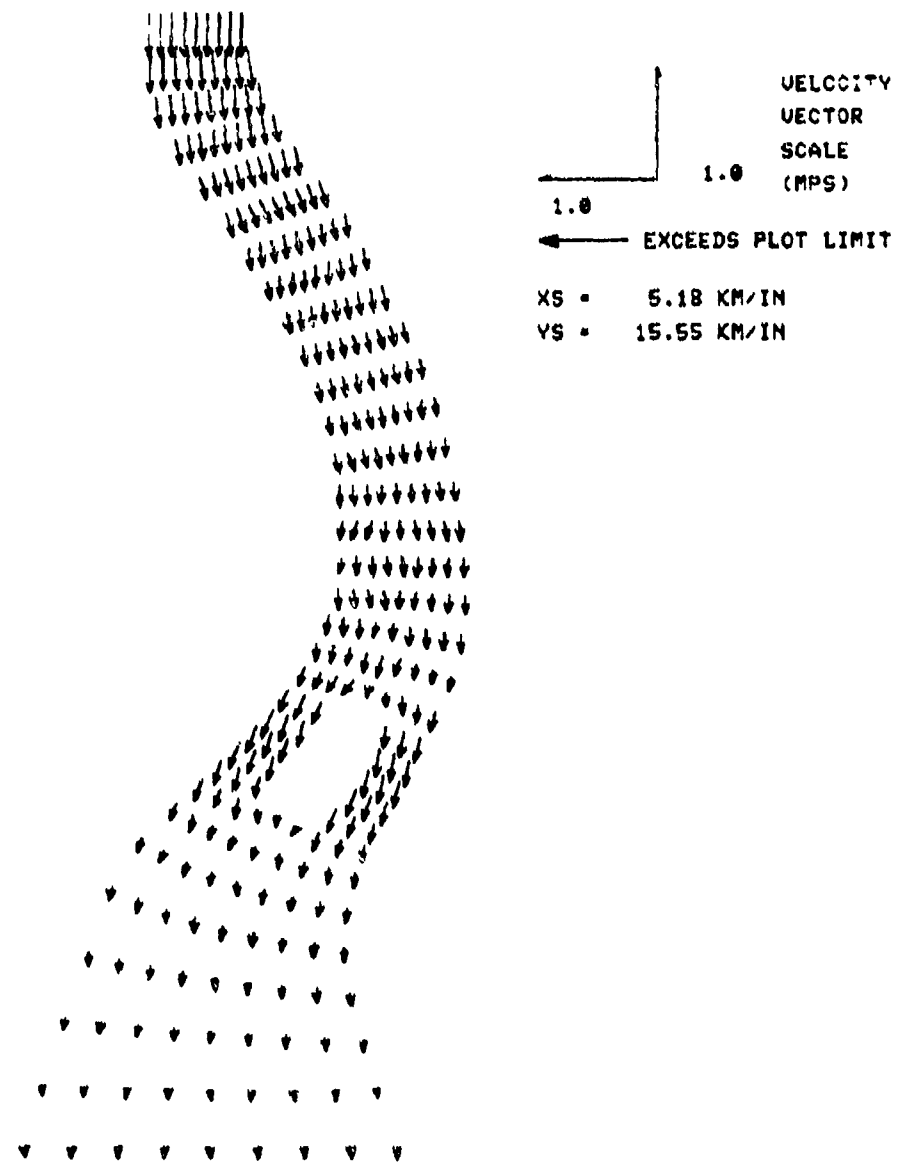
Figure 6. Velocity field after 6 hours, CONVEC = CENTER
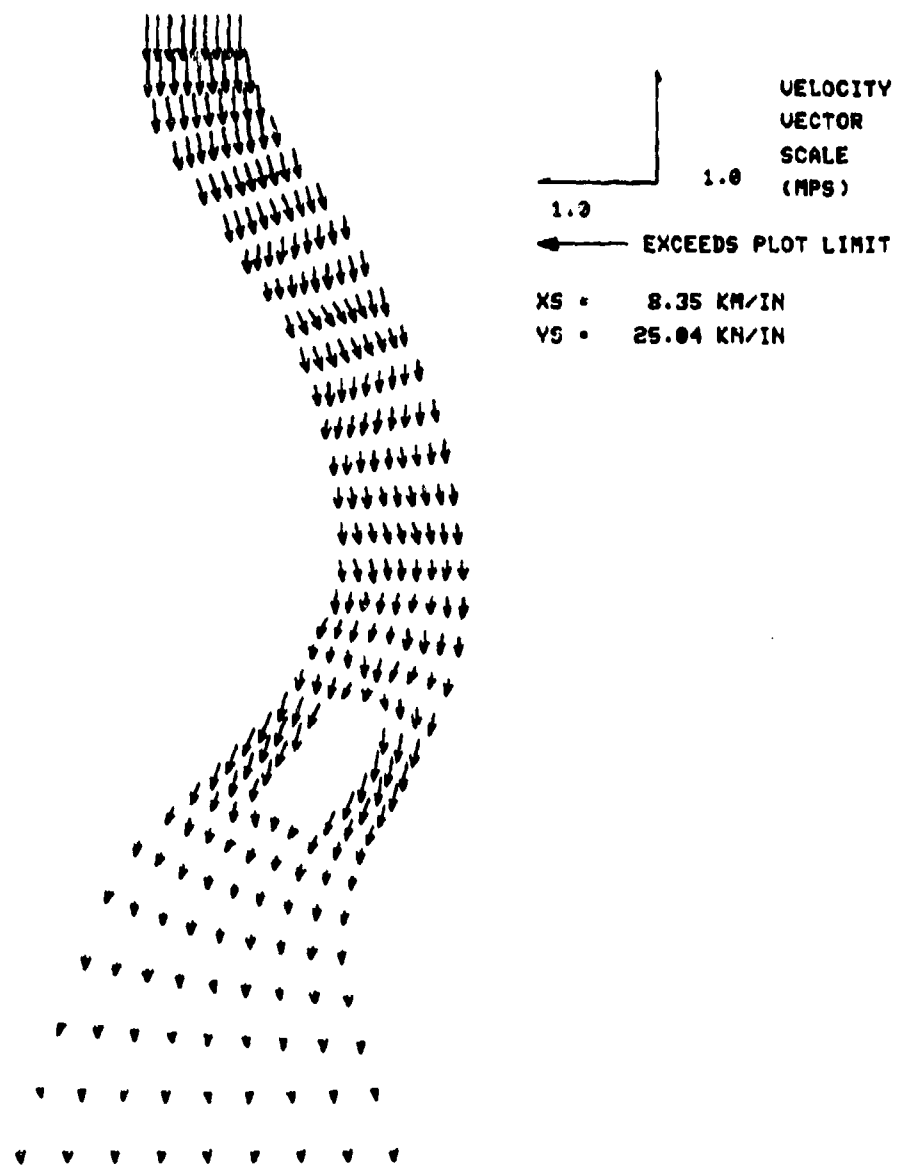
Figure 7. Velocity field after 9 hours, CONVEC = CENTER
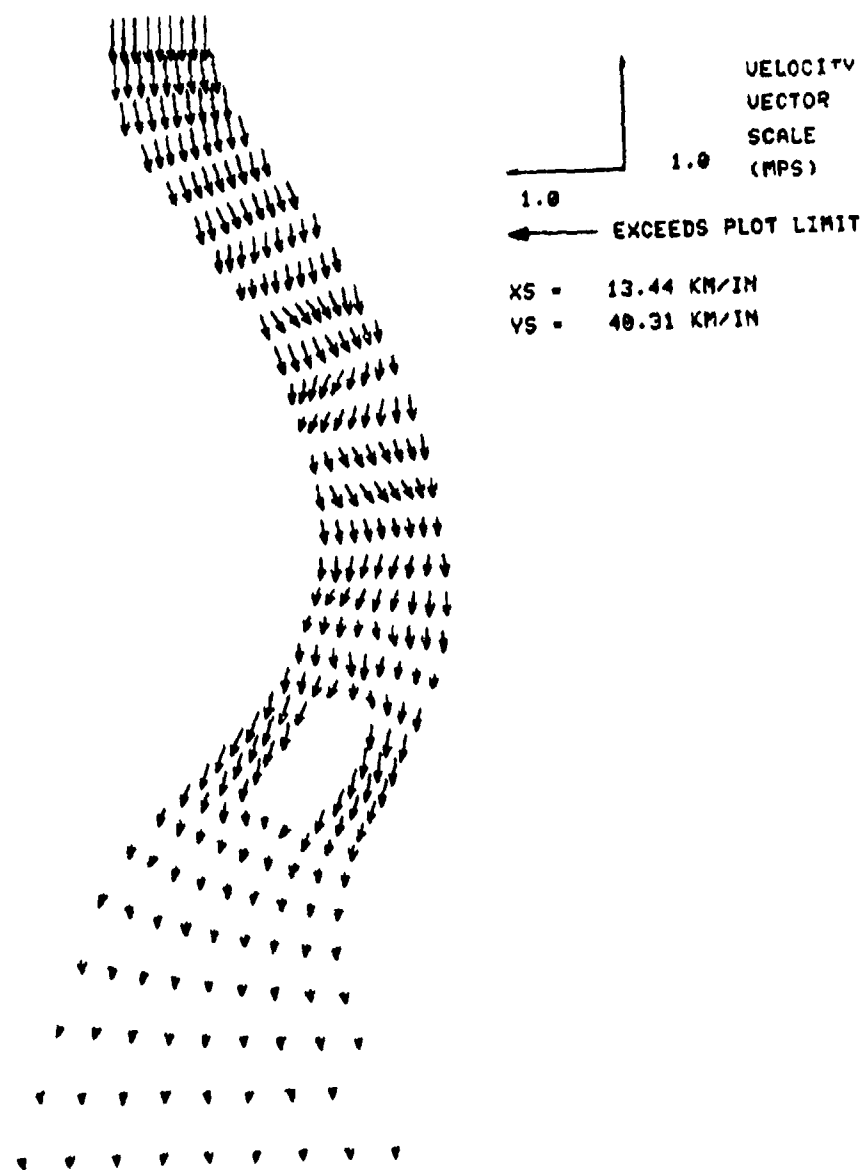
Figure 8. Velocity field after 12 hours, CONVEC = CENTER
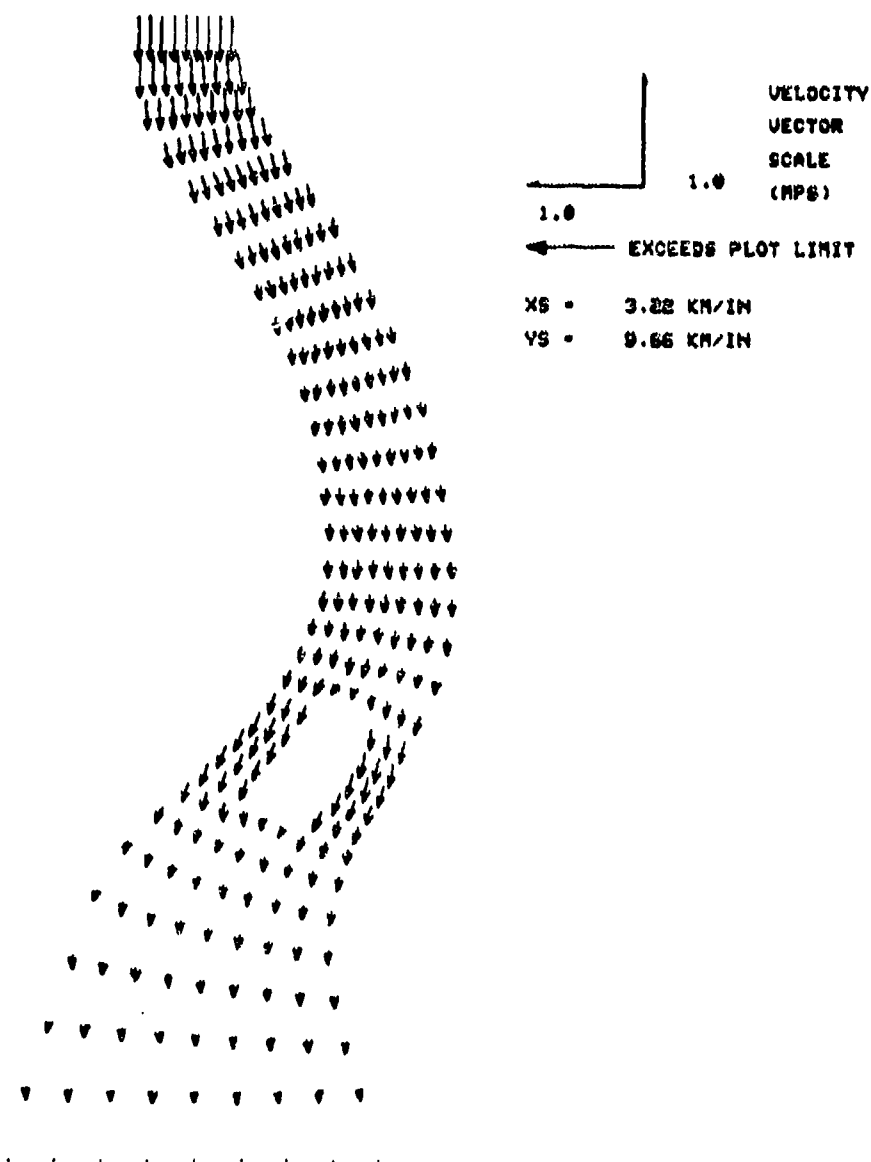
Figure 9.   Velocity field after 3 hours, CONVEC = UPWIND
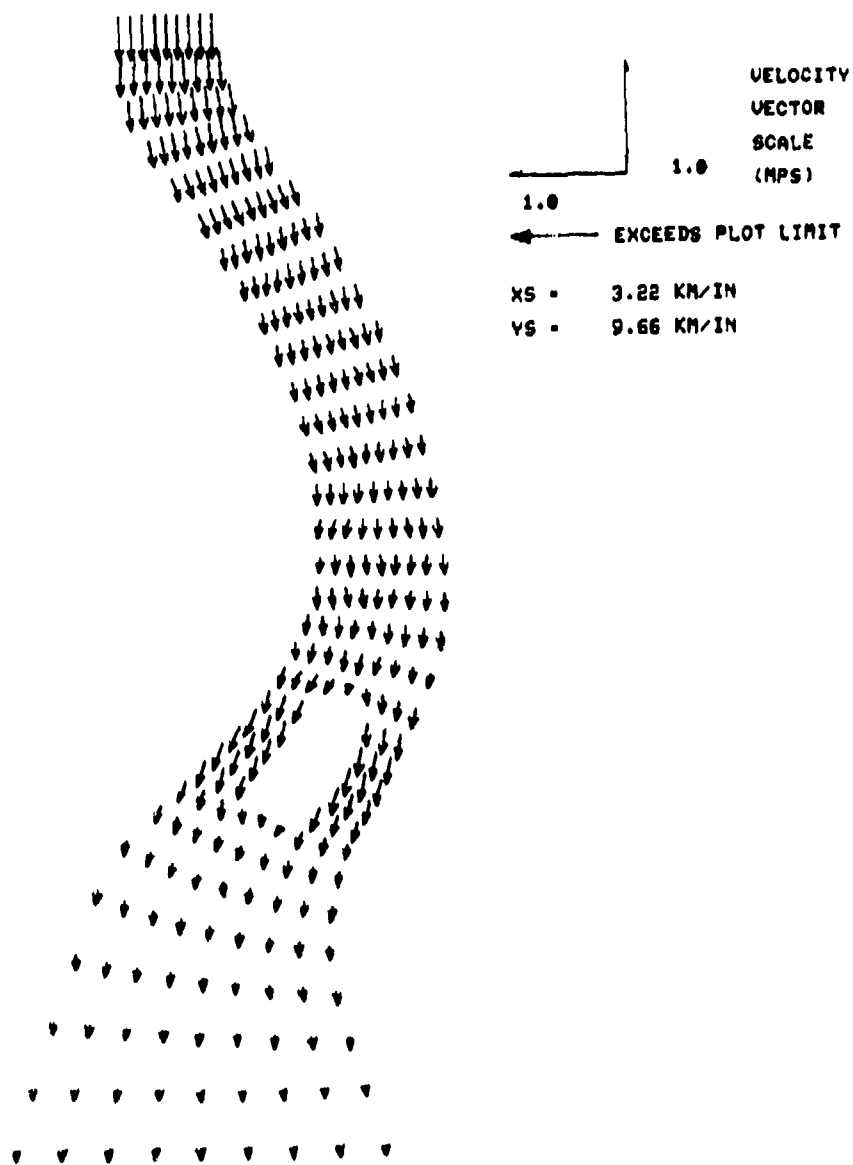
Figure 10. Velocity field after 6 hours, CONVEC = UPWIND

VELOCITY
VECTOR
SCALE
1.0   (MPS)
1.0

EXCEEDS PLOT LIMIT

XS =   3.22 KM/IN
YS =   9.66 KM/IN
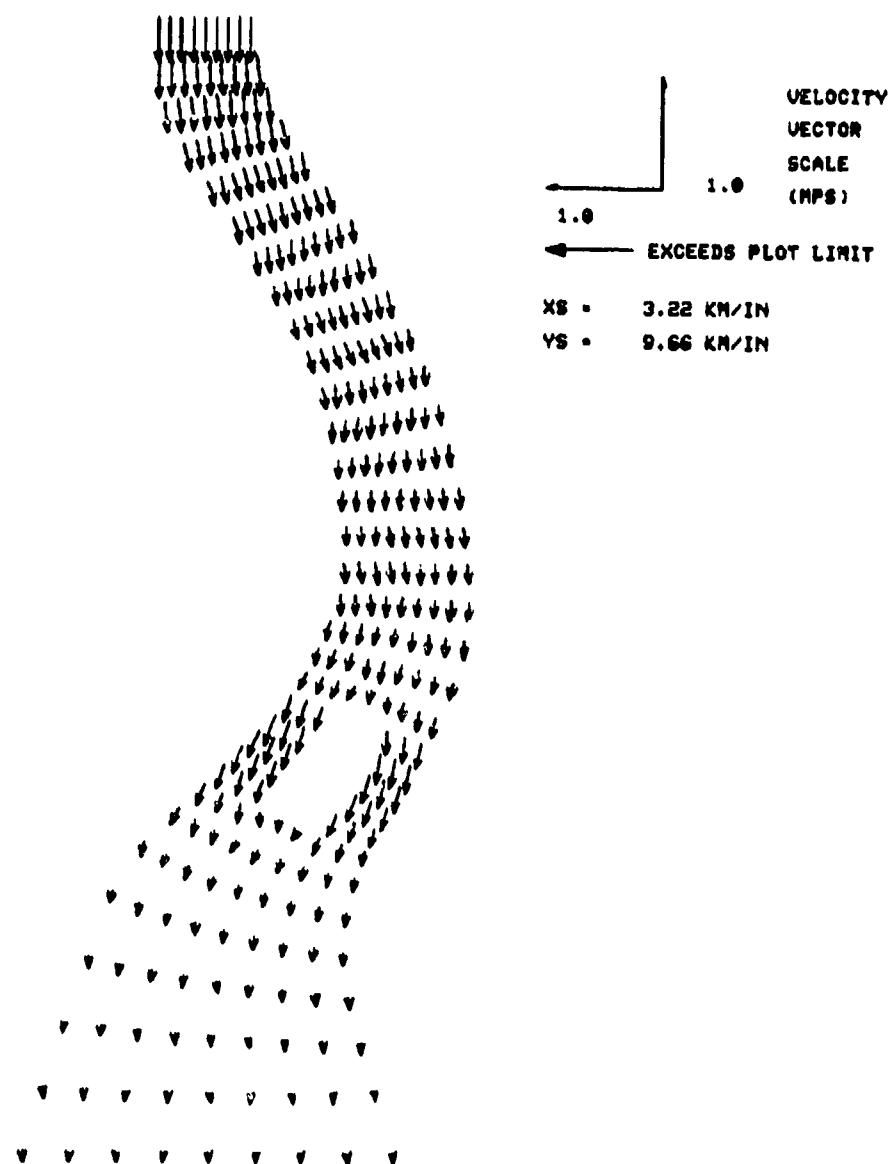
Figure 11.   Velocity field after 9 hours, CONVEC = UPWIND
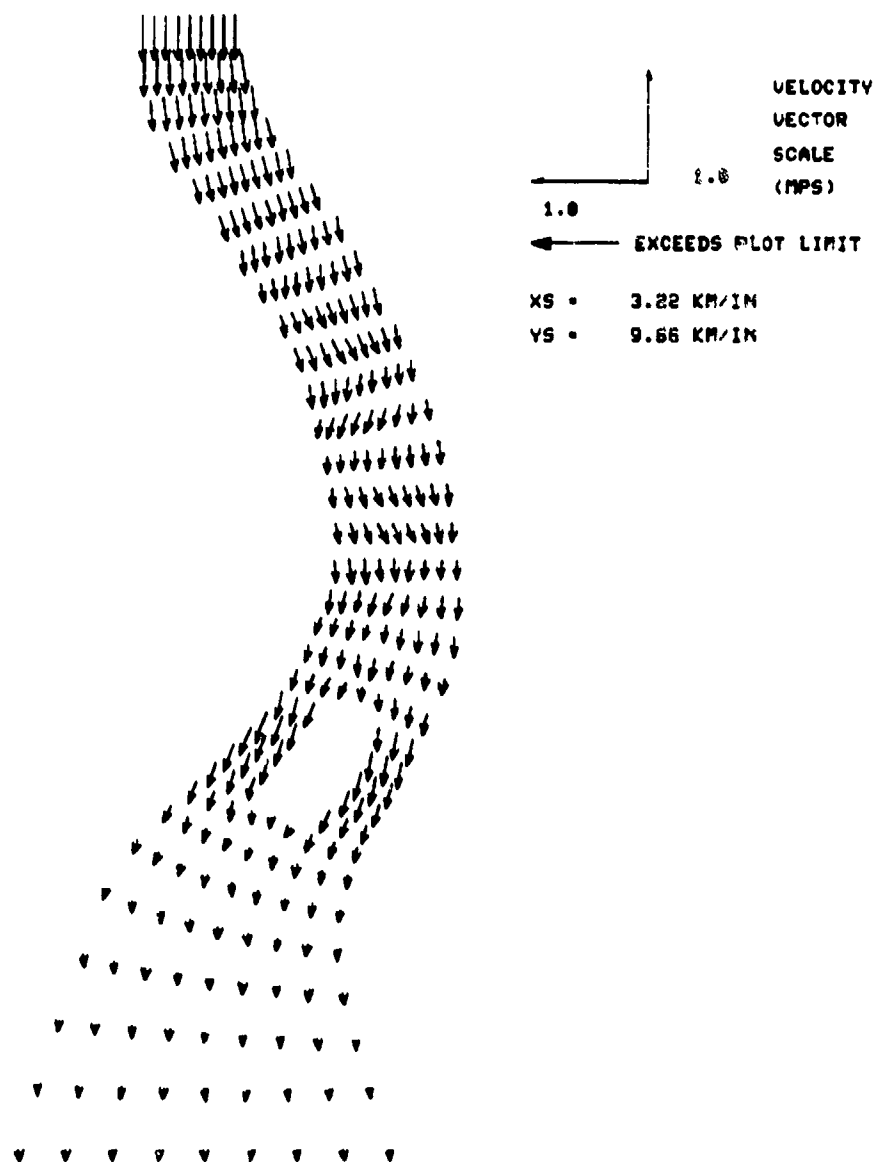
Figure 12. Velocity field after 12 hours, CONVEC = UPWIND
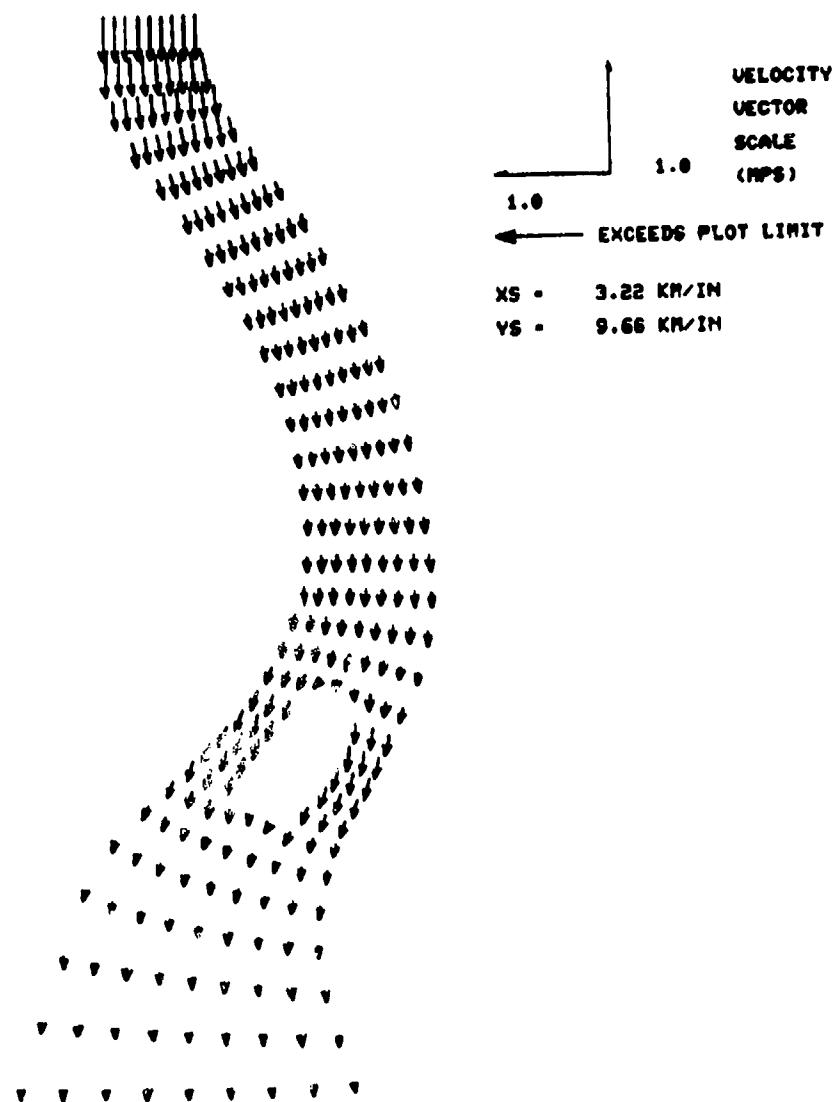
Figure 13. Velocity field after 3 hours, CONVEC = UPWIND, $D_{xx} = D_{yy} = 10$
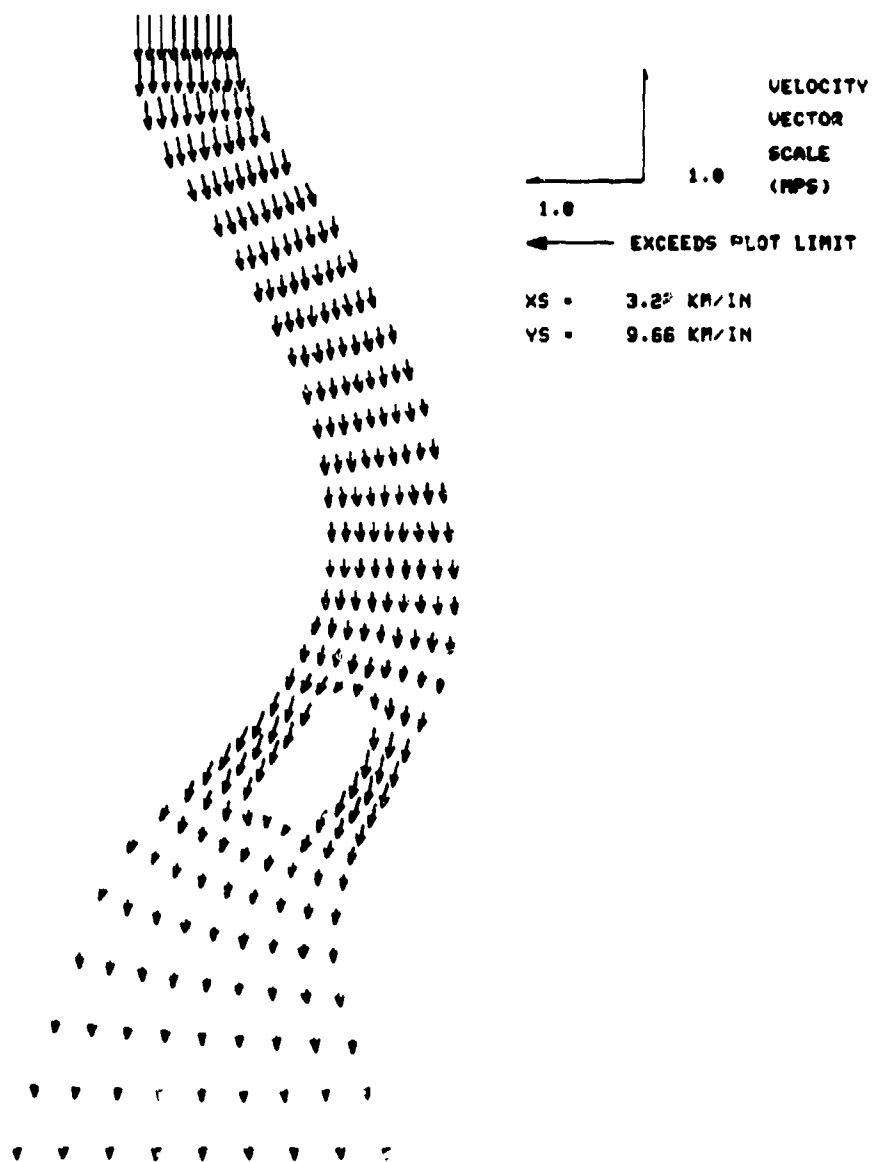
Figure 14. Velocity field after 6 hours, CONVEC = UPWIND, $D_{xx} = D_{yy} = 10$
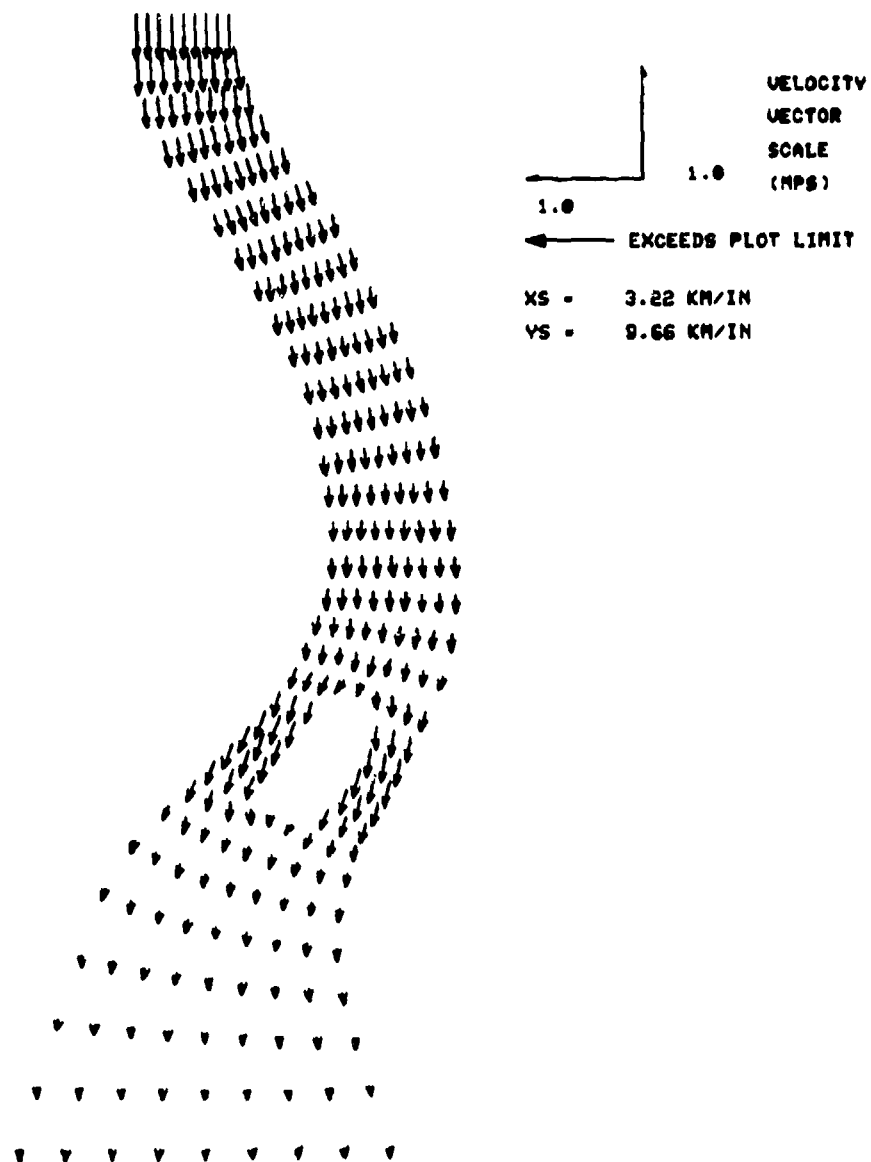
Figure 15. Velocity field after 9 hours, CONVEC = UPWIND, $D_{xx} = D_{yy} = 10$
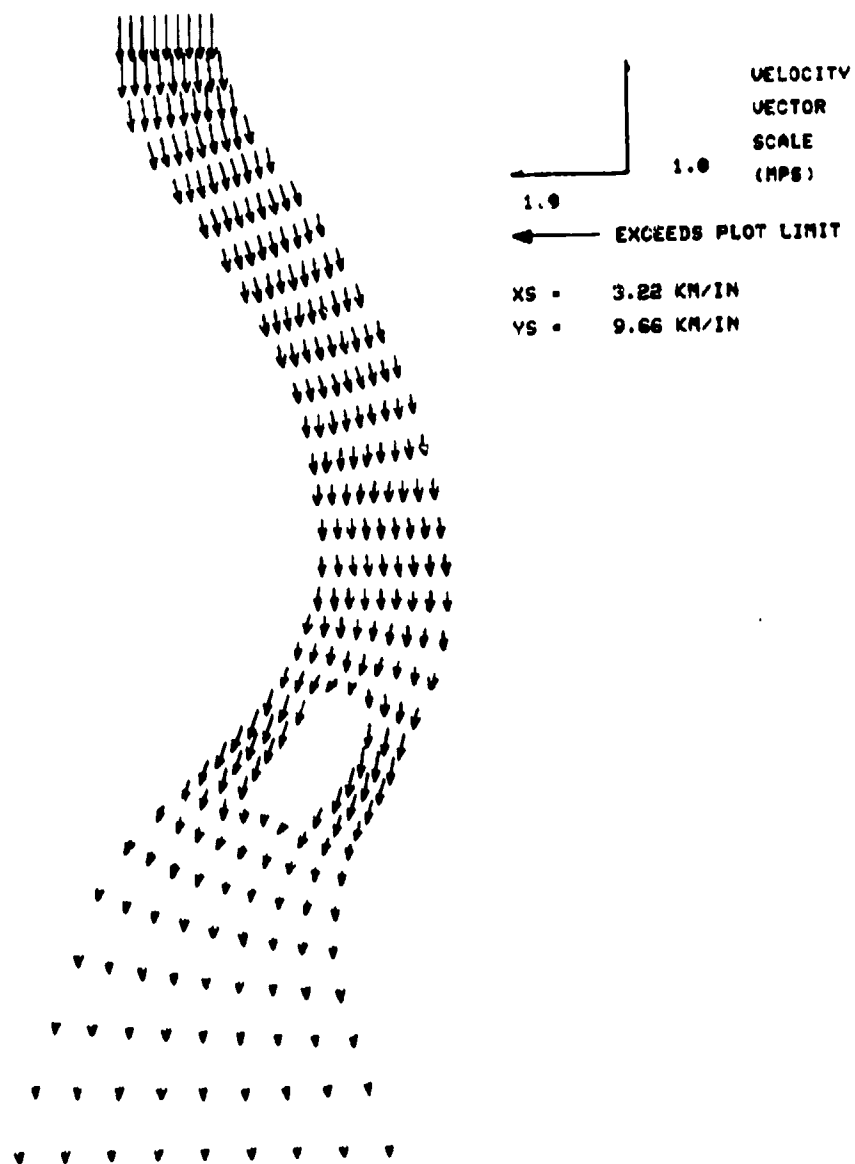
Figure 16. Velocity field after 12 hours, CONVEC = UPWIND, $D_{xx} = D_{yy} = 10$
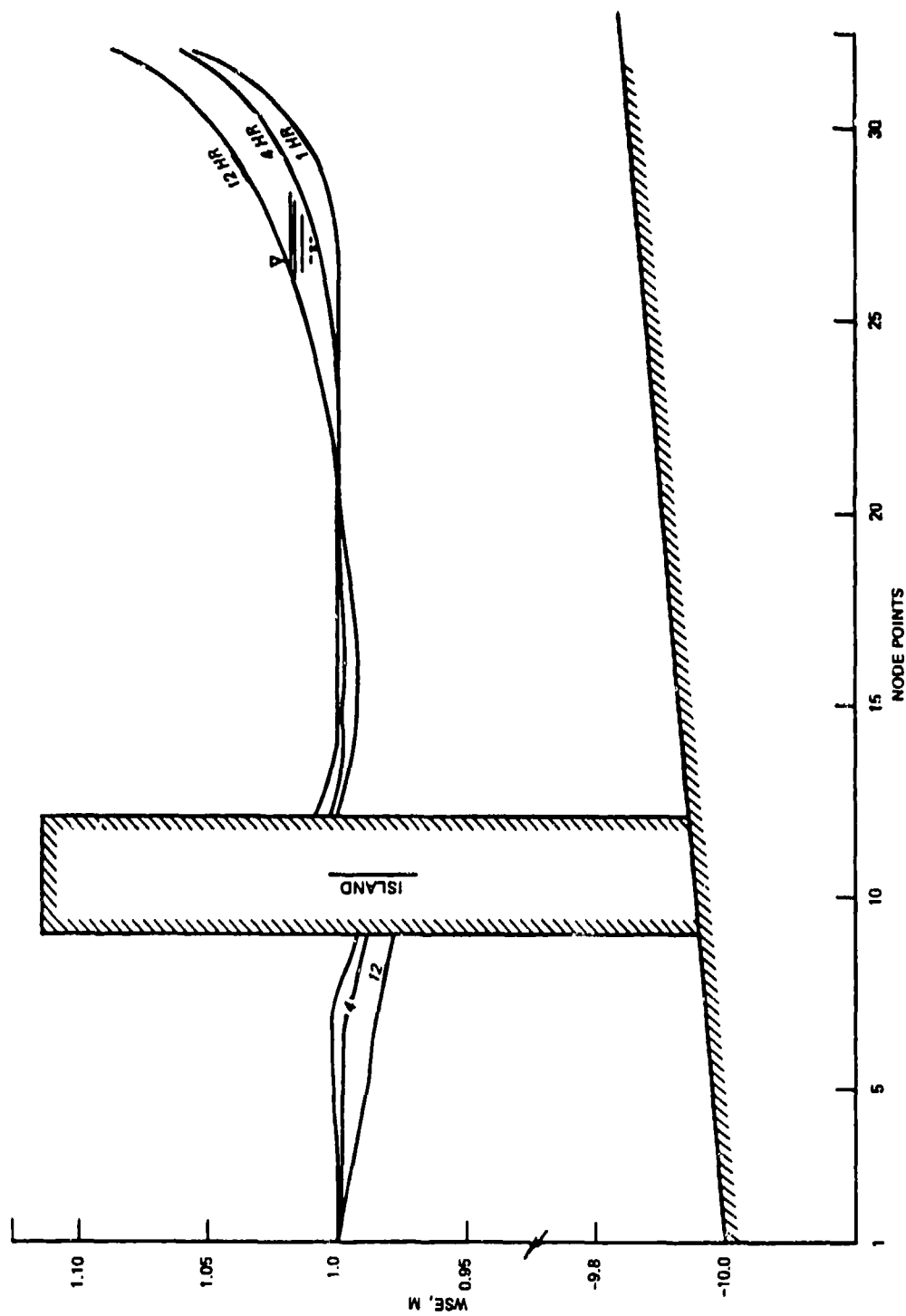
Figure 17. Water surface profile along ξ = 6 line
for a sloping river with control at downstream
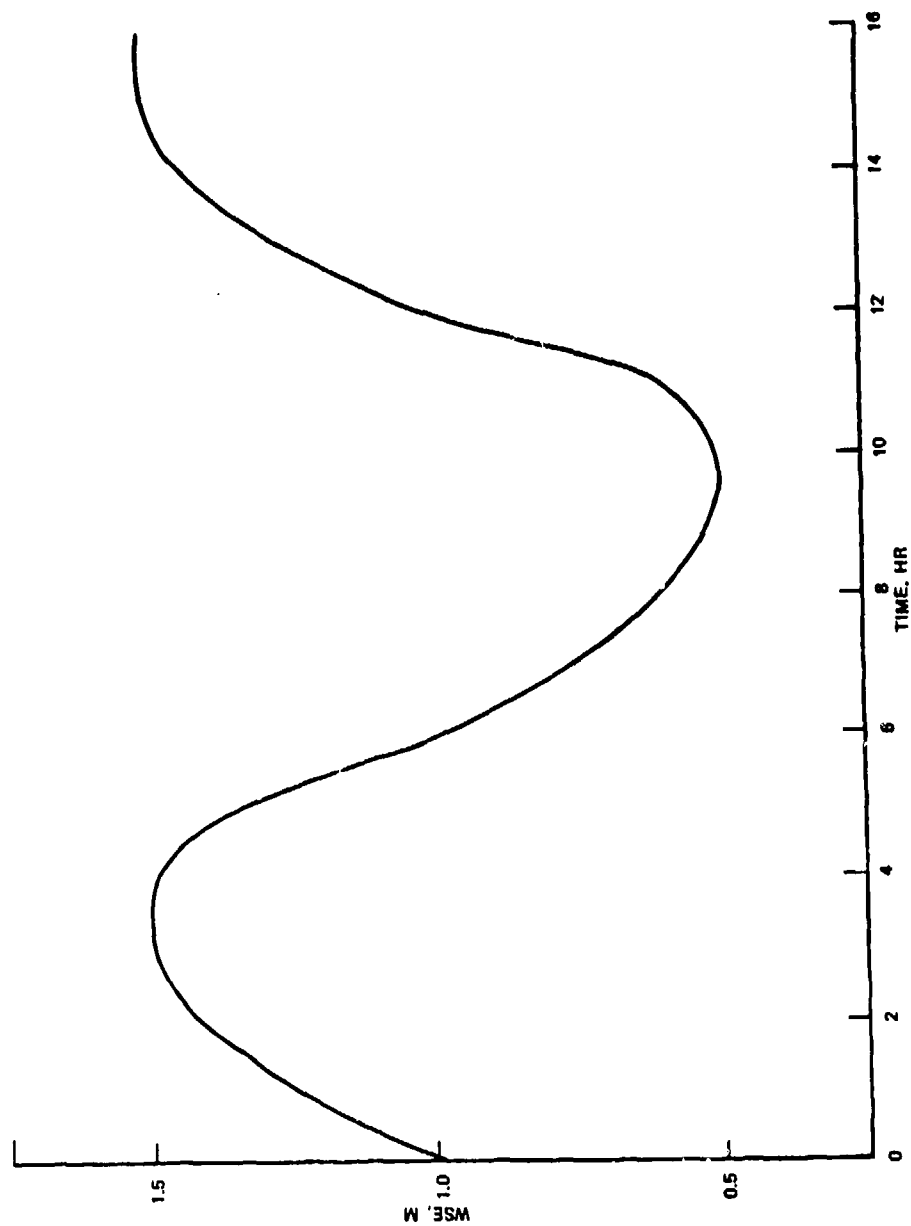
Figure 18. Water surface elevation at ocean boundary
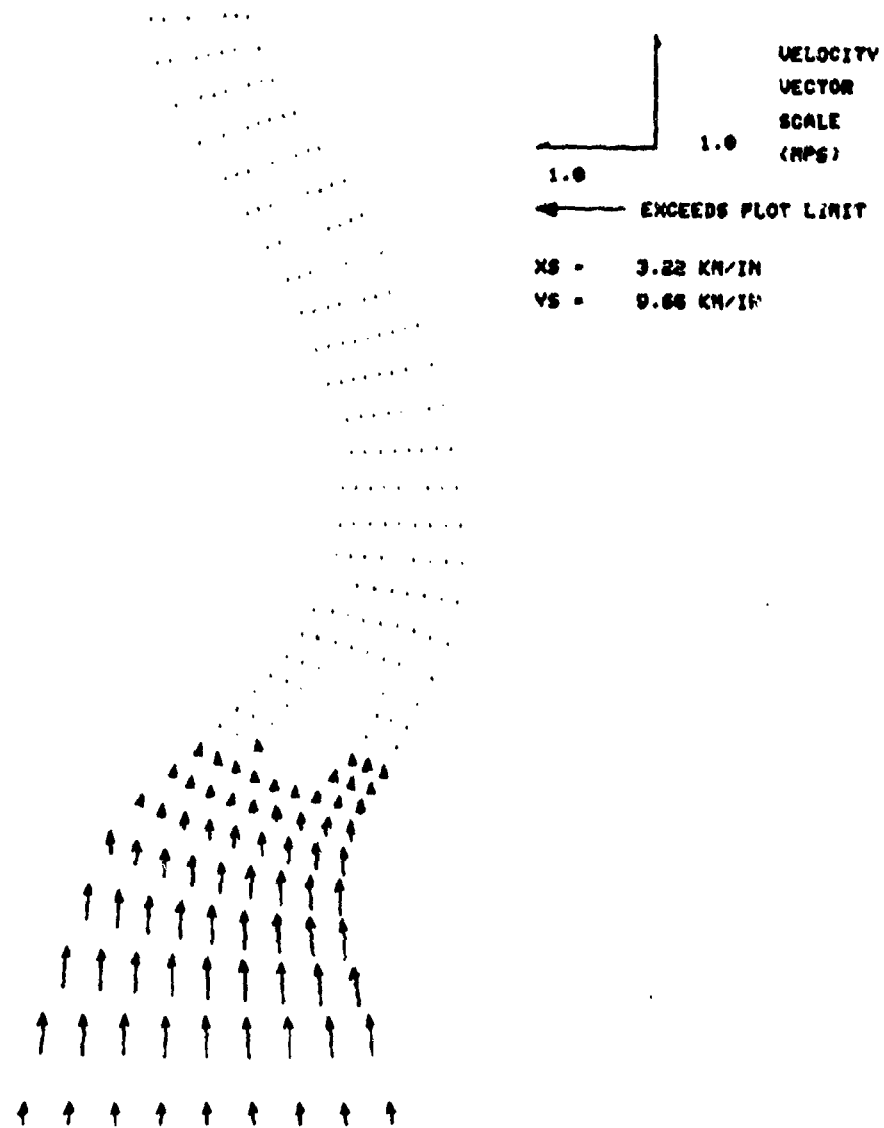
Figure 19. Velocity field after 1 hour with an ocean boundary
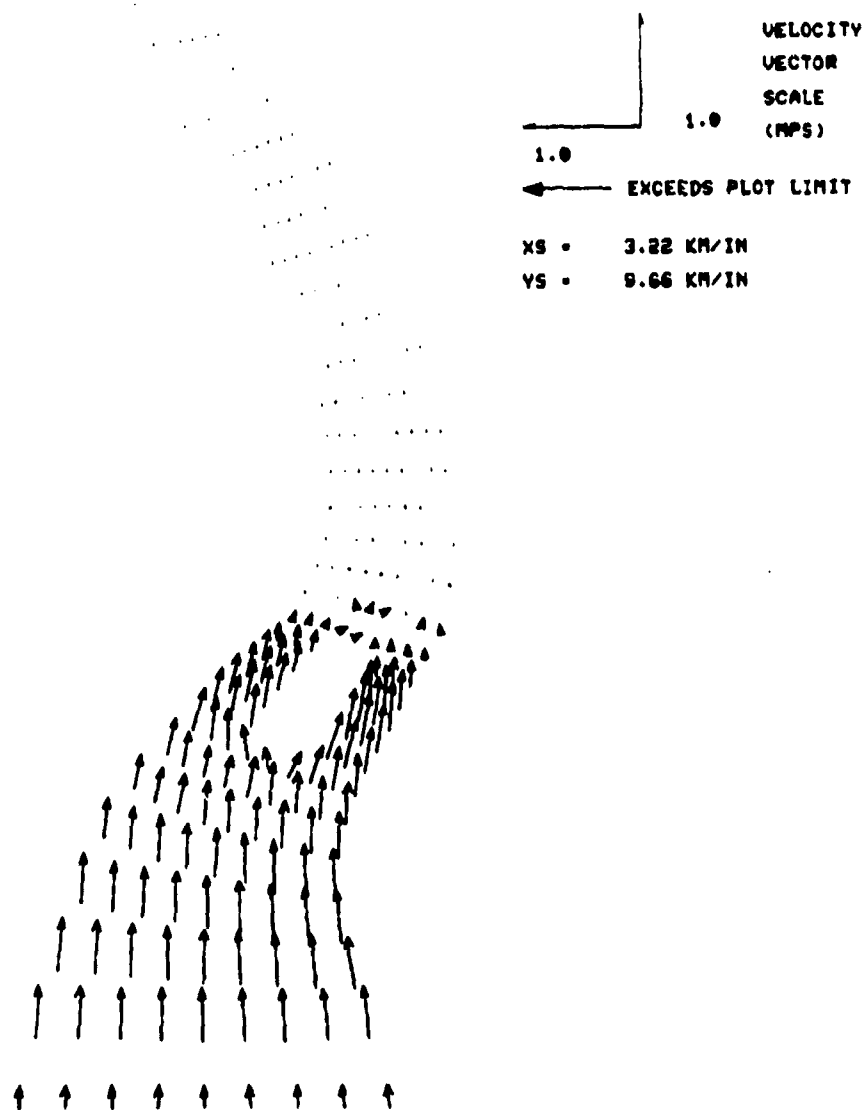
Figure 20.   Velocity field after 2 hours with an ocean boundary
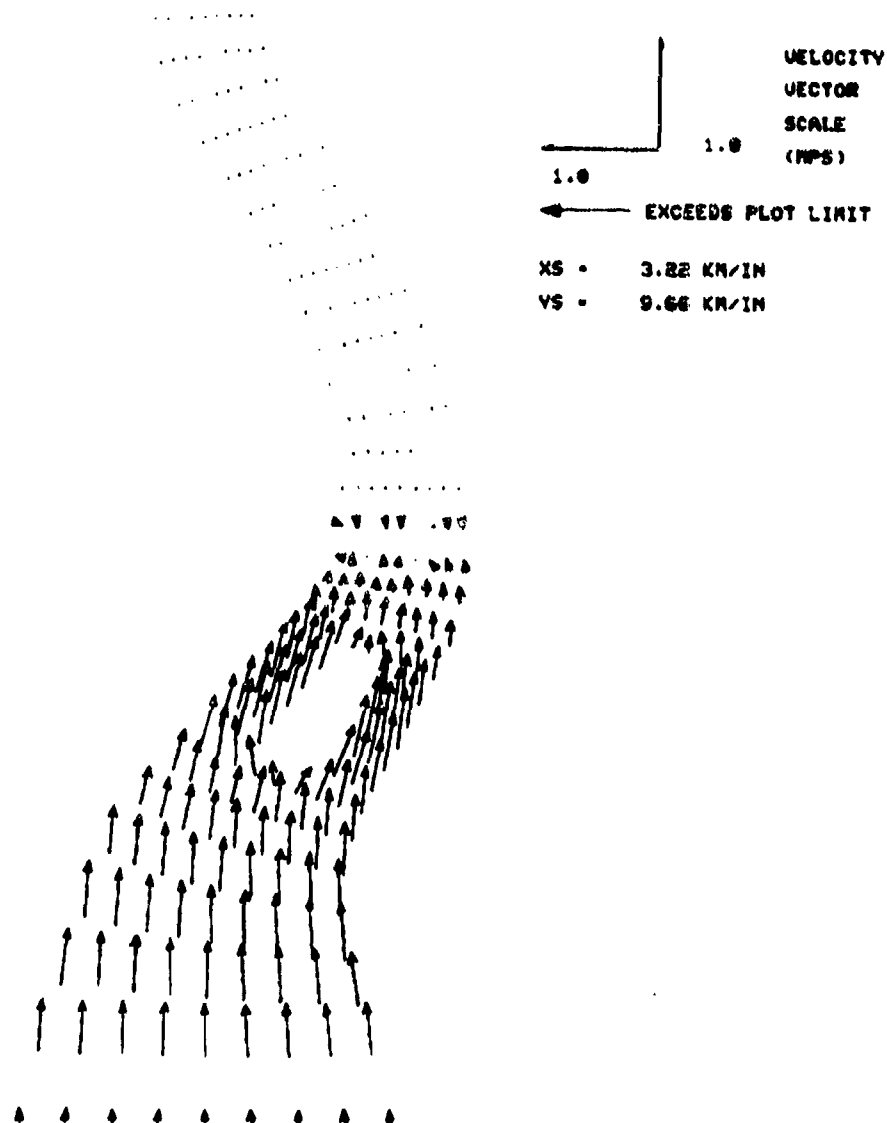
Figure 21. Velocity field after 3 hours with an ocean boundary
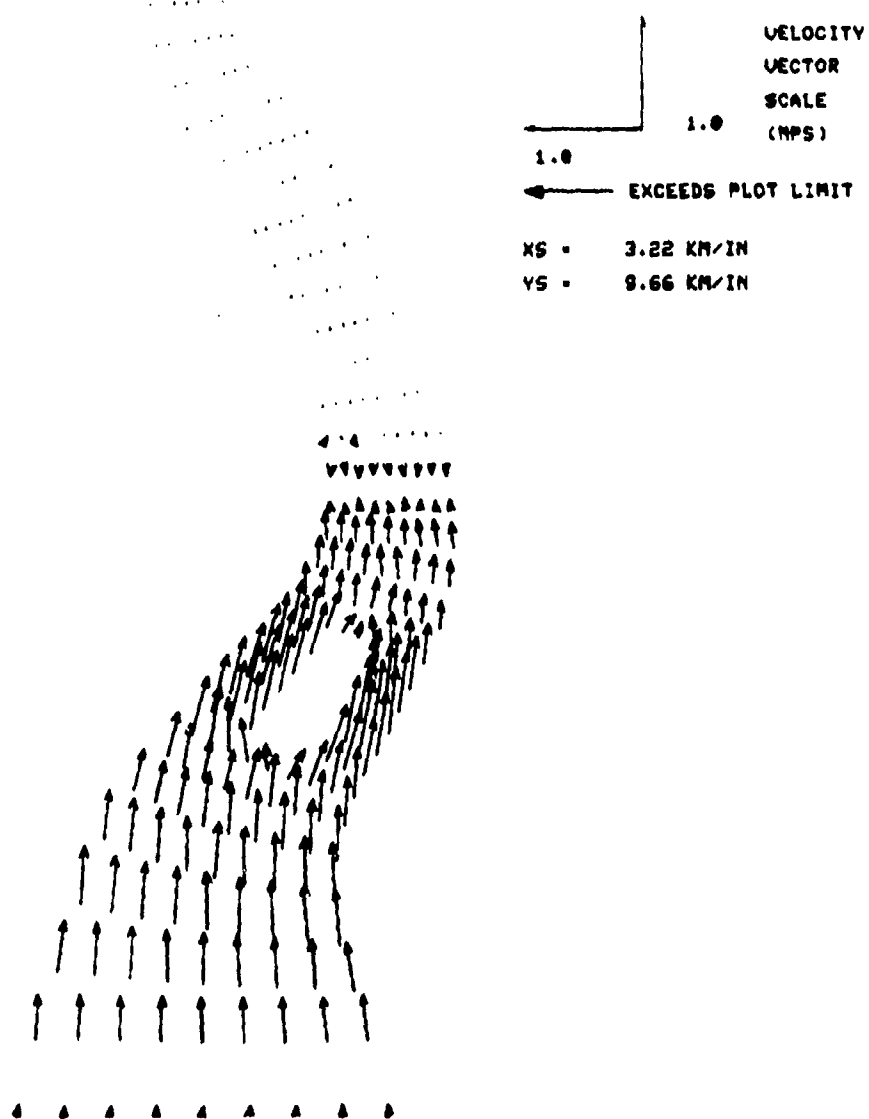
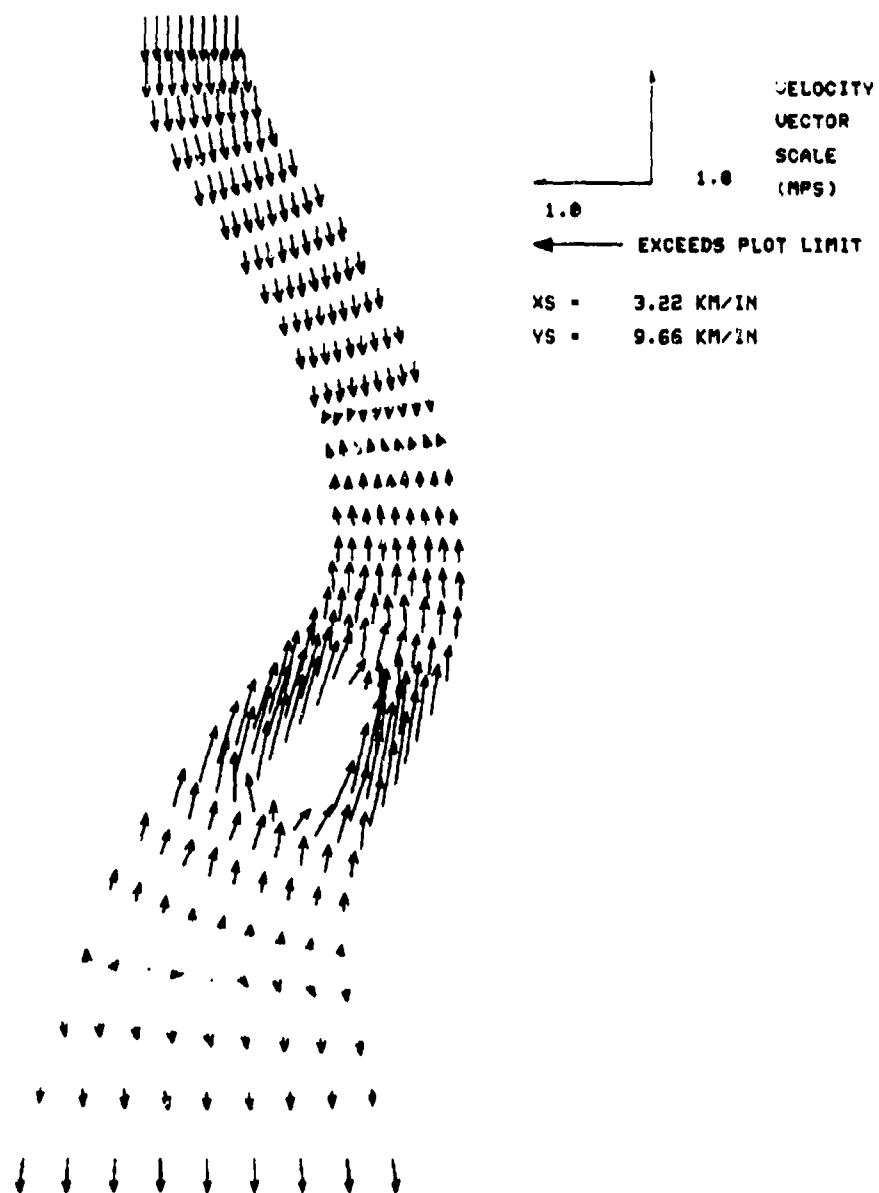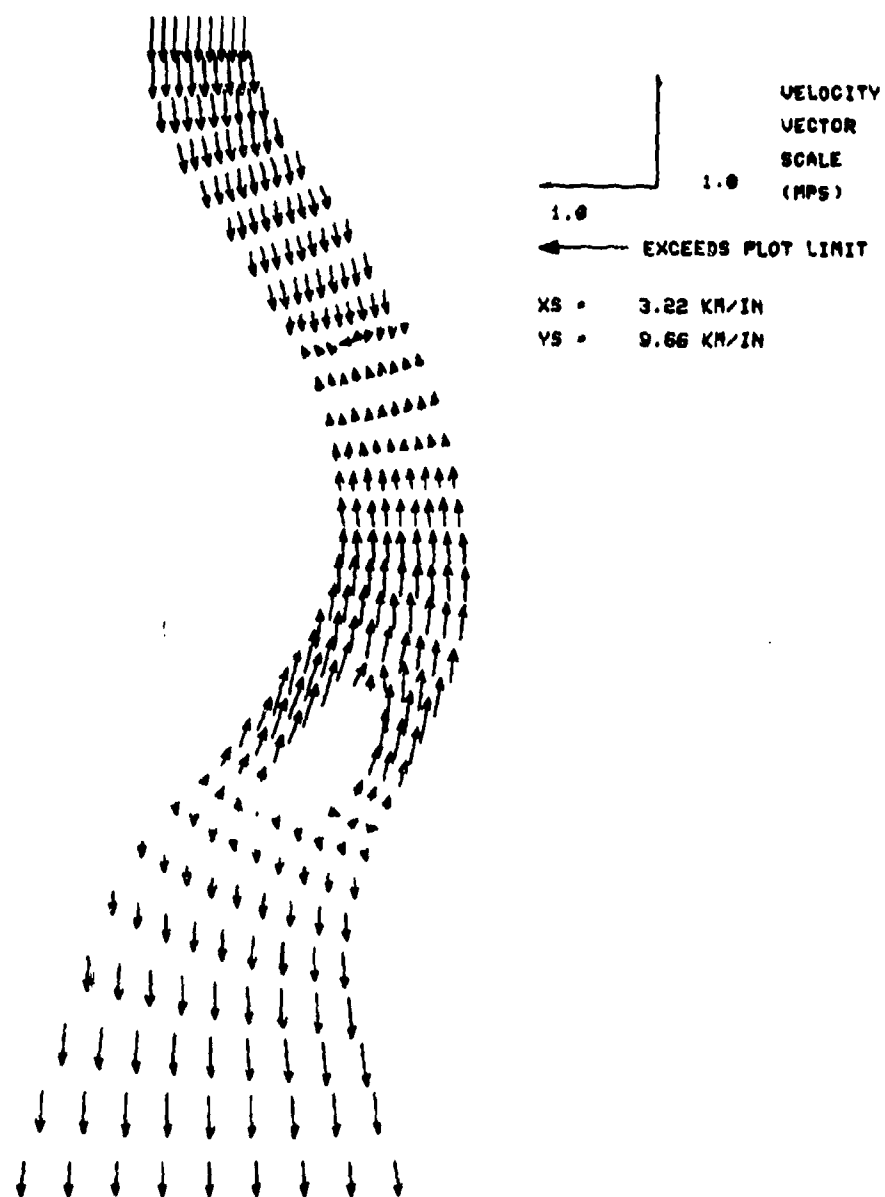Figure 22.   Velocity field after 4 hours with an ocean boundary

VELOCITY
VECTOR
SCALE
(MPS)

EXCEEDS PLOT LIMIT

XS =   3.22 KM/IN
YS =   9.66 KM/IN
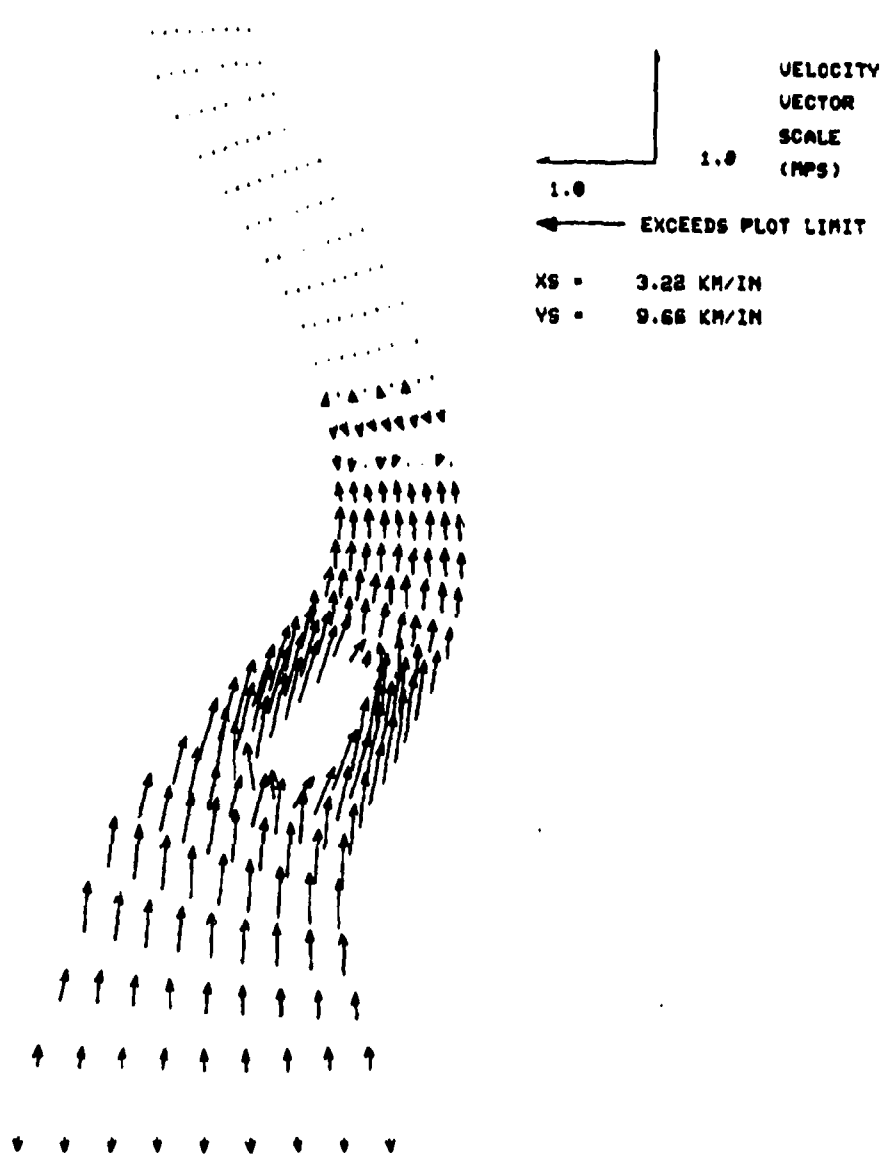
Figure 23.   Velocity field after 5 hours with an ocean boundary
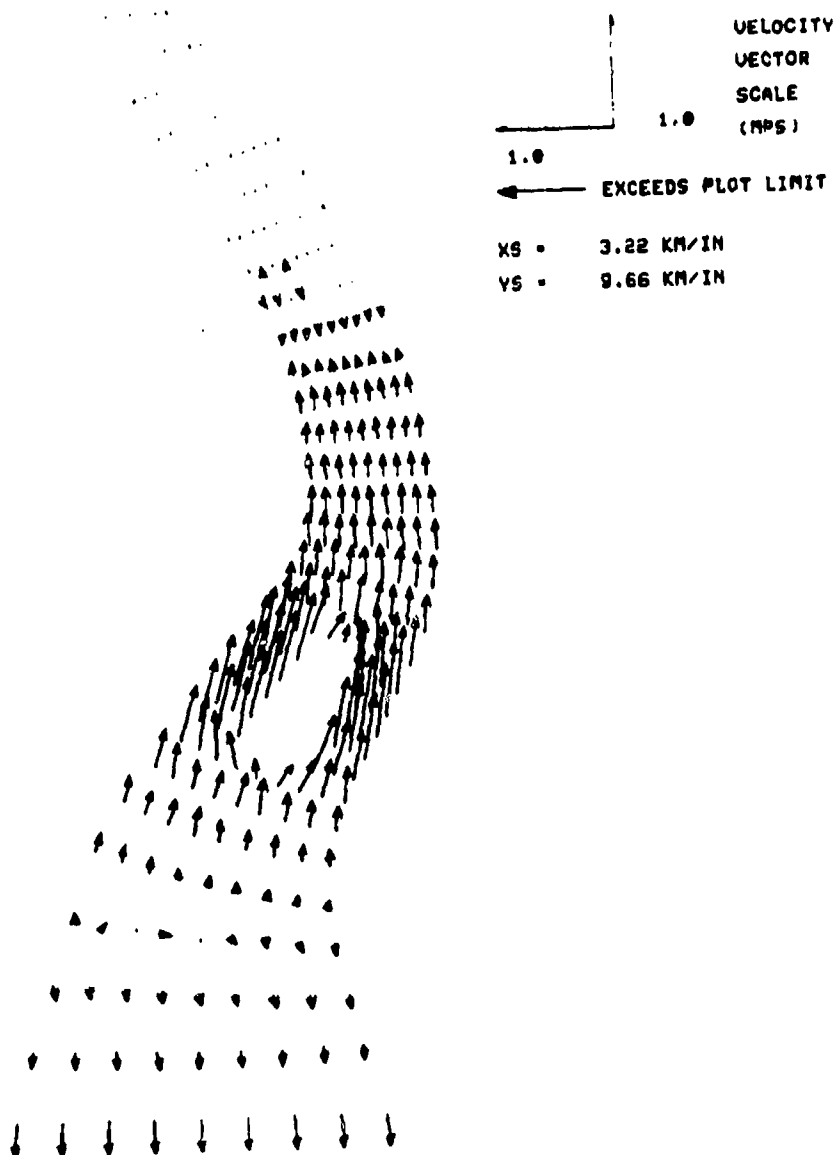
Figure 24. Velocity field after 6 hours with an ocean boundary
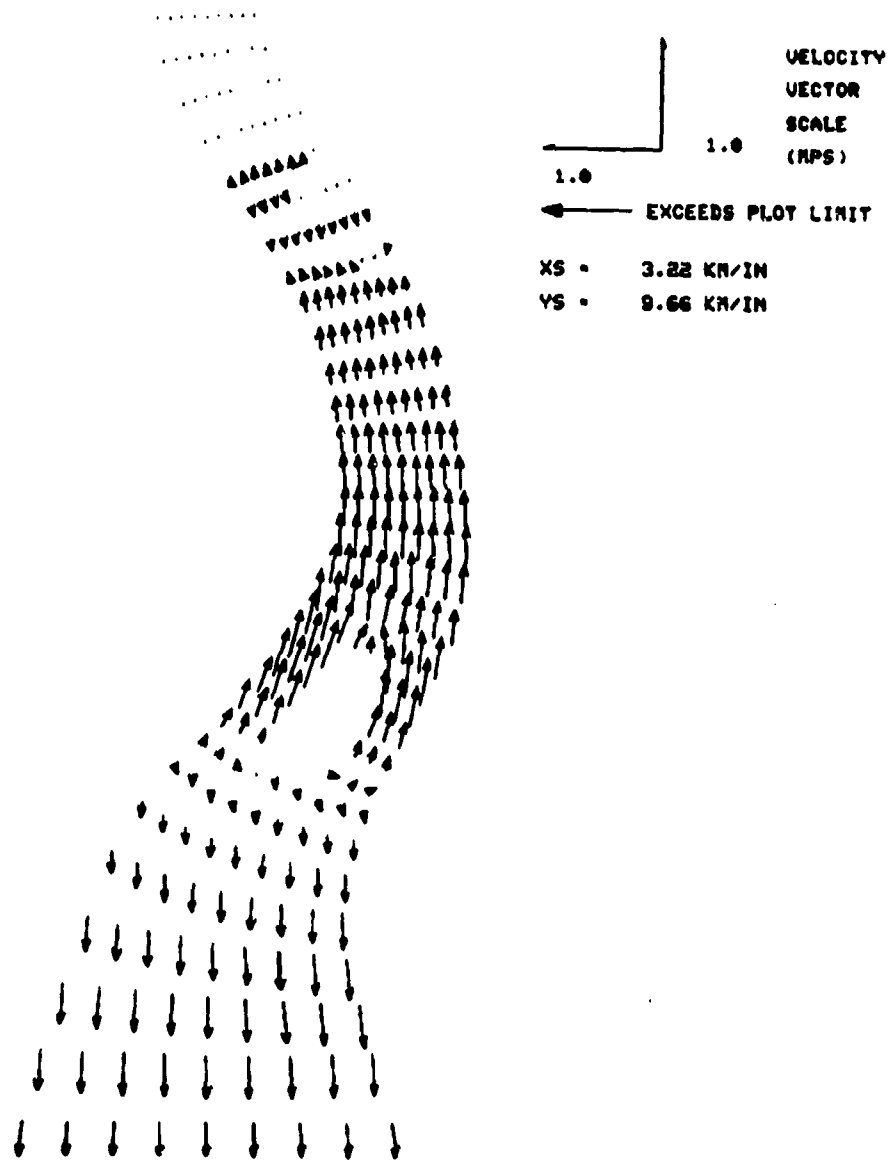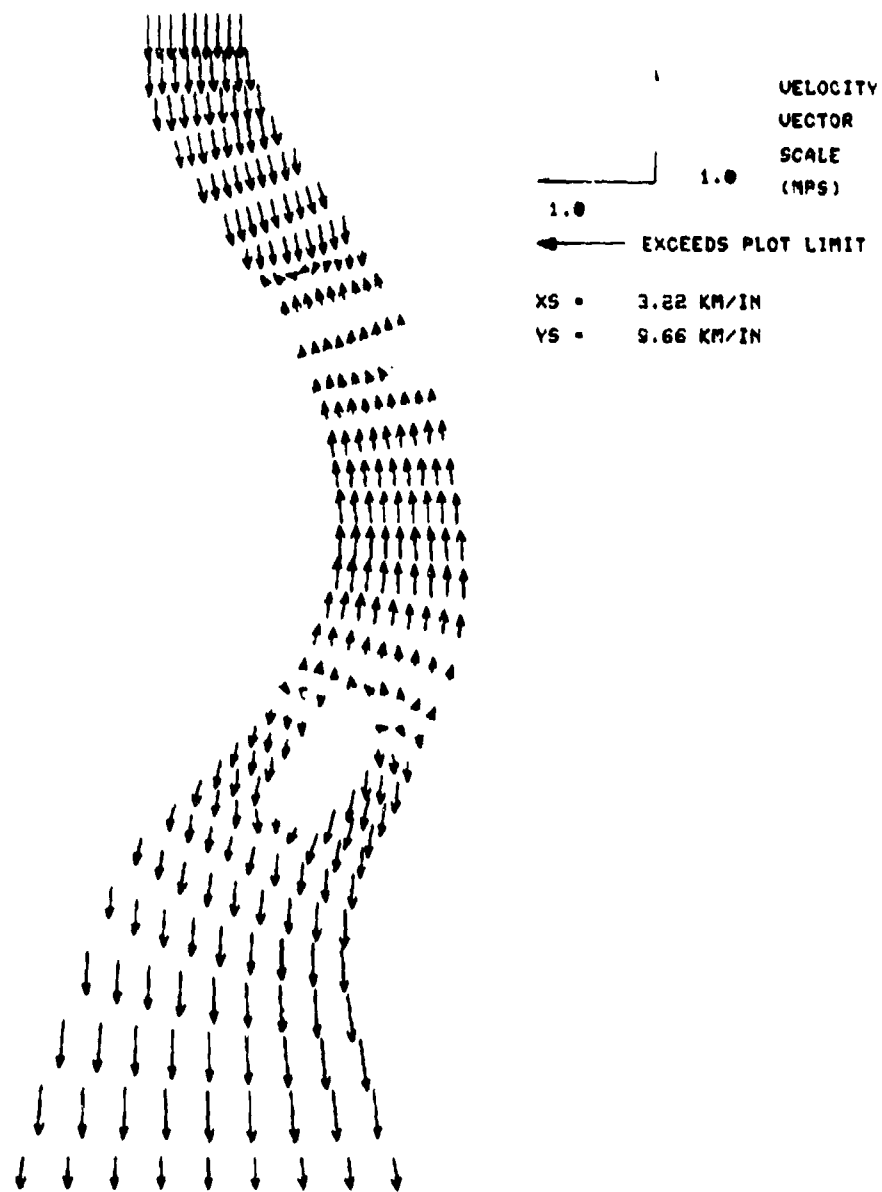
Figure 25. Velocity field after 7 hours with an ocean boundary
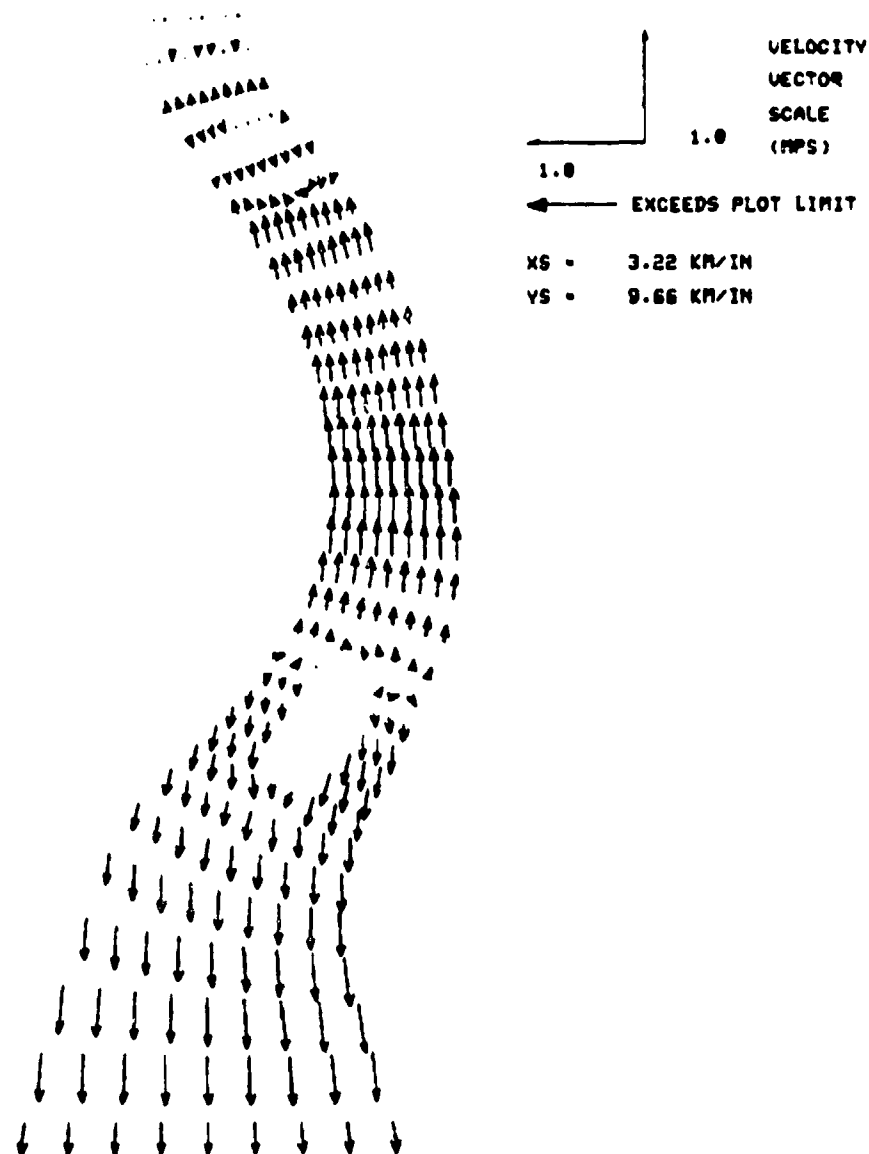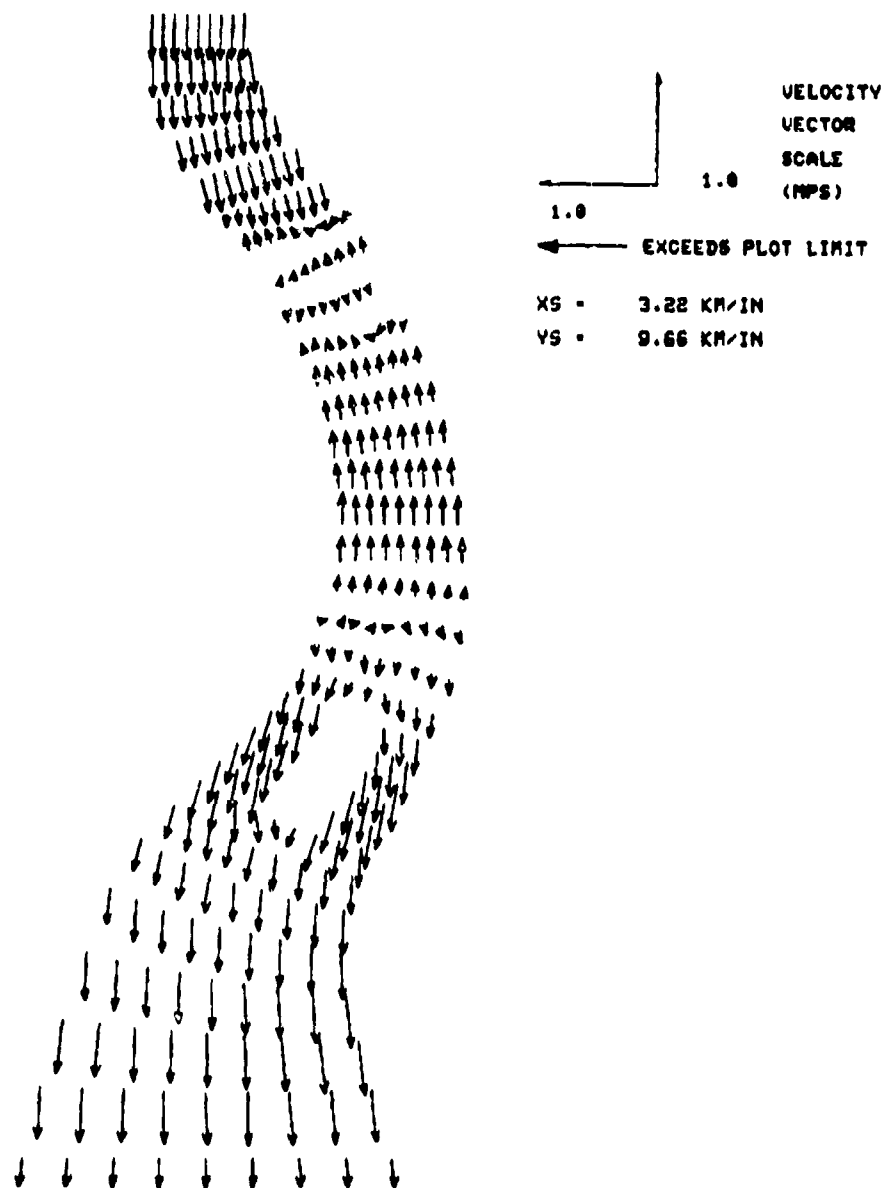
Figure 26.   Velocity field after 8 hours with an ocean boundary
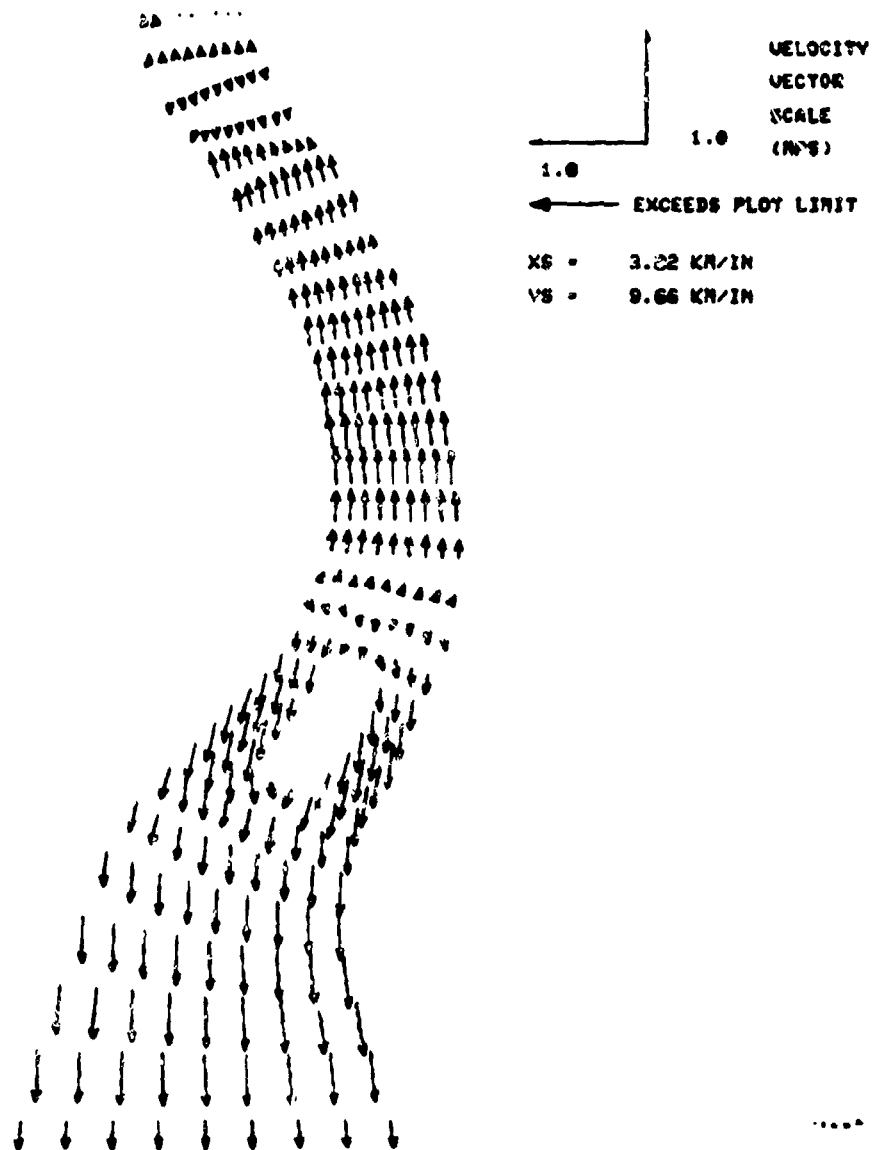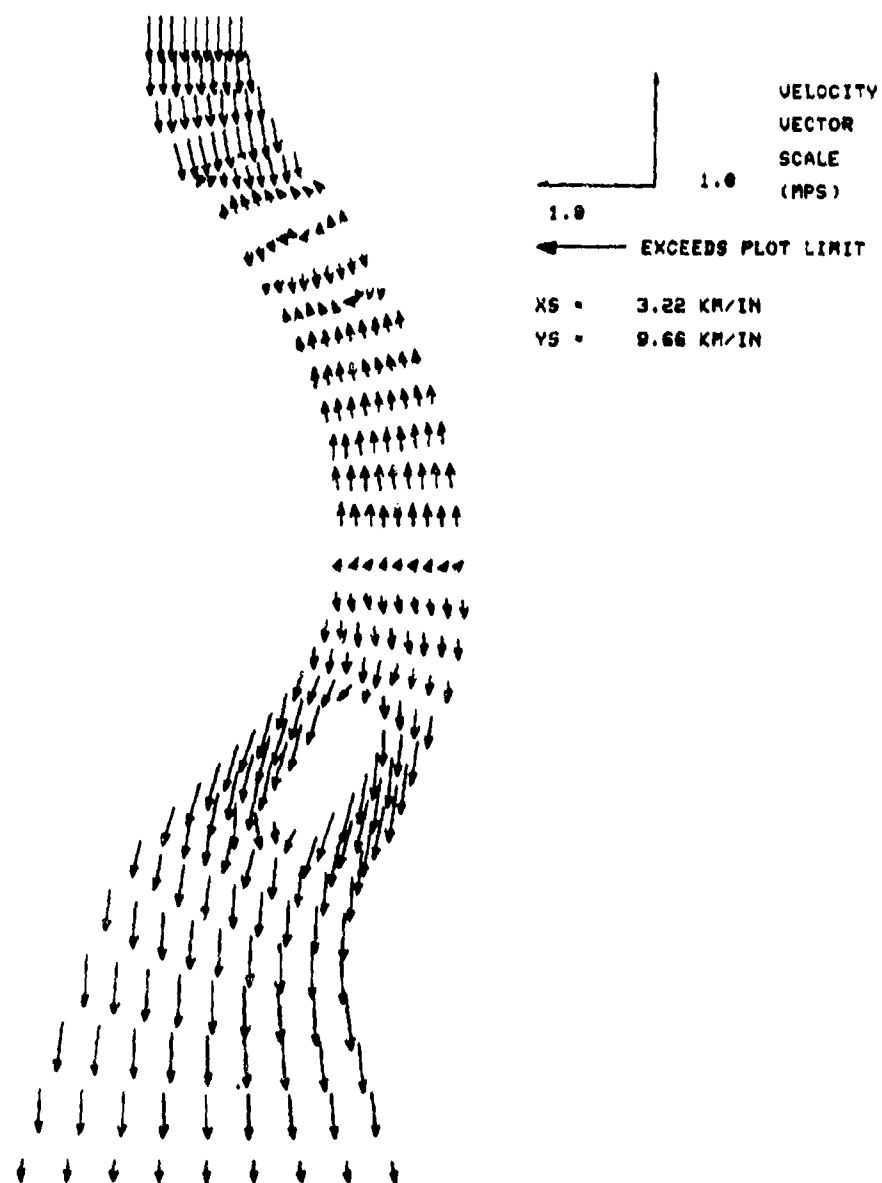
Figure 2). Velocity field after 9 hours with an ocean boundary
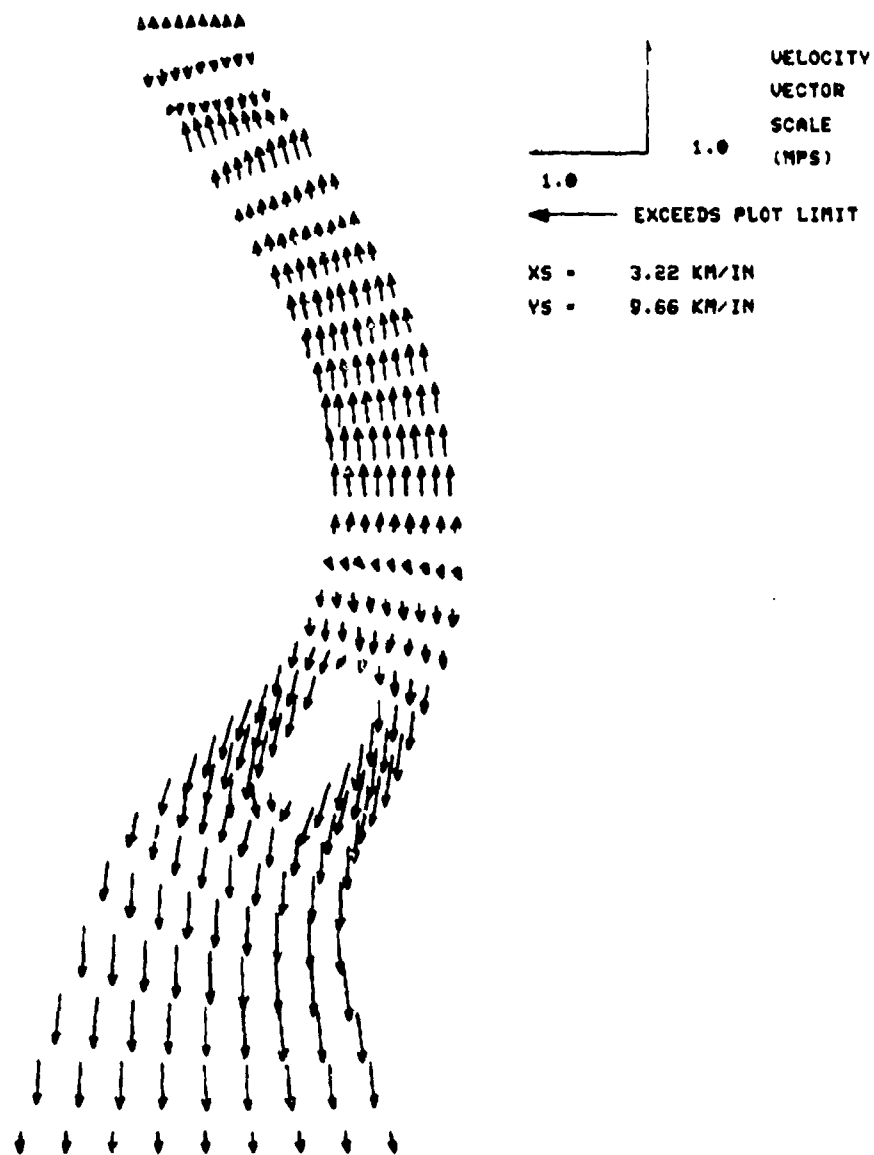
Figure 28. Velocity field after 10 hours with an ocean boundary
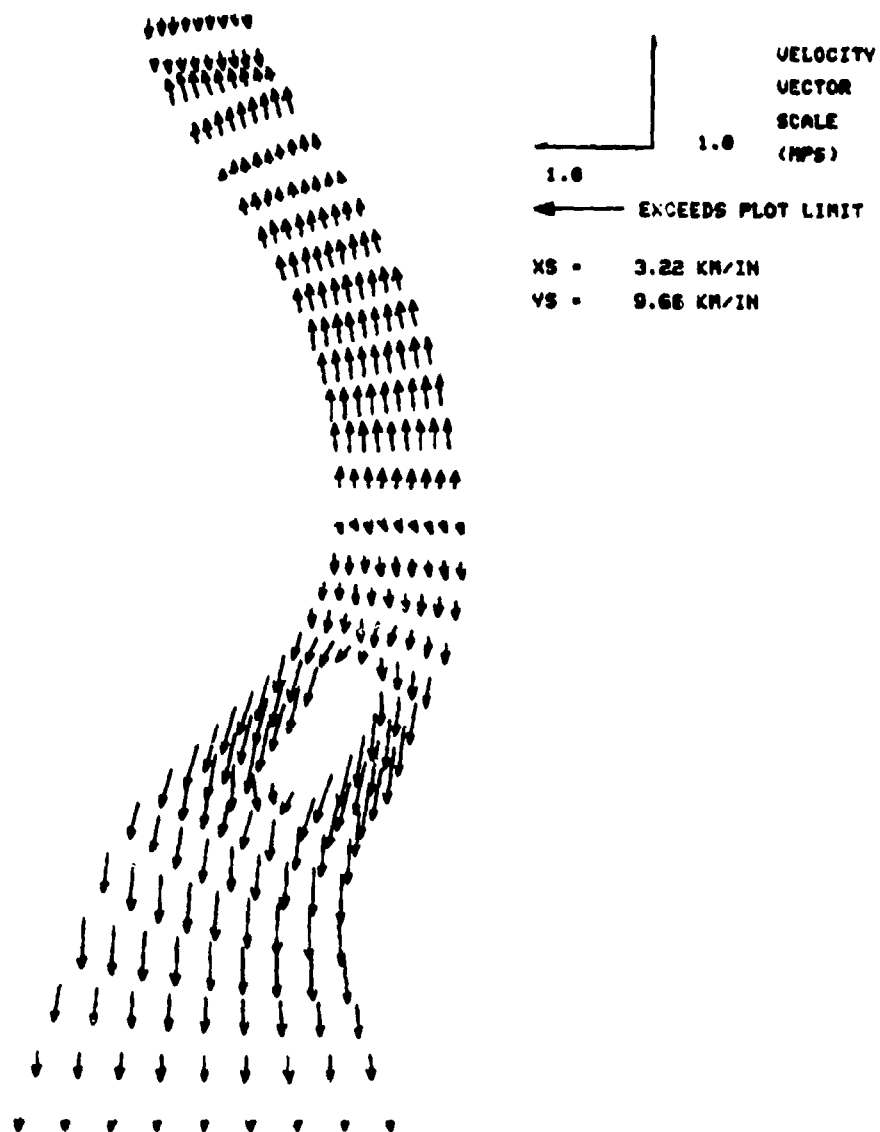
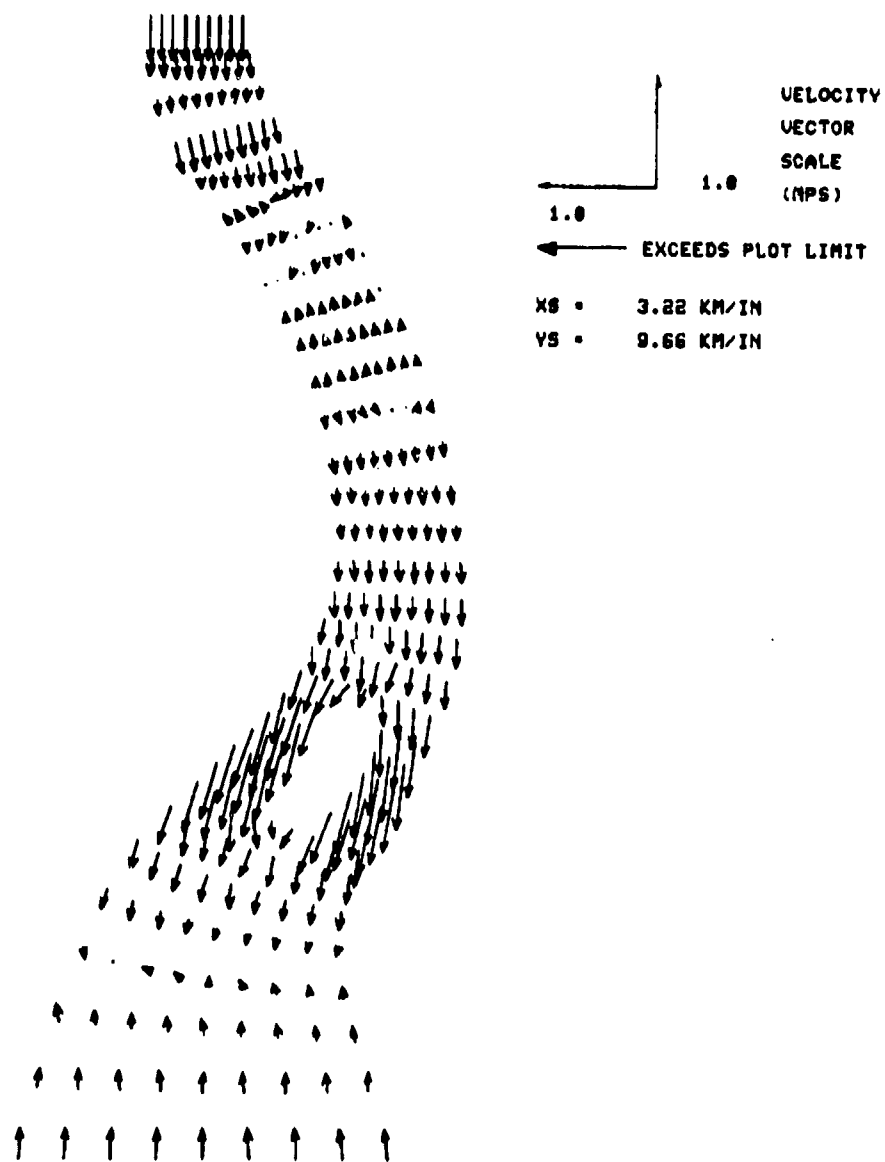Figure 29. Velocity field after 11 hours with an ocean boundary
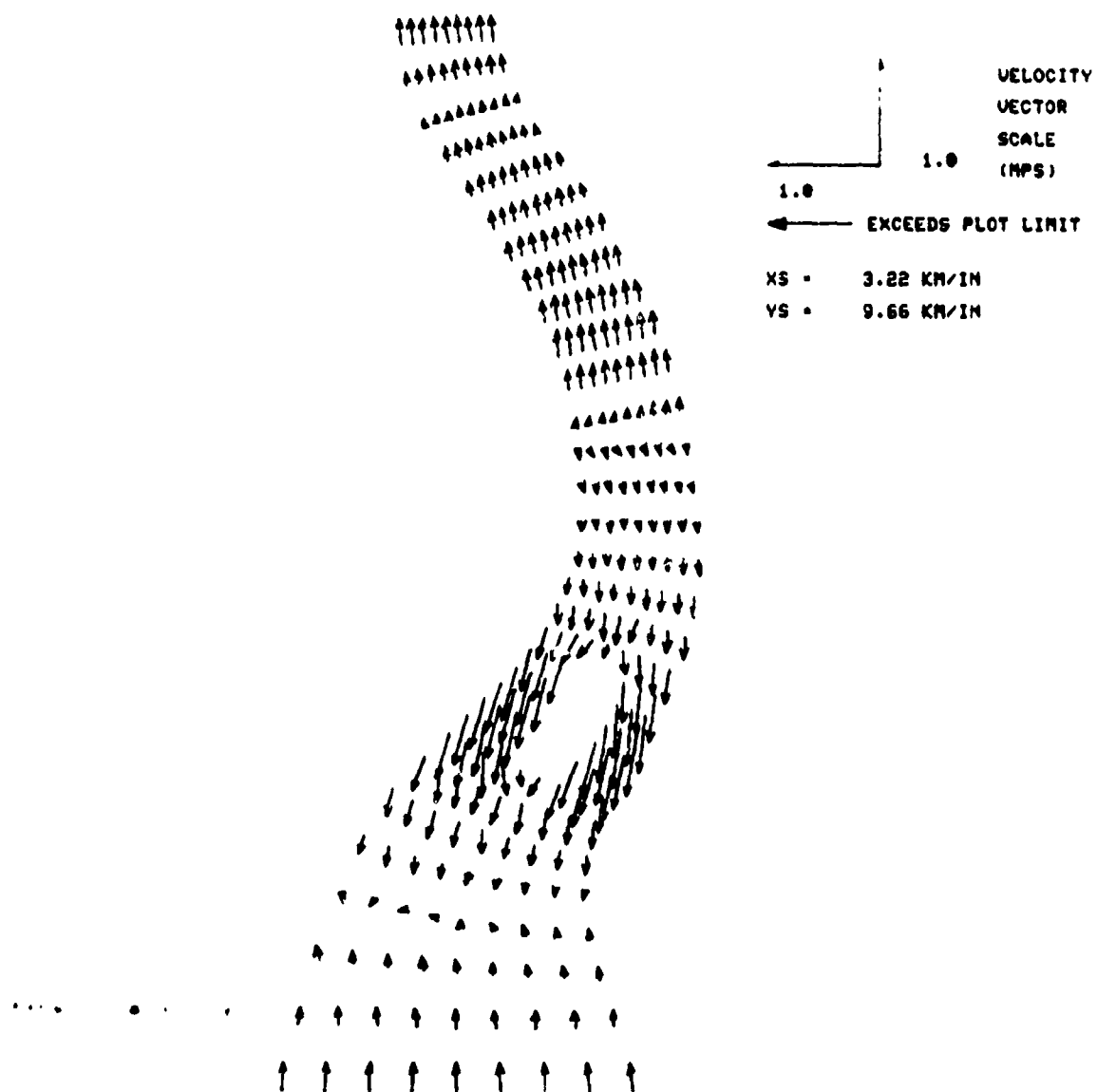
Figure 30. Velocity field after 12 hours with an ocean boundary
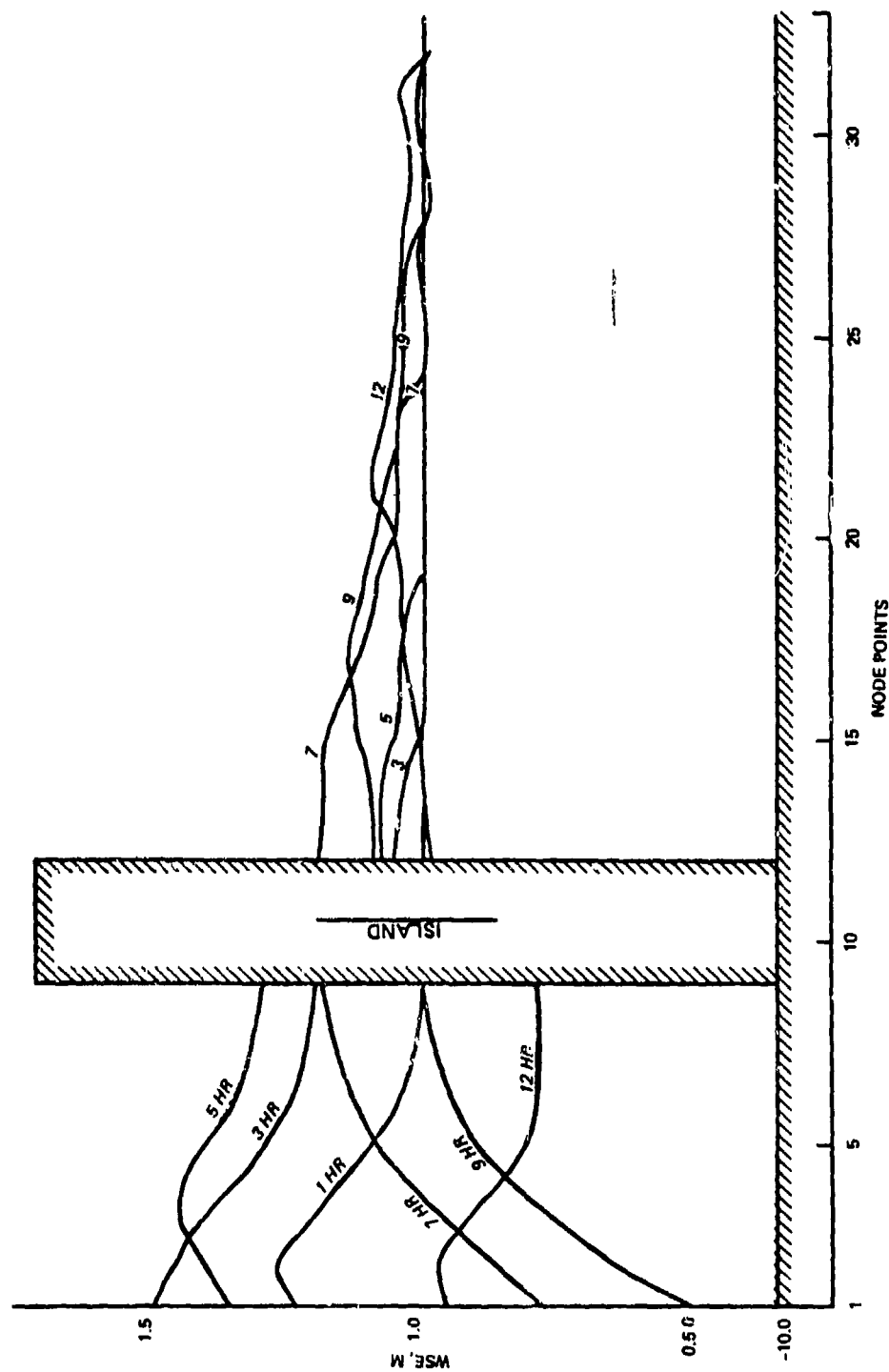
Figure 31. Water surface profiles along $\xi = 6$ line
with only an ocean boundary
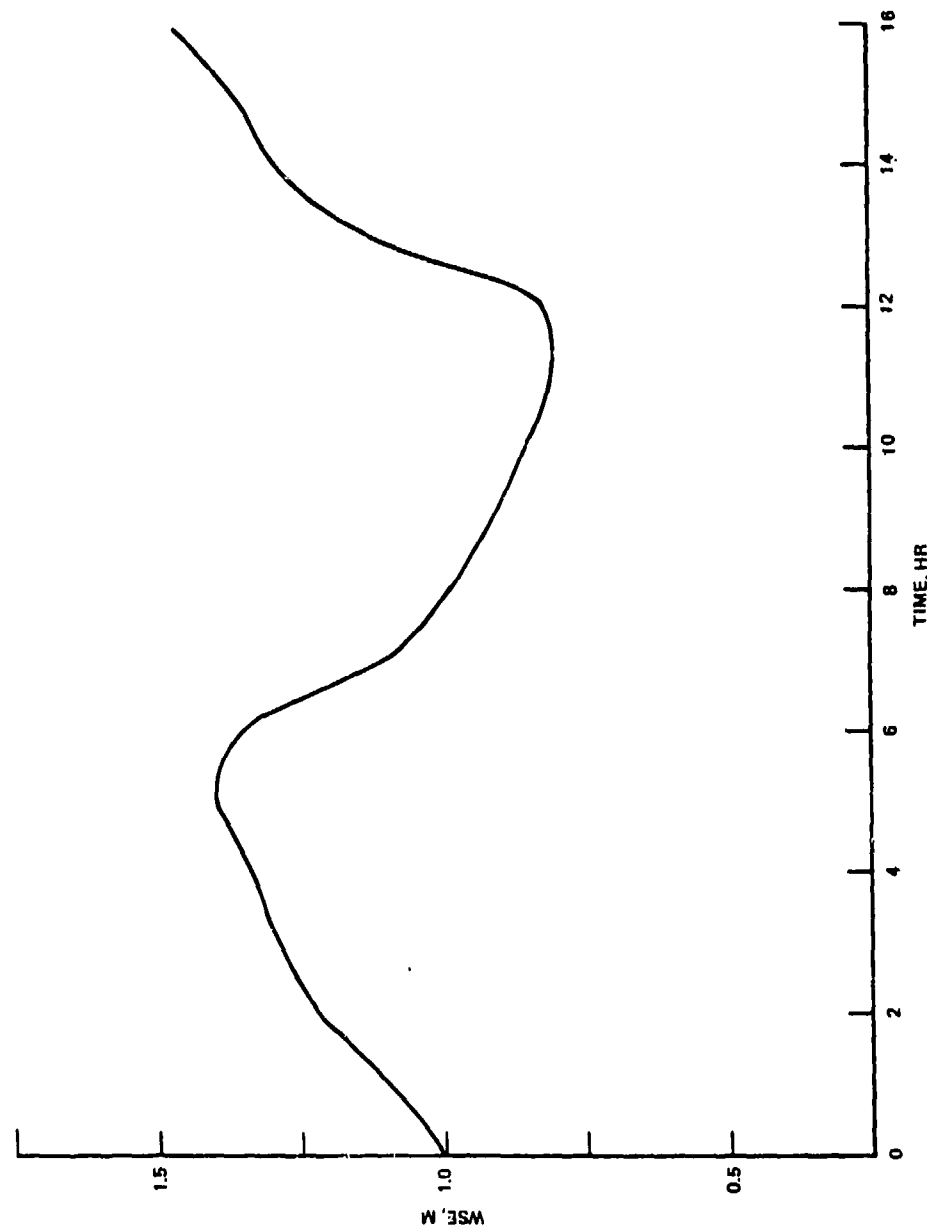
Figure 32. Water surface elevation at $\xi = 6$, $\eta = 5$ with only an ocean boundary
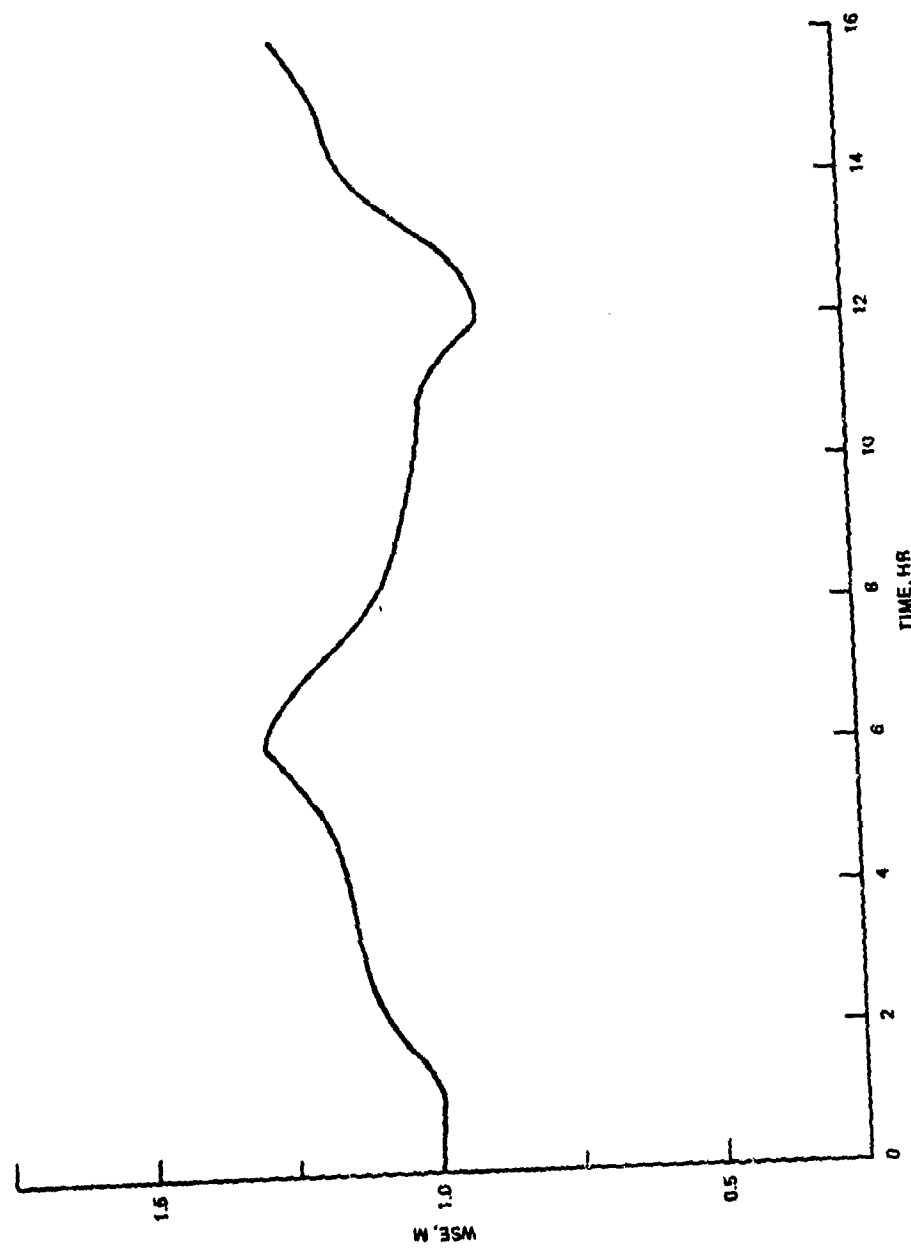
Figure 33. Water surface elevation at $\xi = 3$, $\eta = 10$ with only an ocean boundary
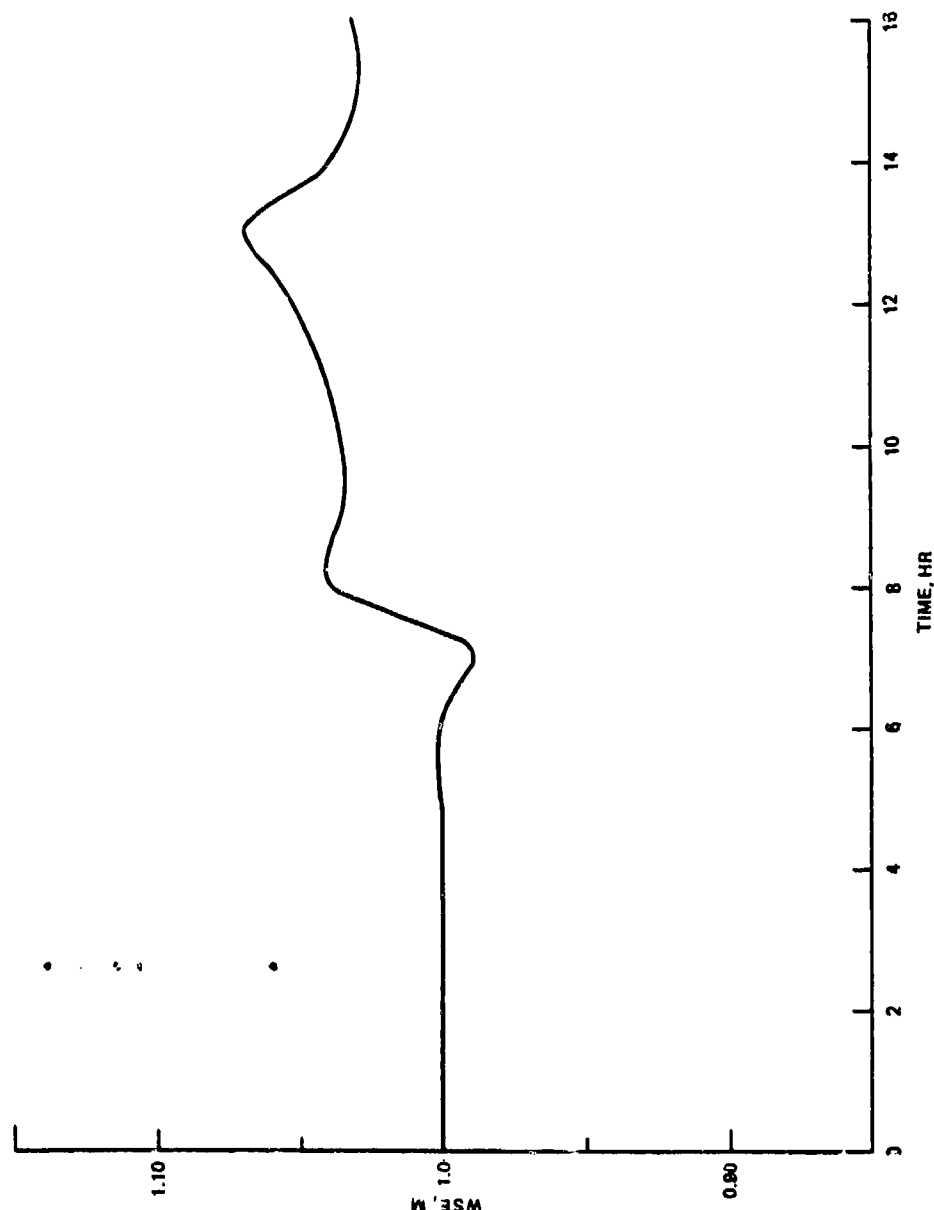
Figure 34. Water surface elevation at $\xi = 6$, $\eta = 25$ with only an ocean boundary
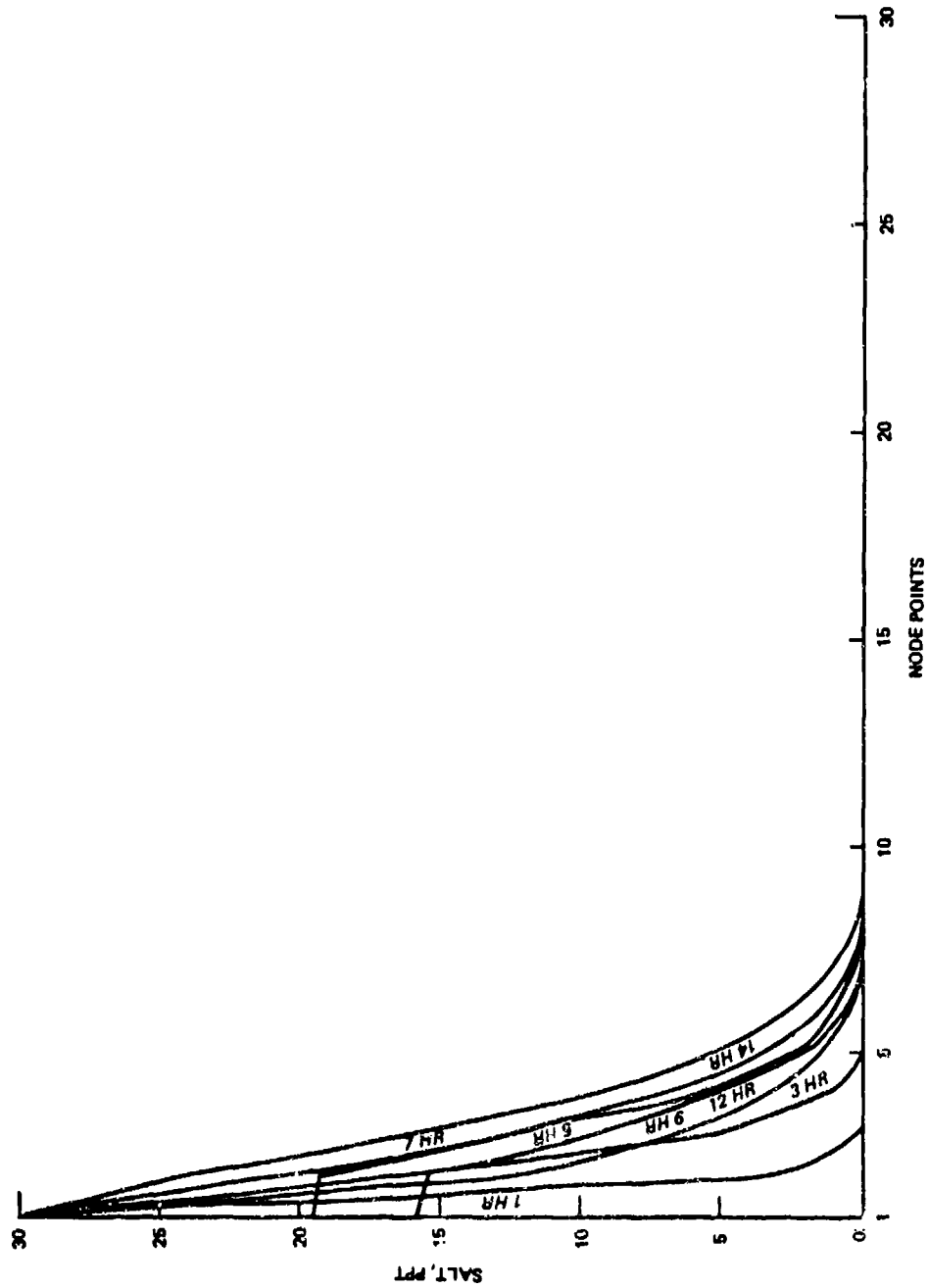
Figure 35. Salinity profiles along $\xi = 6$ with only an ocean boundary
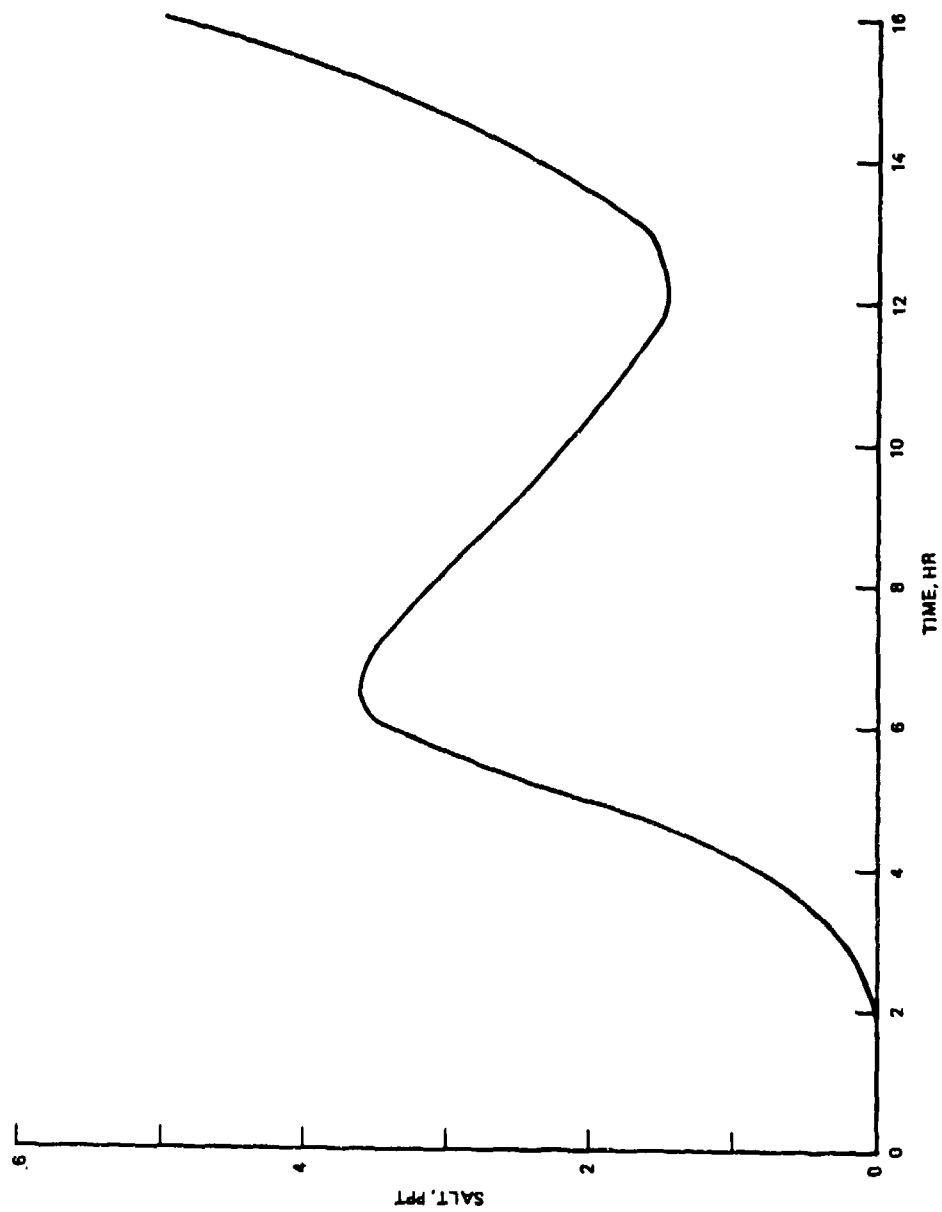
Figure 36. Salinity at $\xi = 6$, $\eta = 5$ with only an ocean boundary
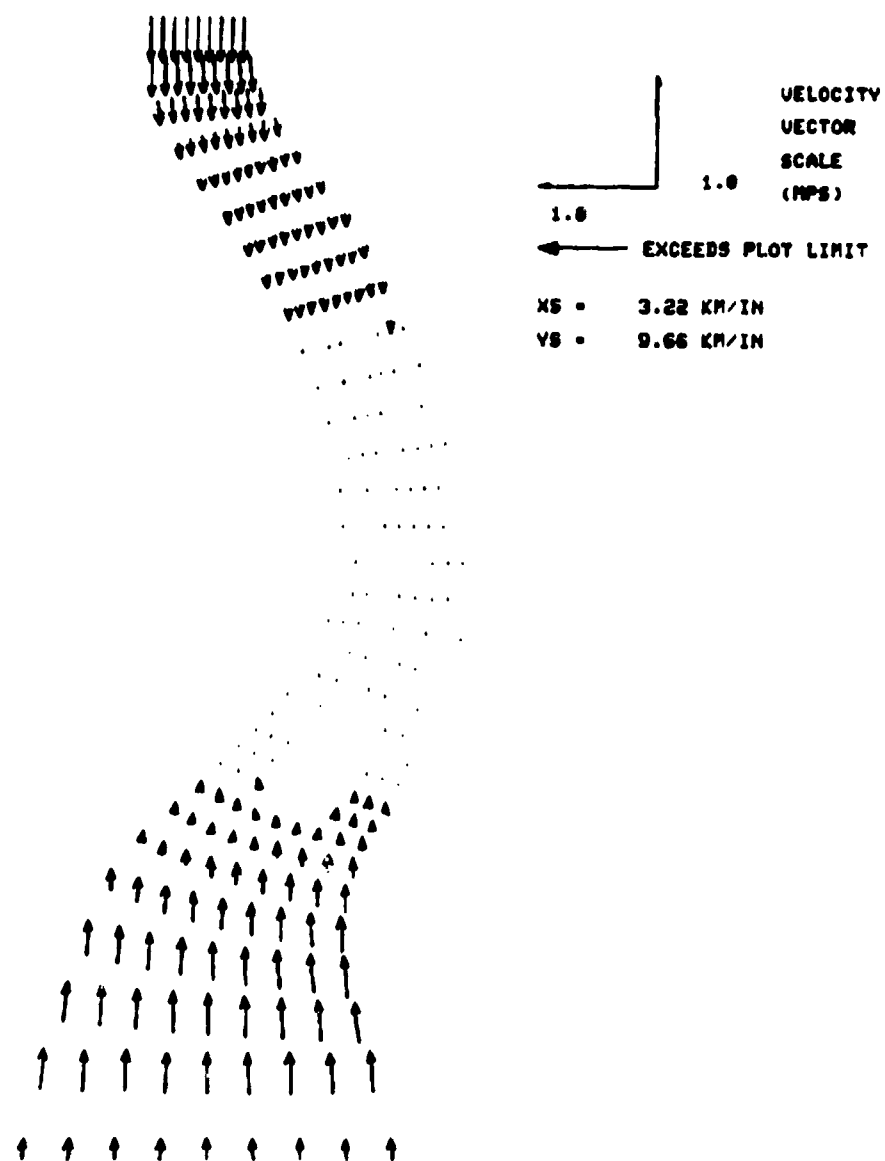
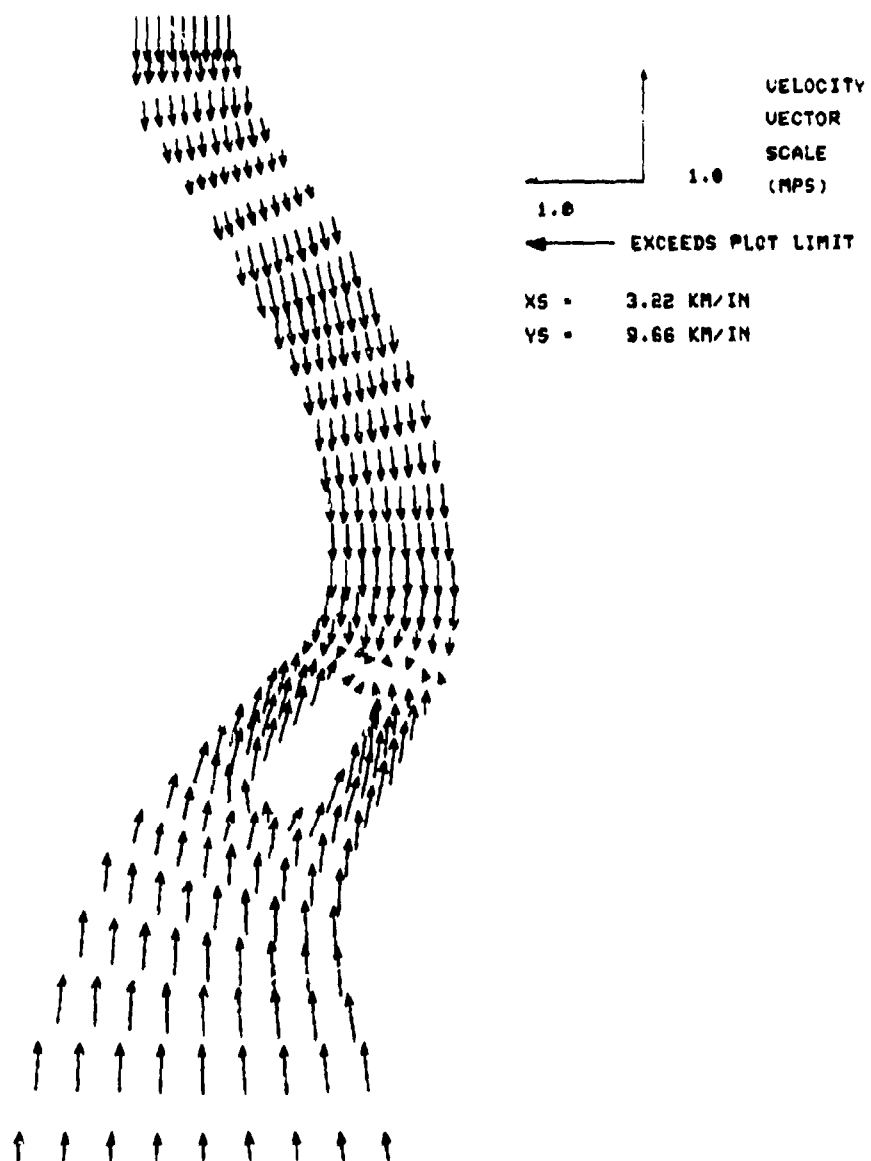Figure 37. Velocity field after 1 hour with an ocean and a river boundary
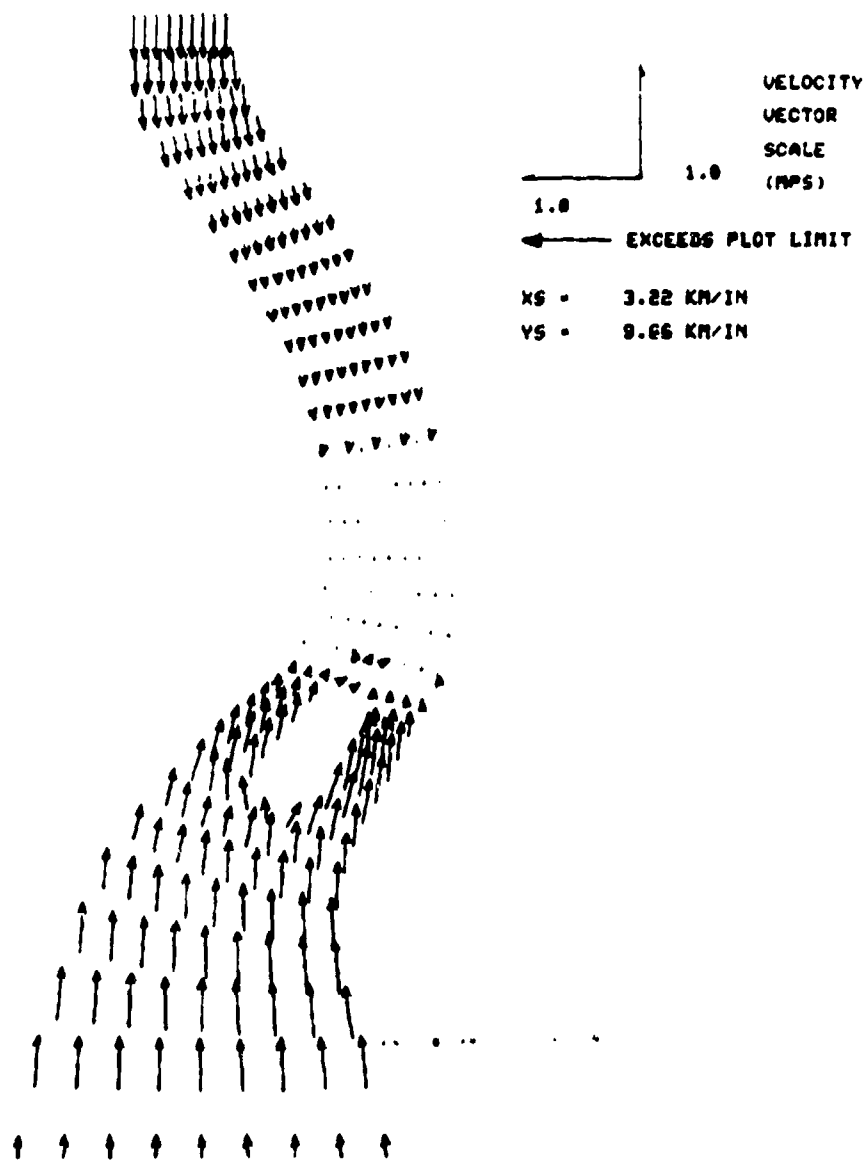
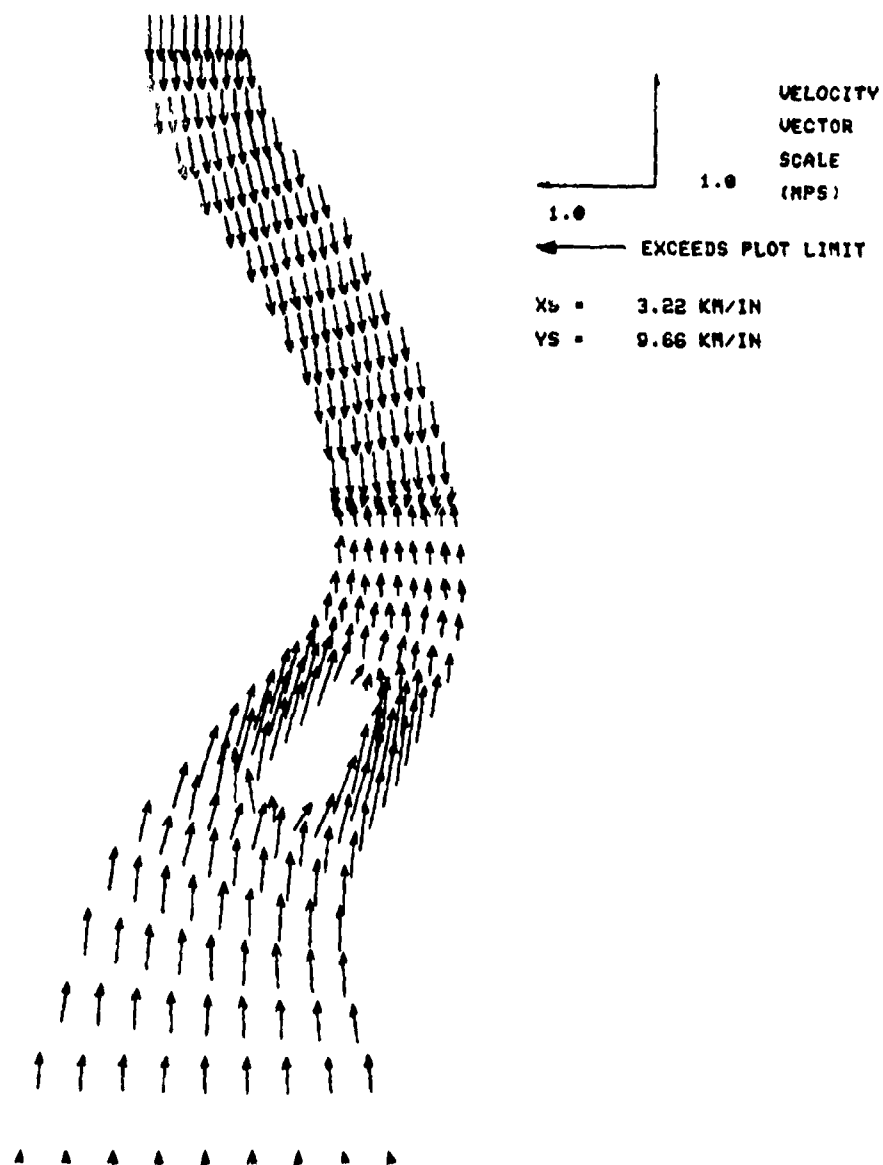Figure 38. Velocity field after 2 hours with an ocean and a river boundary
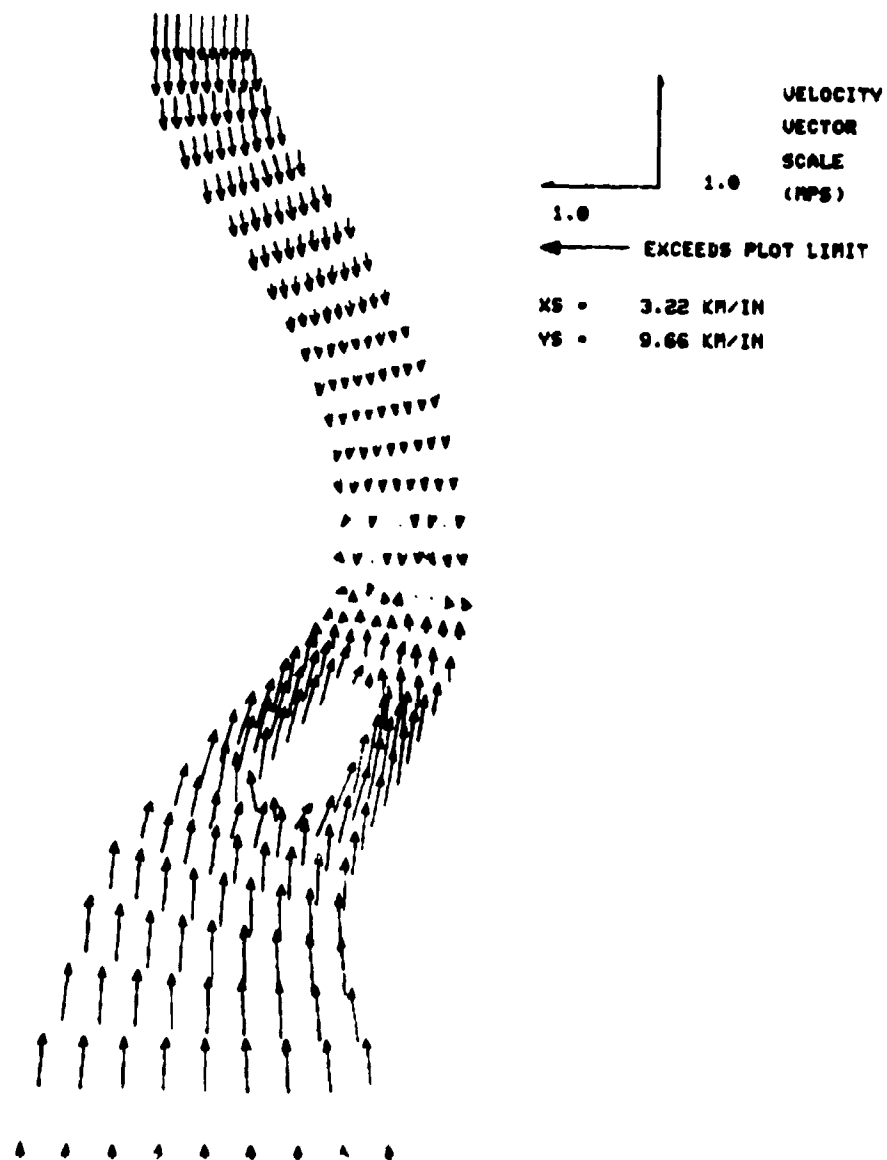
Figure 39. Velocity field after 3 hours with an ocean and a river boundary
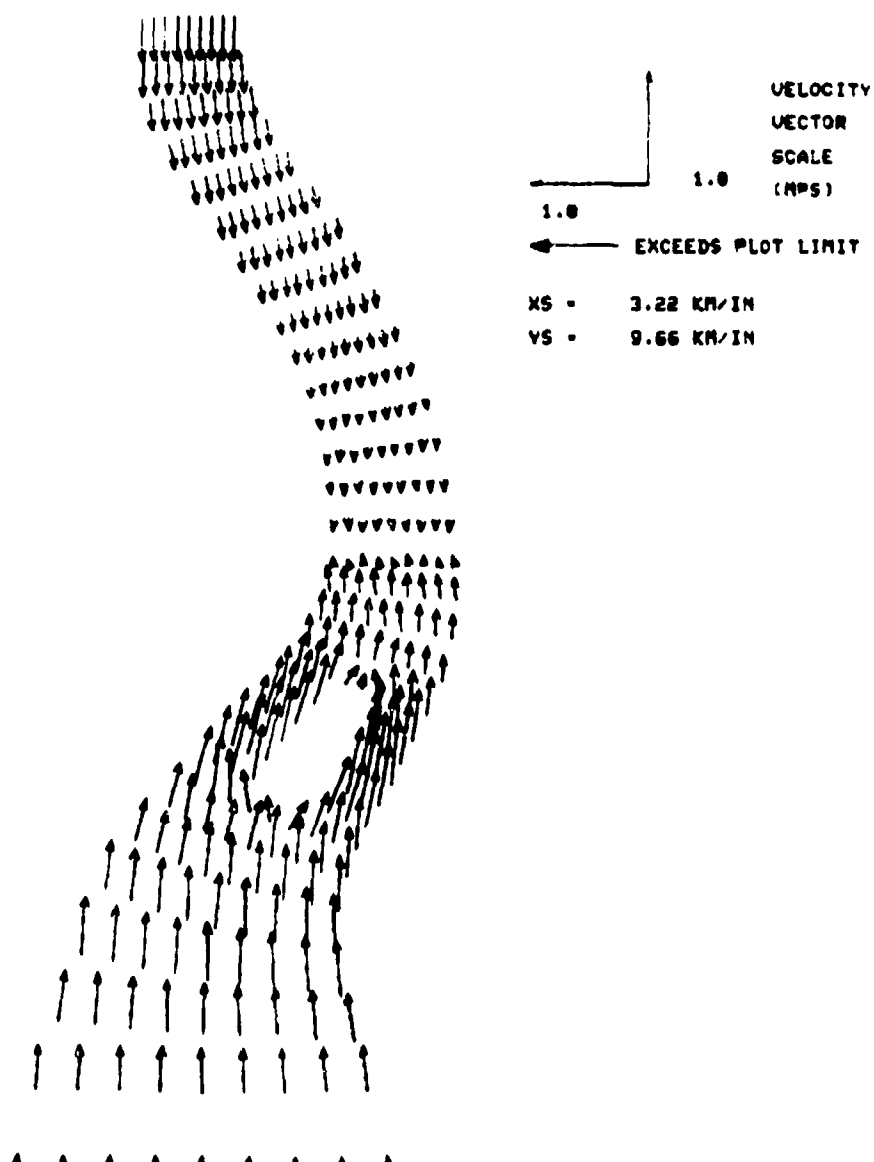
Figure 40. Velocity field after 4 hours with an ocean and a river boundary
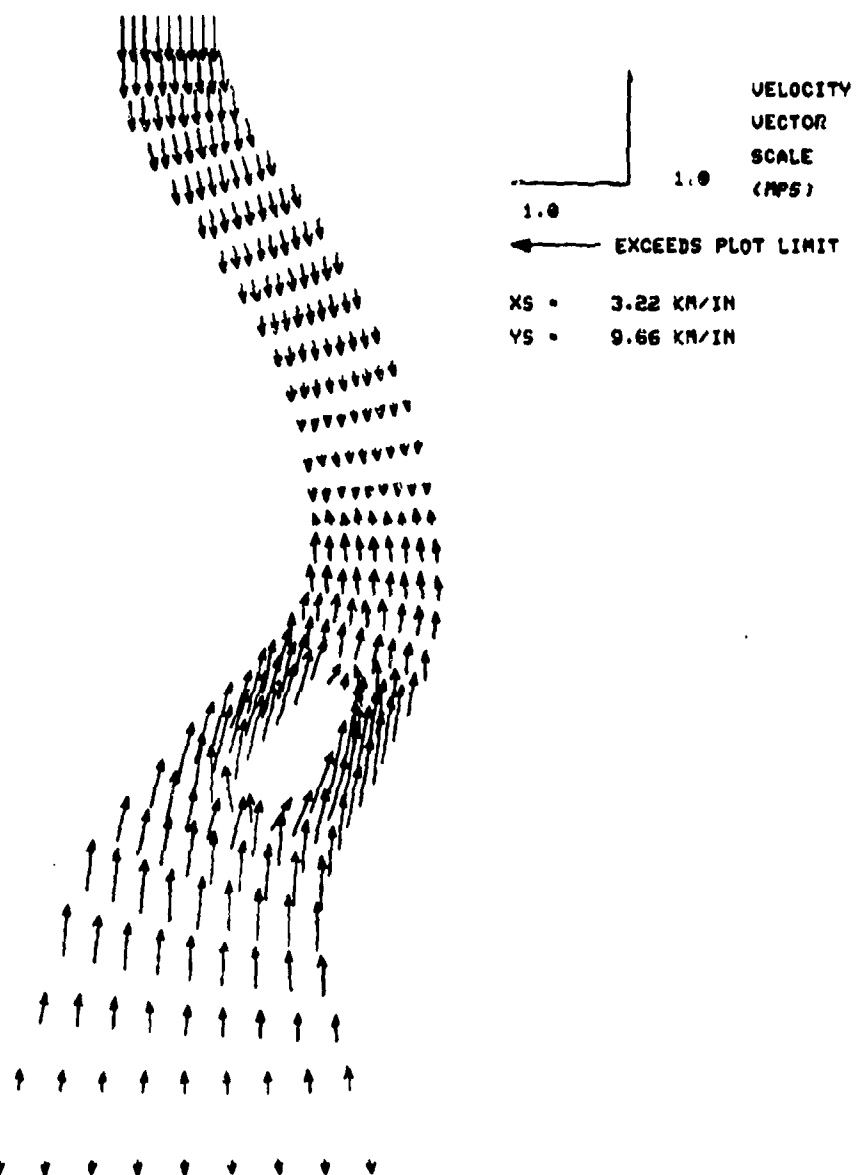
Figure 41. Velocity field after 5 hours with an ocean and a river boundary

Figure 42. Velocity field after 6 hours with an ocean and a river boundary

Figure 43. Velocity field after 7 hours with an ocean and a river boundary

Figure 44. Velocity field after 8 hours with an ocean and a river boundary

Figure 45.   Velocity field after 9 hours with an ocean and a river boundary

Figure 46. Velocity field after 10 hours with an ocean and a river boundary

Figure 47. Velocity field after 12 hours with an ocean and a
river boundary

Figure 48. Velocity field after 14 hours with an ocean and a
river boundary

Figure 49. Velocity field after 16 hours with an ocean and a river boundary
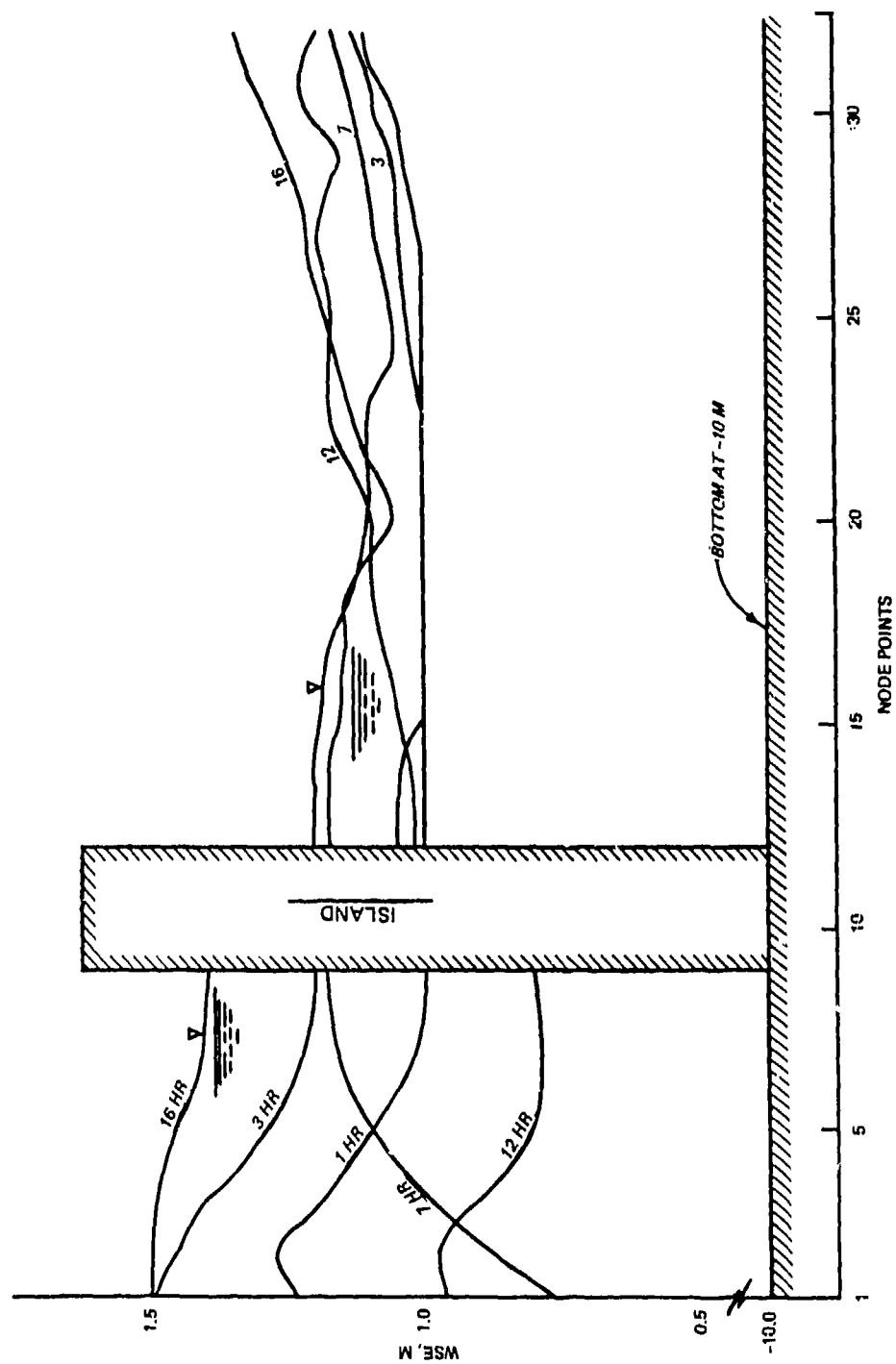
Figure 50. Water surface profiles along ξ = 6 line with ocean and river boundaries
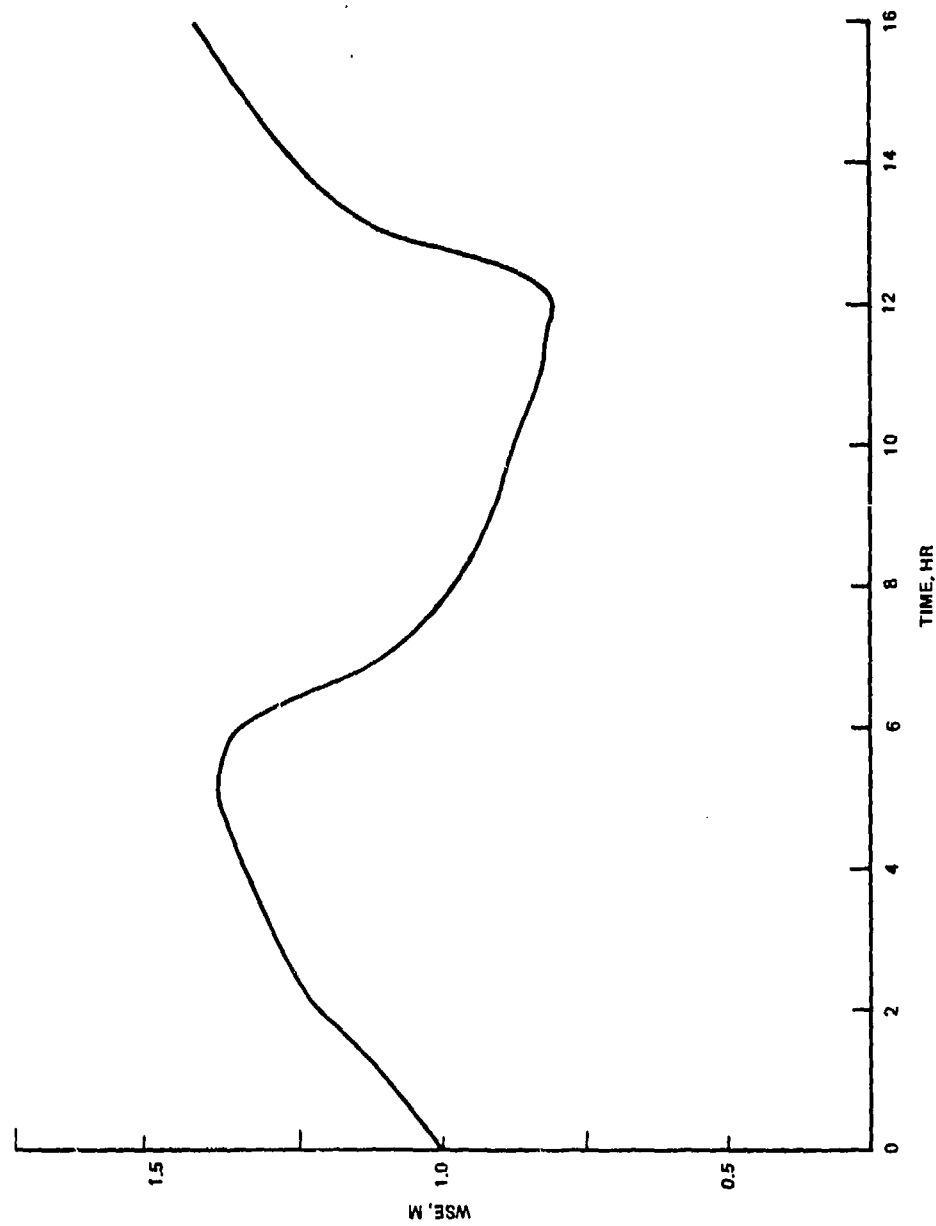
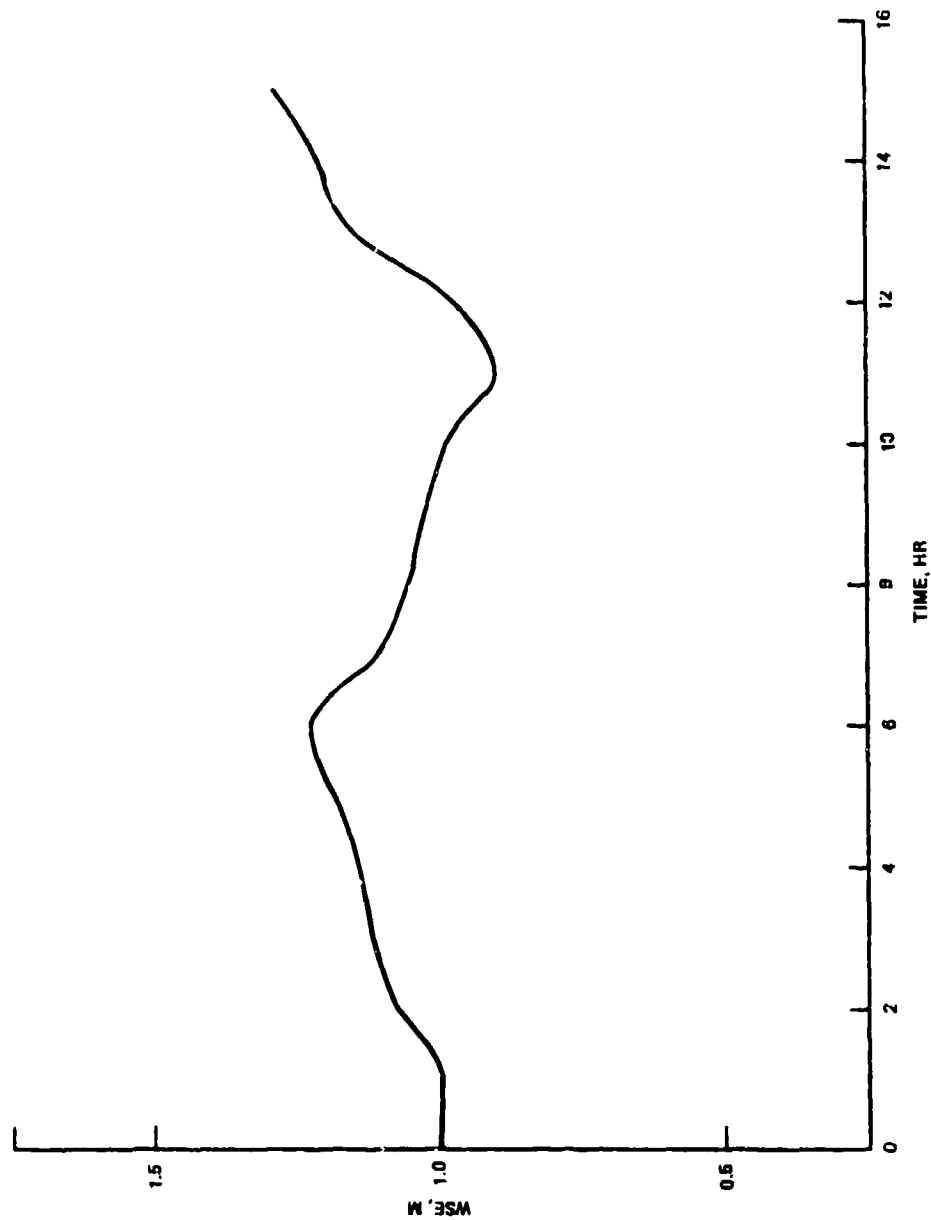Figure 51. Water surface elevation at $\xi = 6$, $\eta = 5$ with ocean and river boundaries

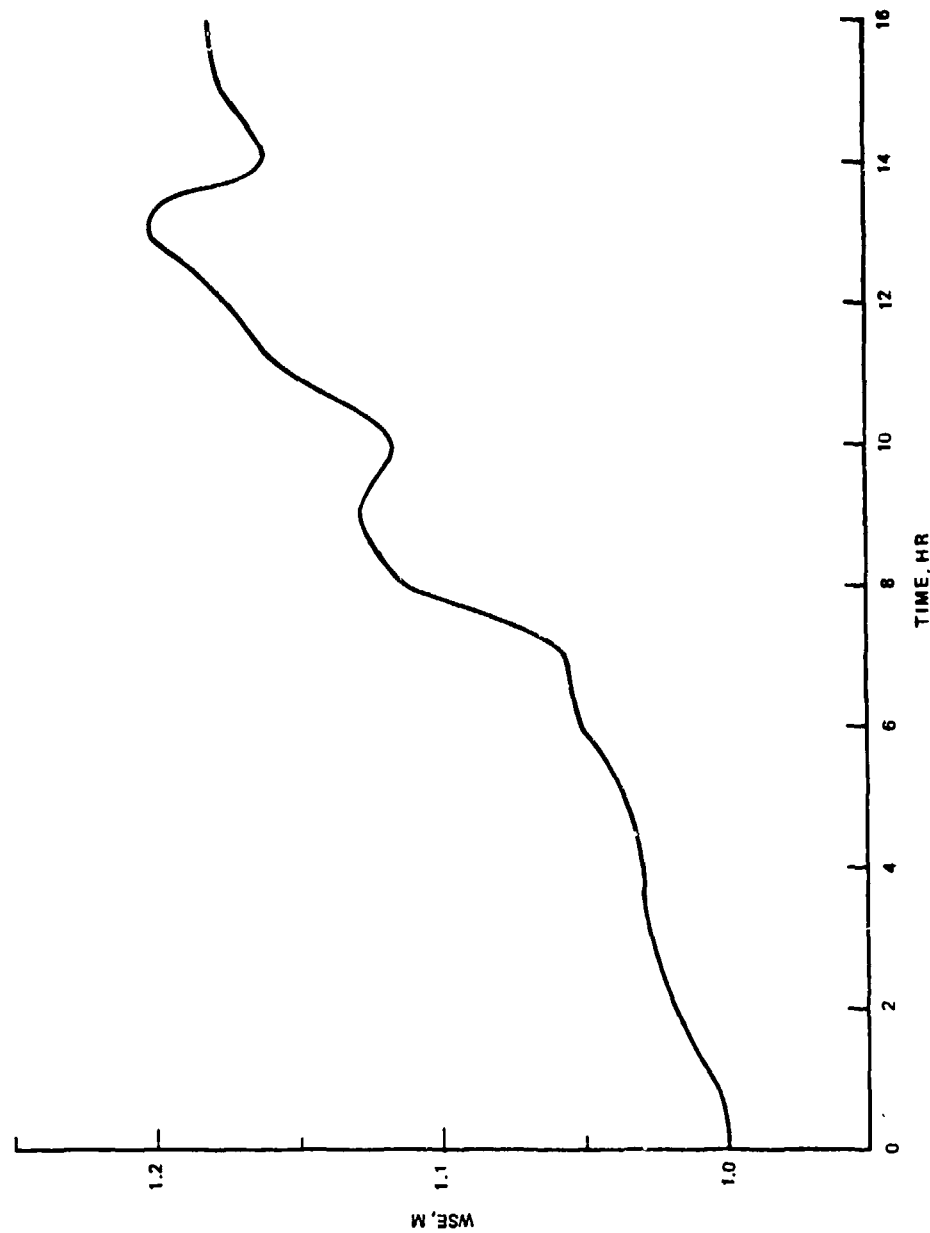Figure 52. Water surface elevation at $\xi = 3$, $\eta = 10$ with ocean and river boundaries

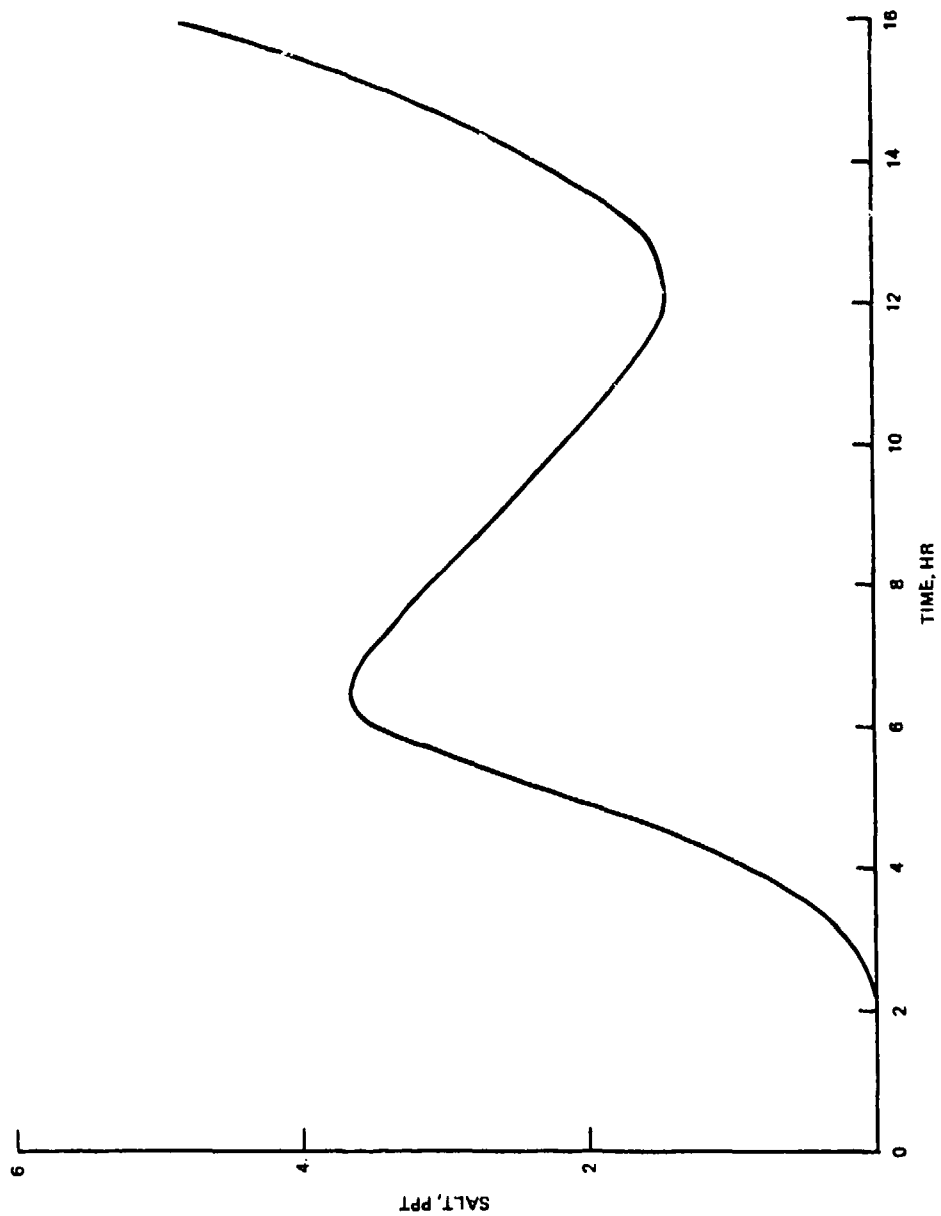Figure 53. Water surface elevation at $\xi = 6$, $\eta = 25$ with ocean and river boundaries

Figure 54. Salinity at $\xi = 6$, $\eta = 5$
with ocean and river boundaries

APPENDIX A: NOTATION

A_{ij}	Eddy diffusivity tensor
A_{ij}	Eddy dispersion tensor
a	Constant
C	Chezy coefficient
d	Constant, distance
D_{ij}	Molecular diffusivity
D_{xx}, D_{yy}	Diagonal components of eddy viscosity tensor
D_{xy}, D_{yx}	Off diagonal components of eddy viscosity tensor
E_x, E_y	Components of eddy dispersion tensor
f	Arbitrary function
$f_x f_y f_\xi, f_\eta$	Derivatives
g	Acceleration of gravity
h	Water depth
J	Jacobian of the transformation
P, Q	Coordinate control functions
P	Pressure
P_a	Atmospheric pressure
r, θ	Cylindrical coordinates
s	Salinity
T	Temperature
Δt	Time step
u, v, w	Components of velocity
u_i, u_j, u_k	Tensor notation for velocity
$\bar{u}_i$	Time averaged velocity
u_i'	Random time varying component of velocity
$\tilde{u}_i$	Time and depth averaged velocity
$\bar{u}_i'$	Random depth varying component of time averaged velocity
v_w	Wind speed
x, y, z	Cartesian coordinates
ξ, η	Boundary-fitted coordinates
$\Delta x, \Delta y, \Delta \xi, \Delta \eta$	Spatial grid steps

A1

ρ	Water density
ρ_o	Reference water density
ρ_a	Density of air
η	Molecular viscosity
ε_{ij}	Turbulent viscosity tensor
ε_{ij}	Eddy dispersion viscosity tensor
ϕ	Water surface elevation; arbitrary variable
τ_{ij}	Stress tensor
ε_{ijk}	Cylic tensor
δ_{ij}	Kronecker delta
$\partial/\partial t$	Time derivative
$\partial/\partial x_i, \partial/\partial x_j$	Space derivatives
τ_{s_x}, τ_{s_y}	Components of bottom shear stress$/\rho$
τ_{B_x}, τ_{B_y}	Components of bottom shear stress$/\rho$
α	Wind direction
λ	Latitude of center of modeled area
ω_e	Earth's angular velocity

A2

In accordance with letter from DAEN-RDC, DAEN-ASI dated
22 July 1977, Subject: Facsimile Catalog Cards for
Laboratory Technical Publications, a facsimile catalog
card in Library of Congress MARC format is reproduced
below.